THE INFLUENCE OF STRUCTURAL OPTIMIZATION ON THE AEROELASTIC PROPERTIES OF A VERTICAL TAIL

THESIS

David G Miller, B. S.
Captain, USAF

AFIT/GAE/ENY/92D-24

AFIT/GAE/ENY/92D-24

THE INFLUENCE OF STRUCTURAL OPTIMIZATION ON THE AEROELASTIC PROPERTIES OF A VERTICAL TAIL

THESIS

David G Miller, B. S.
Captain, USAF

AFIT/GAE/ENY/90D-25

Approved for public release; distribution unlimited

AFIT/GAE/ENY/92D-24

THE INFLUENCE OF STRUCTURAL OPTIMIZATION ON THE AEROELASTIC PROPERTIES OF A VERTICAL TAIL

THESIS

Presented to the Faculty of the School of Engineering

of the Air Force Institute of Technology

Air University

In Partial Fulfillment of the

Requirements for the Degree of

Master of Science in Aeronautical Engineering

David G Miller, B. S.

Captain, USAF

December 1992

Preface

The purpose of this study was to explore the structural and aeroelastic behavior of a standard swept vertical tail. An optimization algorithm was used to minimize the weight of a design. Several different designs were considered by looking at different cases which varied the design load, design variable definition, and design constraints. It is hoped that the qualitative results of this thesis can be easily applied to other lifting surface designs.

The software that was used for this design, MSC/NASTRAN, is based on theory that was not fully explained. Therefore, a major thrust of work for this thesis was to research the theoretical basis of this program and understand and explain the restrictions of the structural and aerodynamic theory. The optimization algorithm was based on a functional approach that needed explanation so that the results from the iterative scheme could be closely monitored.

I wish to give special thanks to my thesis advisor, Dr Peter Torvik, and my thesis sponsor, Dr Jim Olsen, for their guidance in times of need. A word of thanks is also owed to Col Ron Bagley for his assistance and pat on the back when I was making no headway on my thesis.

David G Miller

Table of Contents

List of Figures

List of Tables

List of Symbols

A	Surface area of Wing Panel.
[A]	Aerodynamic Matrix relating Force to downwash.
[B]	Strain-displacement matrix.
b_o	Reference chord length (1/2 of root chord)
[C]	Damping matrix.
{d}	Displacement vector for n discrete nodal points.
$\{d_s\}$	Structural node displacement vector.
$\{d_a\}$	Aerodynamic node displacement vector.
{d}	Displacement modal vector.
[D]	Downwash-pressure coefficient matrix, or stress-displacement matrix.
[E]	Material property matrix.
{F}	Force vector.
$\{F_a\}$	Aerodynamic force vector.
$\{F_s\}$	Structural force vector.
$\{F_2\}$	Vector of aerodynamic forces which are not dependent on structural displacements.
f_i	Aerodynamic doublet line force on panel i.
[G]	Splining matrix.
g	Artificial damping variable.
$G(X_i)$	Constraint equation.
H	Geometric properties of the wing. (size, sweep, etc)

{IC}	Downwash across rigid wing.
k	Reduced frequency, (b_o ω / U) or spring constant.
K	Kernel Function.
[K]	Finite element stiffness matrix or kernel function matrix.
[L]	Coefficient matrix which equates the value of the incremental downwash due to surface displacements due to flexibility.
l_i	Length of bar element i.
[M]	Mass matrix.
M	Mach number.
[N]	Displacement shape function.
{P}	Concentrated forces at discrete points.
$\bar{P}$	Modal Pressure Coefficient.
p	Non-dimensional pressure coefficient.
q	Dynamic pressure. ($\frac{1}{2}$ ρ U^2)
[Q]	General aerodynamic force matrix.
{S}	Search vector in design space.
[S]	Splining matrix.
[T]	Displacement-downwash coefficient matrix.
U	Free stream velocity
u	Displacement function.
$\dot{u}$	Velocity function.
$\ddot{u}$	Acceleration function.

u_k	Aerodynamic nodal point displacements.
u_s	Structural nodal point displacements.
$\{w\}$	Vector containing the value for downwash at n discrete points.
$w,\bar{w}$	Downwash function across wing, modal downwash function.
$\{X\}$	Vector of design variables.
Z	Objective function.
ζ,η	Integration constants.
ε	Strain function vector.
σ	Stress function vector.
Φ	Surface traction function or Lagrangian function.
κ	Damping factor.
ρ	Mass density.
ω	Frequency of oscillation.
λ	Dummy variable used to calculate eigenvalues.
$\{\phi\}$	Eigenvector.

Abstract

The purpose of this thesis is to investigate the influence of structural optimization parameters on the structural and aeroelastic behavior of a vertical tail. The outside geometry of the tail is assumed fixed. The objective of the optimization is to reduce the structural member sizes so that the overall weight of the tail is minimized. The influence that design loads, design constraints, and design variable linking has on the optimal design is observed by examining several design cases. The static aeroelastic properties and flutter speeds of the various design cases are then compared. The doublet lattice method is used to calculate the steady and unsteady subsonic aerodynamic loads and finite element theory is used to model the vertical tail structure.

AN INVESTIGATION INTO THE INFLUENCE OF STRUCTURAL OPTIMIZATION ON THE AEROELASTIC PROPERTIES OF A VERTICAL TAIL

1. *Problem Statement and Background*

1.1 Problem Statement

This thesis investigates the influence of structural optimization on the the minimum weight design and aeroelastic response of the support structure, or tailbox, of a vertical tail. The vertical tail is designed for subsonic, high angle of attack flight conditions. The design loads are based on the maximum aerodynamic loads produced from the tail during steady-state level flight. The aerodynamic loads and the response of the structure to these loads are predicted with a computer generated mathematical model. The exterior geometry, or shape, of the tail and tailbox is assumed to be fixed. Since structural weight is directly related to the size of the structural members, a minimum weight design is calculated by determining the minimum amount of structural material which is required to support the design load without violating any of the design constraints.

To identify the influence that design constraints have on the structural members, an optimal design is calculated for several sets of design constraints. For each constraint set, a minimum weight design is calculated. From the results of each of these design cases, conclusions are drawn on (a) the structural member sizes most influenced by the design constraints, and (b) the cost in structural weight for the

desired aeroelastic response.

1.2 Introduction

Research in the area of aeroelastic optimization has increased dramatically in the last 15 years. This is a result of the emphasis in the engineering community shifting from developing optimal designs at the test and evaluation level, back to developing optimal designs at the product design level. This shift in interest has been fueled by changes in the aircraft industry. Four of the major changes are (35:977)

> (1) new aircraft systems are now very expensive to build resulting in fewer aircraft designs,
>
> (2) fewer current aircraft systems reduce a designer's ability to rely on past experience when making design decisions,
>
> (3) the new aircraft systems are enormously complex and the interdependency of the aircraft's components on the overall performance is difficult for the human mind to conceptualize, and
>
> (4) the processing capability of modern computers has increased dramatically so as to allow the designer to model complex relationships numerically.

These changes have forced the designer to make more and more decisions based on predictions of design behavior instead of actual test data. The most common method for predicting the behavior of a design is to create a mathematical model. These models attempt to duplicate the characteristics of a proposed design and the response of the design to given loading conditions.

The challenge for the engineer is to develop a mathematical model which best predicts the actual behavior of the design. If the model does not closely duplicate the

behavior of an actual design, then an optimal design based on the mathematical model would not be very useful. For the case of the vertical tail, the model usefulness depends on (a) the accuracy of the predicted aerodynamic loads and (b) the accuracy of the predicted structural response to the applied loads. Therefore, before optimal theory can be used to design the structure of the tail, the aerodynamic and structural models must be examined to gauge the quality of the optimal design.

1.3 Prediction of Aerodynamic Behavior

Theoretical prediction of aerodynamic lift forces produced by lifting surfaces pre-dates powered flight. Most of the early work focused on addressing the surface as a single, planar surface in steady flight. These classical approaches can be found in McCormick (27:44-71) or in most undergraduate aerodynamic texts. The prediction of lift with these methods was not very accurate, required empirical correction factors, and was not applicable to oscillating surfaces. In addition, only information on the total lifting surface properties could be calculated. Information on the local values of lift, pressure, and velocity could not be extracted with these methods.

The complexity of the governing equations restricted the bulk of research to inviscid, linear potential flow. In addition, the non-linear viscous effects near the surface are ignored since their influence is isolated to the surface and contribute little to tail deflections. Drag forces are assumed not to influence the aeroelastic properties of a lifting surface either. Therefore, linear potential flow theory reduces the complexity of the problem significantly at only a minor cost in theoretical accuracy.

Theodorsen published the first major paper which addressed the oscillatory nature of aerodynamics over a lifting surface (37:413-440). Though this was an important step forward, his work focussed on a two-dimensional planar airfoil which oscillated in pitch and plunge only and did not account for the flexible nature of the airfoil or provide a function of the pressure distribution across the airfoil.

The first significant success in modeling continuous pressure function across a lifting surface is credited to Kussner (20). He developed a functional relationship between the pressure on a wing and the downwash at the surface of the wing. The relationship was developed from the linear full potential equation. Kussner's relationship between pressure and downwash is referred to as the kernel function. Unfortunately, the kernel function is an integral function which does not have a closed form solution due to multiple order singularities in the integrand. Therefore, approximations to the kernel function have been made in order to obtain a working relationship between downwash and pressure.

A number of researchers continued with Kussner's work by presenting approximations to the kernel function. Watkins, Woolston, and Cunningham (38) modified the kernel function by first including non-planar effects and second approximating terms in the integrand with an exponential expansion and assuming that the time varying pressure distribution can be represented by a finite number of pressure modal shapes. This approximation presented the function in a form more amenable to numerical solution. Ueda presented another method of approximating the integral with an infinite series solution (2:345). Discrete approximations to the kernel

function were used by Hedman for steady flow solutions to the downwash equation (1:280). Albano and Rodden (1:279-285) improved on Hedman's work by including unsteady flow contributions. Giesing later (11:693-702) included a model which would account for interference panels. A thorough review of numerical lifting surface theory progress up to 1968 was written by Landahl and Stark (21:2049-2061).

More recently, Lottati and Nissim (22:1043-1048) presented a method of integrating the kernel function in a piecewise fashion reducing the number of calculations required for a convergent solution. Nierkerk demonstrated a method of reducing the algebra and computation time involved in solving the finite part of the integral (31:1194-1196) by using direct integration methods. Bismarck-Nasr (2:878-880) exactly represented the kernel function as a number of new functions. These new function have properties which permit efficient and accurate numerical evaluation.

1.4 Prediction of Structural Behavior

Because of the complexity of the aircraft structure, solutions to the structural response based on continuum models are not feasible. Instead, a finite element technique (6) is used. This technique models the structure as a number of individual discrete parts or elements. The responses of these elements to applied loads have solutions which are easily derived. The response of the entire structure to an applied load can then be modeled as a linear superposition of the response of each individual member or element of the structure. This technique lends itself nicely to numeric computation. The accuracy of this technique is governed by the accuracy of the

element model and the number of elements used. Most finite element programs available today use elements which are based on the solution to the virtual work or potential energy equation (6:109-112).

1.5 Optimal Theory Applied to Aeroelastic Design

Most of the work in the field of structural optimization as applied to aircraft lifting surfaces before the mid 1970's involved discussion of feasible methods and possible algorithms (14:382). The algorithms used mathematical programming techniques along with the finite element method to model a structure. These algorithms could not be applied at the time because of the large number of computations which are required to complete a rigorous optimization. After the computing power of modern computers advanced, (mid 1970's) software began to emerge. The number of computations still remained high, so researchers reduced the number of calculations by relaxing mathematical restrictions or by reducing the accuracy of the structural model. An example of optimization theory applied to a transport wing is provided by Grossman (12:1050-1058).

Methods by Johnson (18:438-445) and Neill (30:1021-1027) use mathematical programming techniques to vary the physical dimensions of structural members in order to achieve an optimum design. This is the simplest technique to apply since it only requires modifications to each of the element's stiffness matrices.

1.6 Closing

Much work has been done on developing the mathematical models which predict the behavior of an actual design. The accuracy of the aerodynamic and structural models are impressive as long as the design does not violate the limitations imposed on each model. Since the aeroelastic design capabilities are relatively new only a limited number of applications of these models are available. To date no known major system has been designed using these optimal design codes. However, As more applications are published and the results verified, the trust in these optimal codes should increase.

The results from this thesis further builds on the optimal design concept discussed. The variations in the vertical tail design demonstrate how optimal design can be used to influence aeroelastic behavior and to identify which structural members are most influenced by the aeroelastic constraints.

2. *Theory*

2.1 Introduction

This chapter concentrates on establishing the mathematical concepts from which the results in chapter four are based. These concepts include the functional relationship between a moving fluid and the pressure distribution on a lifting surface, and the structural response to an applied load. The aerodynamic and structural model for the tail are based on these relationships. The characteristics of the flow field around the lifting surface, structure, and applied loads are emphasized. The definition of optimization model including the optimization goal, the optimization variables, and any limitations on the variables is described. The algorithm used to reach the optimal design is also presented.

The aerodynamic assumptions of the doublet lattice paneling method (1:279) are given in section 2.2. The finite element structural analysis method is discussed in section 2.3. Section 2.4 develops the equations used to tie together the static or dynamic aeroelastic loads to the structural deformations. The final section addresses optimization theory as applied to structural design.

2.2 Aerodynamic Theory

The aerodynamic model used to predict the loads on the vertical tail is based on the doublet-lattice method presented by Albano and Rodden (1:279). This method assumes that the properties of the flow field can be modeled with linear potential flow. The governing equations for linear potential flow are valid for an inviscid and irrotational fluid. In addition, it is assumed that the free-stream velocity is an order of magnitude greater than any local velocity perturbations near the surface of the vertical

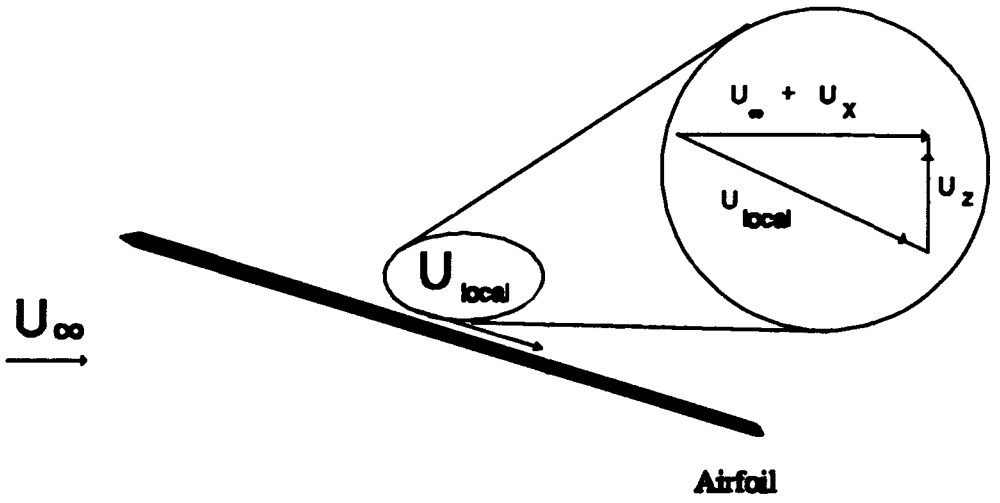

Figure 2-1 : Orientation of aerodynamic velocity vectors used in equation formulations.

tail. (i.e. $U_\infty >> u_x$, u_y, and u_z) The free stream velocity, U_∞, is also assumed to be time invariant in magnitude and direction.

The governing equation for linear potential flow is a second order spatial and time dependent equation. The form of the equation includes the Prandtl-Glauert compressibility effects. The governing equation (7:132) is

$$\nabla^2\Phi - \frac{1}{a_\infty^2}\left[\frac{\partial^2\Phi}{\partial t^2} + 2U_\infty\frac{\partial^2\Phi}{\partial x\partial t} + U_\infty^2\frac{\partial^2\Phi}{\partial x^2}\right] = 0 \qquad (2\text{-}1)$$

where $\nabla\Phi = \bar{u}$. ($\bar{u}$ is a vector of perturbation velocities.) The equation must satisfy the following boundary conditions

$$u_x = u_y = u_z = 0 \qquad as \quad x,y,z \to \pm\infty \qquad (2\text{-}2)$$

$$\frac{\partial\Phi}{\partial z}\Big|_{z=surf} = \frac{\partial z}{\partial t} + U_\infty\frac{\partial z}{\partial x} \equiv w(x,y,z,t) \qquad (2\text{-}3)$$

Equation 2-3 is the surface boundary condition. The surface boundary function is commonly referred to as the downwash function, w(x,y,z,t). Note that the downwash function requires the flow to be tangential to the surface, therefore, the function is only dependent on the tail surface geometry and the motion of the surface with respect to time. By multiplying each side of equation 2-3 by b_o / U_∞ where b_o is a reference

length, the downwash equation can be written

$$\frac{w}{U_\infty} = \left(b_o \frac{\partial}{\partial x} + \frac{b_o}{U_\infty} \frac{\partial}{\partial t} \right) \frac{z}{b_o} \tag{2-4}$$

If z is assumed to vary harmonically with time, $z(x,y,t) = \bar{z}(x,y)\, e^{i\omega t}$, the equation simplifies to

$$\frac{w}{U_\infty} = \left(b_o \frac{\partial \bar{z}}{\partial x} + ik \frac{\bar{z}}{b_o} \right) e^{i\omega t} \tag{2-5}$$

where

$$k = \frac{b_o\, \omega}{U_\infty}$$

The modal amplitude of downwash for each input frequency is then

$$\frac{\bar{w}}{U_\infty} = b_o \frac{\partial \bar{z}}{\partial x} + + ik \frac{\bar{z}}{b_o} \tag{2-7}$$

where the first part is the steady flow downwash and the second part is the oscillatory downwash.

Equation 2-3 provides the downwash as a function of the potential variable. The net aerodynamic pressure acting across the tail can also be represented as a function of the potential variable(7:138).

$$P = -\rho_\infty \left[\frac{\partial \Phi}{\partial t} + U_\infty \frac{\partial \Phi}{\partial x} \right] \tag{2-8}$$

where

P = local perturbation pressure. (P_{local} - P_∞)
ρ_∞ = free stream density.

Both the pressure and downwash equations are a function of perturbation potential, so a functional relationship exists between downwash and pressure. Since the value of the downwash function is known for a given tail geometry, it is desirable to manipulate equations 2-1 through 2-4, and 2-8 to determine the differential surface pressure as a function of the surface downwash. A relationship was developed by Kussner (20:14) by assuming that downwash and the pressure vary harmonically with time or

$$\begin{aligned} w(x,y,z,t) &= \bar{w}(x,y,z)\ e^{i\omega t} \\ P(x,y,z,t) &= \bar{P}(x,y,z)\ e^{i\omega t} \end{aligned} \tag{2-9}$$

The functions, $\bar{w}$ and $\bar{P}$, represent the modal amplitudes of the respective functions. The resulting relationship is commonly referred to as the downwash-pressure function (1:279)

$$\frac{\bar{w}(x,y,z)}{U_\infty} = \frac{1}{8\pi} \int_{-\infty}^{\infty} \int_{-\infty}^{\infty} K[x,\xi,y,\eta,k,M]\ \frac{\bar{P}(\xi,\eta)}{q}\ d\xi d\eta \tag{2-10}$$

where k is the reduced frequency and M is the Mach number. The function K is a singular integral function referred to as the kernel function. This function physically relates the downwash, $\bar{w}$, at the point (x,y) due to a unit pressure flux, $\bar{P}$, at (ξ,η). The limits of integration can be reduced to the tail surface only by the fact that the perturbation pressures are defined to be zero off of the surface. The doublet-lattice method is based on this relationship between the downwash and the pressure function.

Due to the singular nature of the kernel function, equation 2-10 cannot be

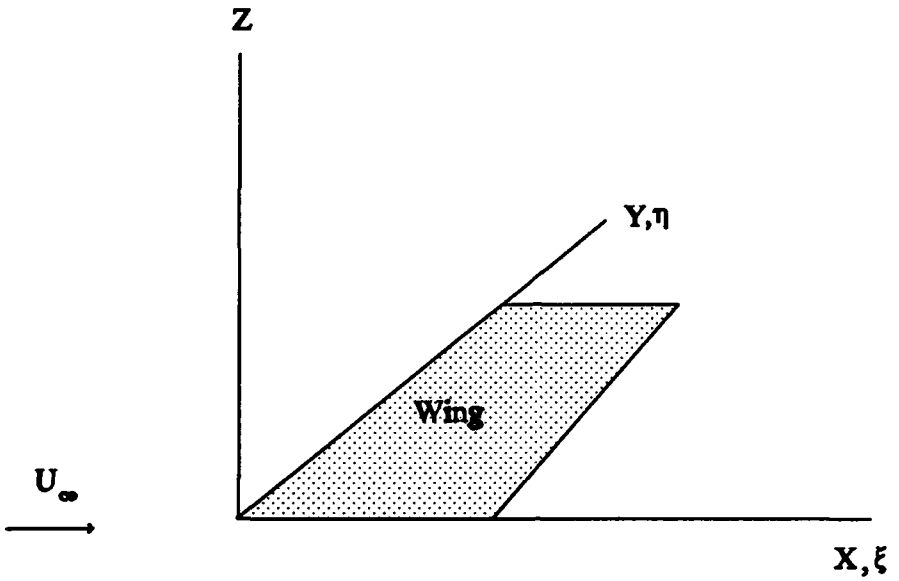

Figure 2-2 : Definition of kernel function coordinate system.

inverted to supply the pressure distribution as a function of downwash. Therefore, this equation does not have a closed form solution for the pressure distribution across the surface. Instead, as was discussed in the background section of chapter one, the terms in equation 2-10 must be approximated in order to get the equation in a form which provides a solution to the pressure function.

First, a solution to equation 2-10 is evaluated at a number of discrete points instead of the continuous domain. The discretization is performed by modeling the surface as a series of planar trapezoidal panels. The panels are arranged in columns parallel to the free-stream velocity vector. A line distribution of acceleration doublets

(2:19,130, and 211) are placed along the one-quarter chord line of each panel. The doublet strength is assumed constant for each panel. The doublet strength is determined by enforcing the known downwash conditions (no flow through) at the mid-span of the three-quarter chord line of each panel. This point is the downwash reference point. By enforcing the no-flow through condition at the downwash reference point, reference 1 found that the Kutta condition is empirically satisfied at the trailing edge.

The strength of the doublet lines of each panel is represented by (1:280)

$$f_j \int_{l_j} d\mu = \overline{P_j} \qquad (2\text{-}11)$$

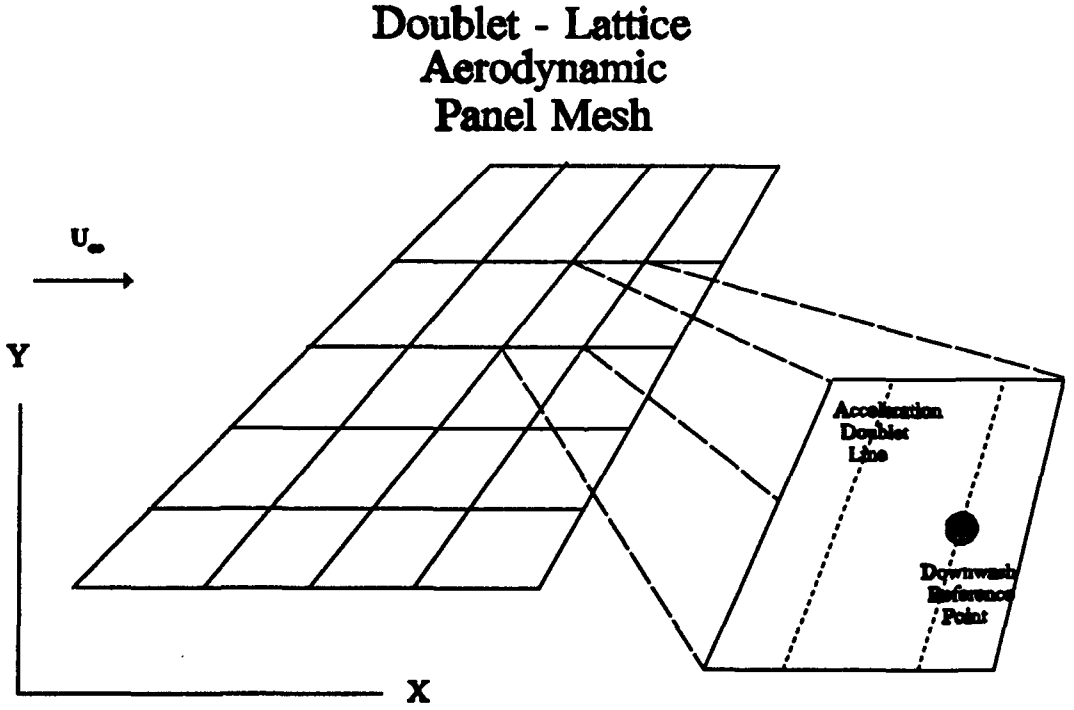

Figure 2-3: Illustration of doublet-lattice mesh.

where

f_j = constant vertical force/unit length.
l_j = direction of panel one-quarter chord span.
$d\mu$ = differential length along l_j.

Inserting this equation into the downwash equation 2-10 reduces the surface integral to a line integral and simplifies the equation to

$$\frac{\overline{w_j}}{U_\infty} = \frac{f_j}{4\pi\rho_\infty U_\infty^2} \int_{l_j} K[x_i, y_i, x_j(\mu), x_j(\mu)] d\mu \qquad (2\text{-}12)$$

($q = \frac{1}{2} \rho U^2$) This equation represents the downwash at a point (x_i,y_i) due to an acceleration doublet at (x_j,y_j). The total downwash produced at the downwash reference point (x_i,y_i) is determined by calculating the influence of all the panels. This is simply the summation of the contribution from each panel or

$$\frac{\overline{w}}{U_\infty} = \sum_{j=1}^{n} \frac{f_j}{4\pi\rho_\infty U_\infty^2} \int_{l_j} K[\ldots] d\mu \qquad (2\text{-}13)$$

where n is the number of panels.

Assume that the net pressure over the panel is the total force produced from the doublets along the panel span, divided over the panel area or

$$\overline{P} = \frac{f_j l_j}{S_j} = \frac{f_j l_j}{\Delta x_j l_j \cos\lambda_j} = \frac{f_j}{\Delta x_j \cos\lambda_j} \qquad (2\text{-}14)$$

where

Δx_j = average panel chord length.
λ_j = panel one quarter chord span sweep angle.

By substituting these equations into the downwash equation 2-10, the downwash

equation simplifies to

$$\frac{\bar{w}}{U_{\infty_j}} = \sum_{j=1}^{n}\left[\frac{1}{8\pi}\Delta x_j \cos\lambda_j \int_{l_j} K[...]d\mu\right]\frac{\bar{P}_j}{q} \tag{2-15}$$

where $q = \frac{1}{2}\rho_\infty U^2$ and the integral term is evaluated numerically. A vector of downwash values can then be calculated and the resulting equations can be written in matrix form *

$$\left\{\frac{\bar{w}}{U_\infty}\right\} = [D]\left\{\frac{\bar{P}}{q}\right\} \tag{2-16}$$

inverting [D]

$$\left\{\frac{\bar{P}}{q}\right\} = [D]^{-1}\left\{\frac{\bar{w}}{U_\infty}\right\} \tag{2-17}$$

Equation 2-17 then provides the pressure at each of the n panels given the downwash values at the n points. The overall force and moment values are determined with an integration matrix [S] (23:86). This matrix acts on $[D]^{-1}\{\bar{w}/U_\infty\}$ and transforms the pressures into forces and moments. Before integrating the pressures, each side of equation 2-17 is multiplied by q (dynamic pressure) so that the pressure values are

* Throughout this thesis a single solid line inside of vector notation,{—}, denotes division, whereas a double line {- -} denotes vector partitioning.

dimensional. The total lift and moment about a given reference point then is represented with

$$\begin{Bmatrix} F \\ -- \\ M \end{Bmatrix} = q[S][D]^{-1} \begin{Bmatrix} \bar{w} \\ \overline{U_\infty} \end{Bmatrix} \tag{2-18}$$

The aerodynamic forces and moments produced by the tail can now be calculated for a given tail geometry. The forces are based on linear potential flow which varies harmonically with respect to time across the tail. Steady flow results are obtained by setting the frequency, ϖ, equal to zero. The linear flow assumption restricts the analysis to small angles of attack because the perturbation velocities must remain much less than U_∞. Finally, it is assumed that the pressure variation can be modeled with a finite number of acceleration doublet lines instead of a continuous sheet of doublets. How these forces are used in conjunction with the structural model will be explained in the aeroelastic model section (2-4).

2.3 Structural Analysis

The finite element method (FEM) is used to model the structural response of the tail to an applied load. This method is a numerical procedure for analyzing

complex structural behavior. Instead of modeling an entire structure with the governing continuum equations, the structure is modeled as an assemblage of discrete pieces. These pieces are referred to as elements. The behavior of each of the elements is relatively simple to model with available equations of motion. (i.e. beam bending, torsion bar, plane stress, etc.) The method is based on satisfying the governing equations at a discrete number of points and assuming the form of the displacement between these points (interpolation). The elements are defined by specifying the connectivity of the element to these points, called nodal points. Each nodal point has up to six degrees of motion (3 translations, 3 rotations). The individual elements are interconnected through the nodal points. The compatibility and equilibrium constraints on the governing equations are imposed at these points.

To simplify the governing equations the following assumptions are made

1. strain (ε) is assumed to be linear with respect to stress (σ).
2. The structure deforms elastically. (no residual strain).
3. Damping is neglected (conservative system).
4. Applied forces are not a function of displacement.

The governing equation for a finite element model with damping is (6:75)

$$[M]\{\ddot{d}\} + [B]\{\dot{d}\} + [K]\{d\} = \{F(t)\} \tag{2-19}$$

where

[M] = Model mass matrix.
[B] = Model damping matrix.
[K] = Model stiffness matrix.
{d} = Generalized nodal displacement vector.
{$\dot{d}$} = Generalized nodal velocity vector.
{$\ddot{d}$} = Generalized nodal acceleration vector.
{F(t)} = Nodal force vector.

which is derived from the virtual work equation. Since damping is neglected, the equation can be simplified to

$$[M]\ \{\ddot{d}\} + [K]\ \{d\} = \{F(t)\} \tag{2-20}$$

The displacement at any point (x,y,z) in the structure is based on the respective displacement at the nodal points. In other words

$$\{u(x,y,z)\} = [N]\ \{d\} \tag{2-21}$$

where {u} represents the continuous displacement field and [N] is the shape matrix which acts as the interpolation matrix with the individual nodal points.

If the inertial contribution ($[M]\{\ddot{d}\}$) is small, equation 2-20 simplifies to

$$[K]\ \{d\} = \{F\} \tag{2-22}$$

The displacement at each of the nodal points can then be determined by inverting the stiffness matrix

$$\{d\} = [K]^{-1}\ \{F\} \tag{2-23}$$

Therefore, given a set of applied loads and the stiffness properties of the finite element model, the resulting displacements can be calculated.

The stress and strain can be calculated from the known displacements by using the strain-displacement relationship

$$\{\epsilon\} = [\partial]\{u(x,y,z)\} = [\partial][N]\{d\} = [B]\{d\} \tag{2-24}$$

where [∂] is the derivative matrix which transforms displacements to strain, and [B] is

referred to as the strain-displacement (6:17) matrix ([B] = [∂] [N]). The stress-strain relationship is $\{\sigma\} = [E]\{\varepsilon\}$ where [E] is the material stiffness properties matrix (6:18). By incorporating the results from equation 2-24

$$\{\sigma\} = [E][B]\{d\} \tag{2-25}$$

If the inertial effects can not be neglected, then the mass term and nodal acceleration term must be included into the solution. To simplify the resulting 2nd order differential equation, the time dependency of the displacement vector is assumed to be harmonic

$$\{d\} = \{\bar{d}\}\, e^{i\omega t} \tag{2-26}$$

After substituting this into equation 2-20

$$(-\omega^2 [M] + [K])\{\bar{d}\}e^{i\omega t} = \{F(t)\} \tag{2-27}$$

The model response becomes infinite for values of ω where the determinant of $| -\omega^2 [M] + [K] |$ is zero. This type of problem is referred to as an eigenvalue problem. The solution involves calculating values of ω_i where the determinant vanishes. These values for ω_i can be substituted back into the governing equation ($\{F\} = 0$) to obtain the corresponding modal shape vectors, $\{\phi_i\}$,

$$\left(\omega_i^2 [M] - [K] \right) \{\phi_i\} = 0. \tag{2-28}$$

The mode shapes are referred to as eigenvectors. These eigenvectors are stored in a square matrix of n eigenvectors, $[\phi_i]$.

Since the model is linear, the response to any set of applied loads is simply a

linear superposition of each of the n modal responses $\{\phi_i\}\ f_i(t)$. For free vibration, the response is

$$\{d(t)\} = \sum_i a_i \{\phi_i\} e^{i[\omega_i]t} \qquad (2\text{-}29)$$

where the coefficient a_i is the amplitude of the ith mode.

The preceding paragraphs demonstrated the usefulness of the FEM in determining the structural response of the vertical tail to both static and time dependent loads. To arrive at equation 2-23 and 2-27, the assumptions had to be made that the structure is continuous in a piecewise manner, the force-displacement relationship is linear, and the material deforms elastically. The forces can only be applied at the structural nodal points so an interpolation scheme is employed to transfer the loads calculated in section (2.2) to the structural nodal points. The method is explained in the following section. Also, the aerodynamic forces are a function of displacement which requires special attention. This, too, is explained in the following section.

2.4 Aeroelastic Analysis

This section develops the equations which tie together the aerodynamic and structural model. Two different approaches are developed; the first is for the static aerodynamic case, and the second is for the critical dynamic response, or flutter, case.

The important issue with aerodynamic loads is that the loads are dependent on the local deflections. The equations in section 2.3 assumed that the loads were not dependent on displacements. The load dependency on displacement results in an aerodynamic 'stiffness' term which is incorporated into the structural stiffness term.

Static Aeroelasticity: For the static aeroelastic case, the structural force equilibrium equation given in section 2-3 is

$$[K]\ \{d\} = \{F\} \tag{2-30}$$

Assume that the force vector is solely produced from aerodynamic loads and can be divided into two force vectors

$$\{F\}=\{F_1\} + \{F_2\} \tag{2-31}$$

where $\{F_1\}$ is a vector of aerodynamic forces which are a function of the structural displacements and $\{F_2\}$ is a vector of forces produced from the tail as if it were rigid. The vector $\{F_1\}$ is assumed to be zero for zero nodal displacements (rigid) and the value for $\{F_2\}$ is determined from the initial conditions (tail angle of attack). Assume the dependence of $\{F_1\}$ on the structural displacements can be represented by

$$\{F_1\} = q\ [A]\ \{d\} \tag{2-32}$$

where q is dynamic pressure and [A] acts as an aerodynamic stiffness quantity. Equation 2-30 can then be rewritten

or

$$([K] - q[A])\ \{d\} = \{F_2\} \tag{2-33}$$

$$[K']\{d\} = \{F_2\} \tag{2-34}$$

Remember that $\{F_2\}$ is independent of the deflections. If, as q is increased, the determinant of [K'] decreases in value towards zero; the displacements, {d}, will have to increase to retain the equality of equation 2-34. If the increase in displacement is only minimal, then there is no need for concern, but if the increase in nodal deflections is large then the structure could exceed elastic limits. This phenomena is called divergence.

There is one major problem with equation 2-31 through 2-34, the equations require that the forces be applied at the structural nodal points, $\{d_s\}$. In the case of this aerodynamic model, the forces are located at aerodynamic nodal points, $\{d_a\}$. The aerodynamic loads can only be utilized in the structural model if they act at the structural nodal points. Therefore an interpolation scheme called 'splining' (23:82) is used to transform the aerodynamic frame of reference into the structural frame of reference. First, a matrix, $[G_{s\to a}]$, is developed which maps the structural deflections into the aerodynamic frame of reference. In other words $[G_{s\to a}]$ calculates the equivalent aerodynamic displacements from the given structural displacements. The interpolation equation (23:82) is

$$d(x,y) = a_0 + a_1 x + a_2 y + \sum_{i=1}^{n} K_i(x,y)\ P_i \tag{2-35}$$

where $K_i(x,y) = (1/16\pi)\ r_i^2 \ln r_i^2$

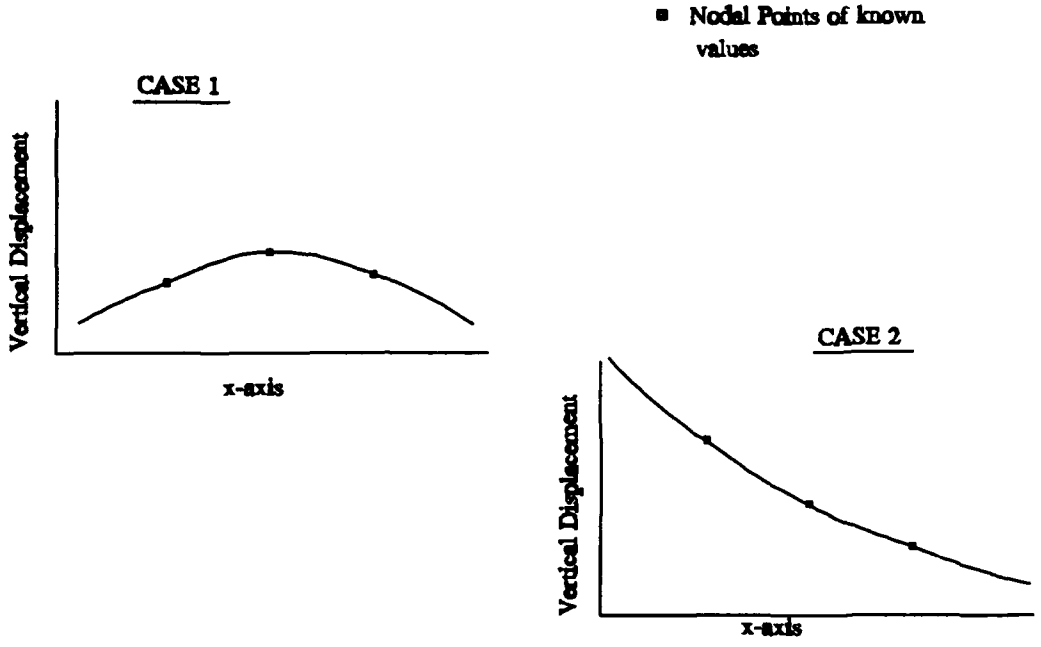

Figure 2-4 : Two 1-D examples of interpolation and extrapolation curves determined from equation 2-35, given three data points.

$$r_i^2 = (x - x_i)^2 + (y - y_i)^2$$

a_i , P_i are coefficients which satisfy

$$\Sigma P_i = \Sigma x_i P_i = \Sigma y_i P_i = 0.$$

The coefficients are determined by repeating this equation for the displacements at the n structural nodal points, (x_j,y_j), to form a matrix equation

$$\begin{Bmatrix} 0 \\ -- \\ d_s \end{Bmatrix} = [C_s] \begin{Bmatrix} a_i \\ -- \\ P_i \end{Bmatrix} \qquad (2\text{-}36)$$

where $[C_s]$ contains the constants for the structural nodal points. The $[C_s]$ matrix is

then inverted to find the coefficients. The displacements at the aerodynamic grid points are then represented by

$$\{d_a\} = [C_a]\,[C_s]^{-1} \begin{Bmatrix} 0 \\ -- \\ d_s \end{Bmatrix} \tag{2-37}$$

where $[C_a]$ contains the constants for the aerodynamic nodal points. Interpolation and extrapolation is then done for the aerodynamic displacements. These displacements will follow the trend of the structural nodal points. If the structural nodal points deflect in a parabolic pattern extrapolation will continue the pattern. If the structural nodal points deflect linearly (for example, wing twist), the leading and trailing edge aerodynamic panels will deflect in the same linear fashion. As the extrapolation is used for data points further from the structural nodal points, the aerodynamic point deflections will tend to converge to a linear behavior.

In simpler form, equation 2-37 is written

$$\{d_a\} = [G_{s-a}]\,\{d_s\} \tag{2-38}$$

To insure that the overall force applied to the structural model is identical to the force applied to the aerodynamic model, identical virtual work of both systems is enforced or

$$\{\delta d_a\}^T \{F_a\} = \{\delta d_s\}^T \{F_s\} \tag{2-39}$$

where the symbol δ refers to the virtual values of displacement, and $\{F_a\}$ and $\{F_s\}$ are the forces in the aerodynamic frame of reference and the structural frame of reference, respectively. Equation 2-38 and 2-39 can be combined to obtain

$$\{d_s\}^T \left[[G_{s-a}]^T\{F_a\} - \{F_s\}\right]=0 \tag{2-40}$$

Since virtual displacements are arbitrary then the terms inside the bracket must equal zero and

$$\{F_s\} = [G_{s-a}]^T \{F_a\} \tag{2-41}$$

This can now be used in equation 2-18 which results in

$$\begin{Bmatrix} F \\ -- \\ M \end{Bmatrix}_s = q[G_{s-a}]^T[S][D]^{-1}\begin{Bmatrix} \overline{w} \\ \overline{U_\infty} \end{Bmatrix}_a \tag{2-42}$$

and provides the aerodynamic loads at the structural nodal points.

In order to determine the contents of the matrix [A] from equation 2-32, downwash must be presented as a function of the displacement vector. This is done with a derivative matrix [T] so that

$$\begin{Bmatrix} \overline{w} \\ \overline{U_\infty} \end{Bmatrix}=[T]\{d\}_a \tag{2-43}$$

or

$$\begin{Bmatrix} \overline{w} \\ \overline{U_\infty} \end{Bmatrix} = [T][G_{s-a}]\{d\}_s \tag{2-44}$$

Equation 2-7 illuminates the task of this matrix. The [A] matrix then has the form

$$[A] = q[G_{s-a}]^T[S][D]^{-1}[T][G_{s-a}] \tag{2-45}$$

The only unknown now left in equation 2-34 is the structural displacement vector {d}. A solution to the structural displacements are then obtained by inverting the modified stiffness matrix [K']. These displacements can then be used to calculate member stresses, strains, etc.

Flutter analysis: Aerodynamic forces naturally will vary due to wind gusts or maneuvers. The wing responds to the fluctuation of aerodynamic loads by oscillating. At low dynamic pressures, the oscillatory aerodynamic loads typically act opposite to the motion of the wing. This effectively dampens the response of the wing. As the dynamic pressure increases, the oscillatory aerodynamic forces may begin to dampen the oscillations less and, in fact, begin to reinforce the motion of the wing. This reinforcement can quickly cause wing components to exceed elastic limits and fail.

The motion of the wing is modeled using equation 2-17 of section 2.2. As in divergence, the main difficulty is modeling the aerodynamic forces accurately. Assuming no structural damping and concentrating on the oscillatory aerodynamic forces only, the governing equation for the structural response can be written

$$[M]\{\ddot{d}\}+[K]\{d\} = q[Q(M,k,H)]\ \{d\} \tag{2-46}$$

where [Q] is the aerodynamic stiffness matrix and the other terms were defined previously. With oscillatory motion, [Q] is a complex matrix which introduces damping into the problem.(the damping terms come from the kernel function)

Before, a solution to this second order differential equation involved assuming the motion was harmonic and oscillated at a frequency $e^{i\omega t}$. To model this problem as harmonic then the damping from [Q] must be removed. To artificially remove the damping from the problem, an artificial damping factor (g) is inserted into the equation. If a value for g is chosen which cancels out the aerodynamic damping of one of the modes then the system can oscillate harmonically in that mode. The sign of the damping factor is important. When the sign of g is negative, the aerodynamic damping is stable and would have caused the oscillations to die out. If g is positive, then the aerodynamic damping would have caused unbounded growth of the response. A velocity/Mach number combination at which g is zero reflects a point at which there is no aerodynamic damping in one of the modes. This is the critical point at which one of the modes of vibration become unstable. The smallest velocity/Mach number pair for which g=0 is considered to be the flutter point.

Equation 2-46 is rewritten to reflect the harmonic assumption and to include the artificial damping term

$$(-[M]\omega^2+(1+ig)[K]-q[Q])\{d_o\}e^{i\omega t}=0. \qquad (2\text{-}47)$$

where $\{d_o\}$ is the modal participation vector. The solution to this equation is solved with a technique referred to as the K method (23:2.6-1). Equation (2-47) is rewritten to accommodate this method and the steps follow. Combine [Q] and [M] within one

set of parenthesis

$$\left[-\left[[M]+\frac{\rho}{2}\left(\frac{\bar{c}}{2k}\right)^2[Q]\right]\frac{\omega^2}{1+ig} + [K]\right]\{d_o\}=0. \tag{2-48}$$

The equation is rewritten by factoring out the $(\bar{c}/2k)^2$ term.

$$\left[\left[\left(\frac{2k}{\bar{c}}\right)^2[M]+\frac{\rho}{2}[Q]\right]\left(\frac{-U_\infty^2}{1+ig}\right)+[K]\right]\{d_o\}=0. \tag{2-49}$$

With this representation, the eigenvalue is

$$(\alpha+i\beta)^2=\frac{-U_\infty^2}{1+ig} \tag{2-50}$$

or

$$(\alpha+i\beta) = i\ U_\infty(1-i\frac{g}{2}) \tag{2-51}$$

$$(\alpha+i\beta) = \frac{U_\infty g}{2} + iU_\infty \tag{2-52}$$

From this, the velocity and damping factor can be found to be

$$U_\infty=\beta$$
$$g =\frac{2\alpha}{U_\infty} \tag{2-53}$$

Note that as $g \rightarrow 0$, the imaginary part of eigenvalue also tends to zero. Solution to equation 2-49 then requires the user to input a value for k, m, and ρ. Inputting these

values into the equation and solving the resulting eigenvalue problem will produce a solution for g and V. The flutter speed is the velocity for which the artificial damping factor is zero. For a more complete investigation on this subject, the reader is referred to references 3 and 5.

2.5 Structural Optimization

The optimal design for the vertical tail is determined using a numerical optimization algorithm. This section introduces the general problem statement and the basic concepts and definitions of the optimization problem. The application of these concepts to the structural design problem is then outlined.

Before an optimal design can be determined three characteristics need to be known about the design; (1) what end result is desired, (2) what changes in the design are allowed to best attain that result, and (3) what limitations are there, to these changes. To mathematically model the design process each of these characteristics is represented as function relationships. The first characteristic is called the objective of the design. The values that are allowed to be changed during the optimization process are referred to as the design variables. The objective function should be a function of the design variables. This way the design variables can be changed in order to better meet the design objective. The objective function is constructed so that the optimal design is reached only when the function is at it's minimum value. The design

variables most often are restricted to a range of values. If the value of all of the design variables is within this defined range then the design is considered to be a feasible design. If any of the design variables fall outside of the defined range the design is considered to be an infeasible design. The range is defined by an equation called the constraint equation. A design may have many constraint functions.

For the structural design problem the objective function could be to minimize the structural weight by decreasing the sizes of all the structural members. If the weight was directly proportional to the member sizes and the problem definition did not state any constraints, it should be obvious to see that the optimal design is achieved when the member sizes are zero. This, of course is not true so constraints are placed on the member sizes to account for maximum stress values, maximum displacement allowed, and any other structural behavior that the designer wishes to avoid. The finite element method is used to produce the equations necessary for the constrained optimization problem. The optimal solution is determined with an iterative scheme referred to as the method of modified feasible directions (20:A-11).

The objective and constraint function can be non-linear, but each function and its first derivative must be continuous and be defined for every point in the design space. The general non-linear constrained optimization problem is stated as follows:

Find $\{X\} = \lfloor X_1, X_2, ..., X_n \rfloor$

such that

$Z = F(\{X\}) \rightarrow$ Minimum Value,

for values of {X} which satisfy the constraints

$G_j(X) \leq 0 \qquad j = 1,2,....,C$

$X_i^{lower} \leq X_i \leq X_i^{upper} \qquad i = i,2,....,n$

where F({X}) is the objective function, {X} is a vector of the design variables, and G({X}) is the constraint function. As an example of a two design variable, $\{X_1, X_2\}$, constraint problem, consider a constraint function $G(\{X\}) \equiv a^2 - (X_1^2 + X_1^2)$. (see figure 4) A special case of the constraint equation is the side constraint. This constraint limits directly the value of a design variable, such as $X_1 > 0$ and $X_2 > 0$. (see figure 4) Before explaining how these equations can be applied to structural optimization, an overview of how the solution to this problem is found is necessary.

The solution of this problem is determined with an iterative first order procedure called the method of modified feasible directions. An initial set of design variable values, $\{X^o\}$, must first be given. Assume that these values do not violate any of the constraints. This is referred to as a feasible design. A new guess on an improved design is then calculated by

$$\{X^q\} = \{X^{q-1}\} + \alpha \{S^q\} \tag{2-54}$$

where q is the iteration number, $\{S^q\}$ is a vector which defines the direction in the design space where the new guess will move, and α defines the magnitude or distance of the move. Values for the search vector, {S}, and α must now be determined.

The search vector is required to point in a direction which reduces the value of the objective function, F({X}),

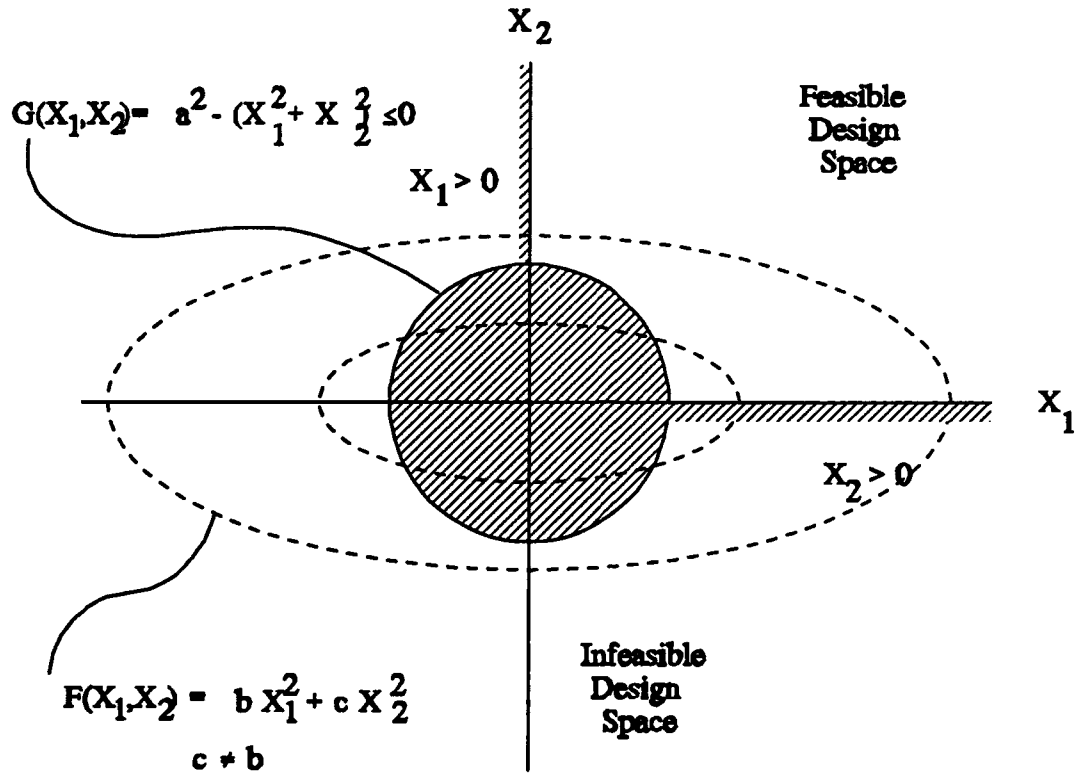

Figure 2-5: Example optimization design space. (F(X) objective function)

$$\nabla F \cdot \{S\} \leq 0 \tag{2-55}$$

or

$$|\nabla F| \cdot |\{S\}| \cos\theta \leq 0 \tag{2-56}$$

The gradient of F({X}) points represents the direction for which F increases most rapidly, therefore, the direction for most rapid decrease is the negative of that direction. As long as the cosine of the angle between the two directions is less than zero, then {S} is in a direction which will decrease the objective function.

For the starting vector, {X°}, assume that the values are not close to any

constraint boundaries. For this case, the direction which would minimize the objective function most quickly is the negative of the gradient of F({X}), or -∇F. So for the unconstrained problem the search direction would be

$$\{S\} = -\frac{\nabla F}{|\nabla F|} \tag{2-57}$$

where {S} is a normalized with respect to the euclidean norm of ∇F. Now, the magnitude or distance of the search vector, α, must be determined.

The value of α is limited to a magnitude which does not cause one of the constraint equations to be violated. To determine a value for α, the constraint functions are calculated at a number of prescribed values for α. When the first value of α for which a constraint is violated, $G_j(\{X\}) > 0$, is calculated, an polynomial interpolation scheme is used to estimate the maximum value of α which can be used which will not violate the constraint. This value is then used for the iteration equation.

By using equation 2-54, a new guess value for the design variables can now be calculated. This value should be close to one or more of the constraint boundaries. The new vector {X} will result in a reduced value of F({X}).

The new vector $\{X^q\}$ still might be able to be changed so that the objective function is reduced even though it is against one or more constraint boundaries. First, the new search direction must still satisfy equation 2-55 but to insure the direction does not violate the constraint equations, the search direction must also satisfy the constraint

$$\nabla G^j(\{X\}) \cdot \{S\} \leq 0 \tag{2-58}$$

which, as in equation 2-56, also states that the angular difference between the ∇G and {S} must be between 90 and 270 degrees.

If during the optimization process, the design variable vector moves to a point in the design space that one or more constraints are violated, equation 2-55 and 2-58 are modified slightly to bias the {S} vector in a direction which will return {X} to the feasible region (20:77).

The process is considered to have converged when the objective function can not be reduced further. For example, when a modified design does not reduce the objective function by 0.1 percent. Several other convergence criteria are used to insure that the code does not continue unnecessarily. These criteria are useful in problem specific cases, so they are not discussed here.

This was a quick overview of the method of modified feasible directions. For the sake of brevity the mathematical intricacies as well as the variations of this method for particular cases has been excluded. However, a thorough explanation can be found in references 14, 23, or 28. The attention will now be shifted to the structural design problem and how the equations of force equilibrium are modified in order to be in a form similar to the constrained optimization problem.

The design properties, or design variables, for the vertical tail are the cross-sectional area and thickness of the wing box bars and panels respectively. It is assumed that the material is homogenous so that the weight varies directly with the

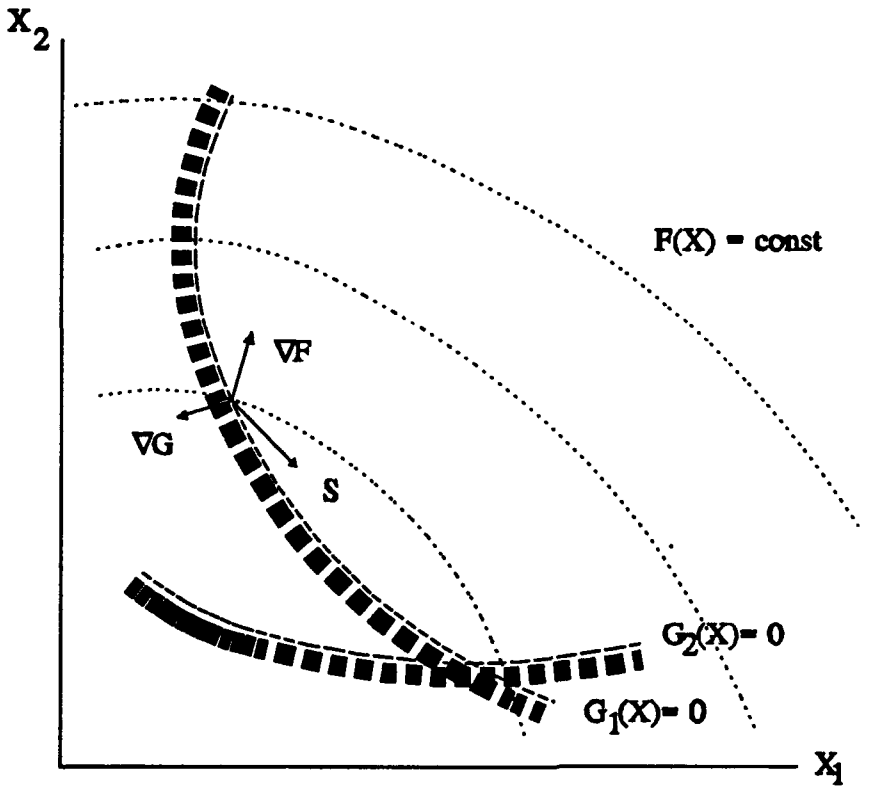

Figure 2-6: Graphical representation of ∇F, ∇G, and {S}.

material volume. The value for these properties must then be reduced in order to produce a lighter weight design. The design variables effect the force equilibrium equation through the stiffness matrix [K] and the mass matrix [M]. For example the stiffness matrix for a simple two degree of freedom rod has a common factor of EA/L where E, A, and L represent the modulus of elasticity, cross-sectional area, and bar length respectively. So, the stiffness matrix can be written as $[K] = EA/L\ [K_{mod}]$ (23:125) where A represents the design variable and K_{mod} is the factored [K] matrix. For the mass matrix of the bar element, the cross-sectional area can be factored out of the mass matrix so that $[M] = \rho\ A\ L\ [M_{mod}]$ where ρ is the material mass density and

$[M_{mod}]$ is the factored mass matrix. Similar operations can be done on other element stiffness and mass matrices although the design variable may not be factorable out of the respective matrices. The design variables now are used to set up the objective and constraint function.

The objective of the design is to minimize the weight of the overall structure. The weight of the design can be determined by summing the weight of each of the m elements or

$$F(\{X_i\}) = Weight = \sum_{i}^{m} \rho V(X_i) \tag{2-59}$$

where $V(X_i)$ is the volume of the ith element. For a bar element the volume is $V(X_i) = \pi A_i L_i/4$. The variable L_i is fixed since geometry of structure is given.

The form of the objective function for the structural design problem is now known. It is desirable to modify the design variable definition slightly to linearize some of the constraint equations. The design variable is defined as

$$X_i = \frac{1}{A_i} \tag{2-60}$$

The advantage gained by this definition will be seen during the constraint equation development.

Assuming the design variables are the cross-sectional area, the gradient of the objective function in equation 2-59 is

This can then be used to calculate the direction of steepest descent.

Several constraints are used during the design of the vertical tail. In particular,

$$\nabla F_{(1 \times m)} = \sum_{i}^{m} \left(-\rho \frac{\partial V\left(\frac{1}{X_i}\right)}{\partial X_i} \right) \tag{2-61}$$

stress constraints, displacement constraints, frequency constraints, and size constraints are used to limit the values of feasible design variable values. The constraint equations as well as the constraint gradient which is used in equation 2-58 are presented next.

A minimum size constraint is a linear constraint which is also referred to as a side constraint. It's purpose is to limit the upper and/or lower bound of the design variable. This constraint might be enforced because of manufacturing limitations or assembly and fit restrictions. The constraint equation is

$$\begin{aligned} G_i(X_i) &= (X_i - X_{upper}) \leq 0 \\ &= (X_{lower} - X_i) \leq 0 \end{aligned} \tag{2-62}$$

Where X_{upper} and X_{lower} are the respective limits of the design variables. There would be 2 equations for each of the m design variables and the gradient of each of these equations would be a vector of zeros except at the ith entry which would have a ± 1 depending on whether it was the upper or lower limit equation.

For a displacement sensitive design, a displacement constraint equation would restrain the displacement at a node j to a minimum and or maximum value. The constraint equation is similar to the minimum gauge function and is defined as where the subscript j denotes the jth node. Note that the constraint equation will now most likely be a function of most or all of the design variables. The gradient function

$$G(\{X\}) = (d_j - d_{upper}) \le 0$$
$$G(\{X\}) = (d_{lower} - d_j) \le 0 \qquad (2\text{-}63)$$

for displacement constraints represent the change in displacement due to a change in each of the design variables.

$$\nabla G = \begin{cases} -\dfrac{\partial d_j}{\partial \{X\}} \; ; & \textit{lower limit} \\ \dfrac{\partial d_j}{\partial \{X\}} \; ; & \textit{upper limit} \end{cases} \qquad (2\text{-}64)$$

The gradient function is derived from the force equilibrium equation (29:134). The force equilibrium equation developed in section 2.3 is

$$[K]\{d\} = \{F\} \qquad (2\text{-}65)$$

Let the design variable for each element be represented by {X}. The change in equation 2-58 due to a change in the design variable can be represented by

$$\frac{\partial F}{\partial X_i} = \frac{\partial [K]}{\partial X_i}\{d\} + [K]\frac{\partial d}{\partial X_i} \qquad (2\text{-}66)$$

Assume that {F} does not vary with respect to X_i. Then equation 2-45 can be written as

$$\frac{\partial \{d\}}{\partial X_i} = -[K]^{-1}\frac{\partial [K]}{\partial X_i}\{d\} \qquad (2\text{-}67)$$

All the variables on the right hand side of the equation are known from the problem formulation and initial analysis. This equation provides the gradient of the displacement constraint function with respect to any of the design variables {X}.

The stress constraint equation limits the values of the design variables so that the yield stress values for each element are not violated. Therefore there will be a constraint equation for each element. The constraint equation is written

$$\begin{aligned} G_i(X_i) &= \sigma_i - \sigma_{max\text{-}Tension} \leq 0 \\ &= \sigma_{max\text{-}Compression} - \sigma_i \leq 0 \end{aligned} \tag{2-68}$$

where σ_{max} is the tensile or compressive yield stress. The governing equation for member stress was given by equation 2-25 and is repeated

$$\{\sigma\} = [E][B]\{d\} \tag{2-69}$$

The dependence of stress on the design variables is determined by taking the derivative of $\{\sigma\}$ with respect to X_i which is

$$\frac{\partial\{\sigma\}}{\partial X_i} = \frac{\partial[D]}{\partial X_i}\{d\} + [D]\frac{\partial\{d\}}{\partial X_i} \tag{2-70}$$

where [D] = [E] [B]

Substituting in equation 2-67 and noting that $\frac{\partial[D]}{\partial X_i} = [0.0]$

$$\frac{\partial\{\sigma\}}{\partial X_i} = -[D][K]^{-1}\frac{\partial[K]}{\partial X_i}\{d\} \tag{2-71}$$

where all the terms on the right hand side are known from the initial problem analysis.

The last constraint that is enforced on the tail design is a frequency constraint. This constraint requires that the first natural frequency be less than some given maximum or

$$G(\{X\}) = \omega_i^2 - \omega_{max}^2 \leq 0 \tag{2-72}$$

This constraint would put a ceiling on the maximum value for the fundamental frequency. This might be important to the functioning of electronic equipment or the fatigue life of a component. Note that ω^2 is used instead of ω to simplify the gradient function. The gradient of this function then is

$$\nabla G(\{X\}) = \frac{\partial \omega_i^2}{\partial \{X\}} \tag{2-73}$$

The gradient of the frequency is determined from equation 2-28 by noting that for the ith frequency

$$[K]\{\phi_i\} - \omega_i^2[M]\{\phi_i\} = 0 \tag{2-74}$$

where ϕ_i is the ith mode shape or eigenvector. Differentiating this equation with respect to $\{X_i\}$ results with

$$([K] - \omega_i^2[M])\frac{\partial \phi_i}{\partial X_i} - \frac{\partial \omega_i^2}{\partial X_i}[M]\{\phi_i\} = -\left(\frac{\partial [K]}{\partial X_i} - \omega_i^2 \frac{\partial [M]}{\partial X_i}\right)\phi_i \tag{2-75}$$

If it is assumed that the motion is primarily from one mode, this can be simplified by noting that [K] - ω^2 [M] = 0 (equation 2-68) and if ϕ_i is scaled so that ϕ_i^T [M] ϕ_i = 1.0. This reduces equation 2-69 to

$$\frac{\partial \omega_i^2}{\partial X_i} = \phi_i^T\left(\frac{\partial [K]}{\partial X_i} - \omega_i^2 \frac{\partial [M]}{\partial X_i}\right)\phi_i \tag{2-76}$$

after premultiplying both sides of the equation by ϕ_i^T. The frequency is then

dependent on both the variation of [K] and [M] with the design variables whereas the previous constraints were solely based on the variation of [K] with respect to the design variables.

Representations for the design variables, objective function, and constraint functions have been presented. These equations can now be used to calculate the minimum weight design for the vertical tail by reducing the sizes of each of the structural members to the minimum size which will not violate any of the active constraints.

3. *Vertical Tail Model.*

3.1 Introduction

The mathematical tools developed in chapter two are now used to create a working mathematical model which, theoretically, replicates the structural response of the vertical tail to aerodynamic loads. The mathematical model is created for analysis with a program called MSC/NASTRAN (Reference 25). To create the model, specific information about the design is necessary. This information is used to build finite element matrices such as the structural stiffness matrix (equation 2-22) and the pressure-downwash matrix (equation 2-16).

The mathematical model can be broken into three major components. A description of the three major components of the vertical tail model is given in the following sections. The next section (3.2) describes the structural model. The physical properties, geometry, and limitations of the model is presented. Section 3.3 explains how the optimization problem is setup. The next section, 3.4, describes the aerodynamic grid, which generates the aerodynamic loads that are used for the structural model.

The final section, 3.5, addresses the reasons for choosing MSC/NASTRAN as the analysis tool. The advantages, as well as the disadvantages, of using this package are featured in this section. Comments on the performance of NASTRAN in calculating the thesis results are delayed until chapter five.

3.2 Vertical Tail Structure

The vertical tail is a highly-swept lifting surface. It is assumed that the root of the tail is cantilevered, or attached to a rigid surface. The tail span is 3 meters and the total surface area is 5.4 m^2. The chord length tapers from 2.4 meters at the root to 1.2 meters at the tip. The leading edge of the tail is swept 45 degrees. The tail is oriented in a vertical fashion with respect to the fuselage of the aircraft. Structural support for the tail surface is provided from a tail box. The tail box has a typical 3 spar configuration.

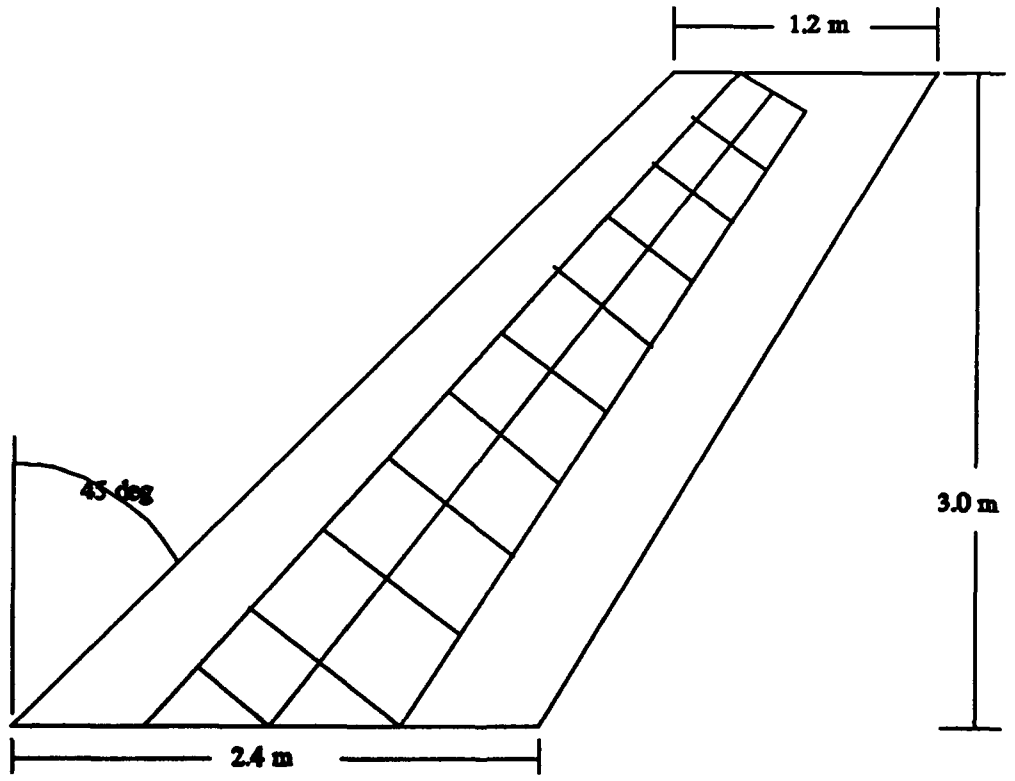

Figure 3-1: Vertical Tail Dimensions.

The tail box is a 3 spar, 10 rib design. The box is thickest at the root of the middle spar (16 cm). The forward and aft spar are 12 cm thick at the root. The thickness of the wing box tapers to 8 cm at the tip of the tail box. This can be seen in figure 3-2. The 10 rib sections interconnect the three spar sections and are evenly spaced along the span of the tail box.

The tail box is assumed to be made of Aluminum 2017. The material properties are given in table 3-1.

Table 3-1: Material Properties of Aluminum 2017 (T-4).

Properties	Values
Modulus of Elasticity	$72.4(10^9)$ N / m^2
Poisson's Ratio	0.33
Yield Stress	$2.76(10^8)$ N / m^2
Specific Gravity	$2.8(10^3)$ kg / m^3

To simplify the structural analysis only the tail box is modeled. The elastic behavior of the leading and trailing edges of the tail are not modeled. This is a reasonable simplification since a majority of the leading and trailing sections of the tail are directly attached to the tail box and will deform only slightly with respect to the tail box. The aerodynamic model does model the entire tail surface, however, and the loads applied to the leading and trailing edge sections are transferred to the tail box as a force-moment couple. Reducing the structural model to just the tail box greatly simplifies the model and allows the designer to focus on the structural members which redistribute the majority of the applied forces.

By making this assumption, however, the effect of the aerodynamic forces which act over the entire surface of the tail must somehow be transferred to the tail box. This technique, referred to as splining, was discussed in section 2.3. This technique transfers the loads so that the moment and forces produced by the applied forces on the tail box are identical to the forces and moments produced by the entire surface of the tail. (See Figure 3-2)

The tail box structural members are divided into six groups. The groups are the

(1) Rib Bars
(2) Spar Bars
(3) Post Bars

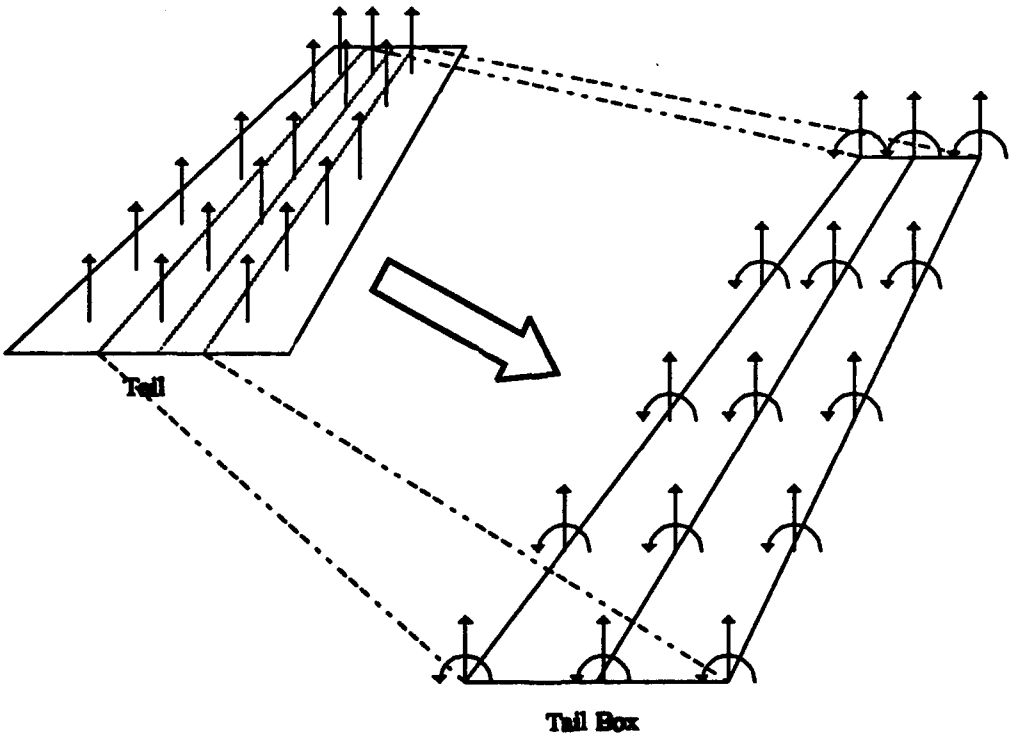

Figure 3-2 : Equivalent transfer of loads from tail surface to tail box.

(4) Skin Panels
(5) Spar Panels
(6) Rib Panels

Groups 1 - 3 are modeled with bar elements whereas groups 4 - 6 are modeled with panel elements. Skin panels are located on the top and bottom surface of the tail box and provide stiffness against vertical motion along with the spar panels. Skin panels provide tensile and compressive stiffness whereas the spar panels provide stiffness with their shear strength properties. Resistance to torsional forces in the tail box is provided primarily from the shear properties of the rib panels which are positioned perpendicular to the mid-spar. Bars are located along the edge of each of the panels to represent the bar covers which are used along each panel connection.

The bar elements provide stiffness in the axial direction of the bar. No stiffness is provided in any direction other than the axis of the bar. Therefore, forces in directions other than the axis of the bar must be resisted by adjacent elements. The displacement along the span of the bar element is assumed to vary linearly. Therefore, from equation (2-24) and (2-25) the stress is constant through each bar element. The panels are modeled with elements which replicate plane-stress behavior. These are referred to as panel elements. These elements provide stiffness in the plane of the element against tensile, compressive, and shear forces. The displacement function of each panel element is assumed to be quadratic. Therefore, the stresses vary linearly throughout the element.

The elements are connected at points referred to as nodal points. All displacements are calculated at these nodal points. The bar element requires two nodal points per element. Two types of panel elements are used. A common type is the

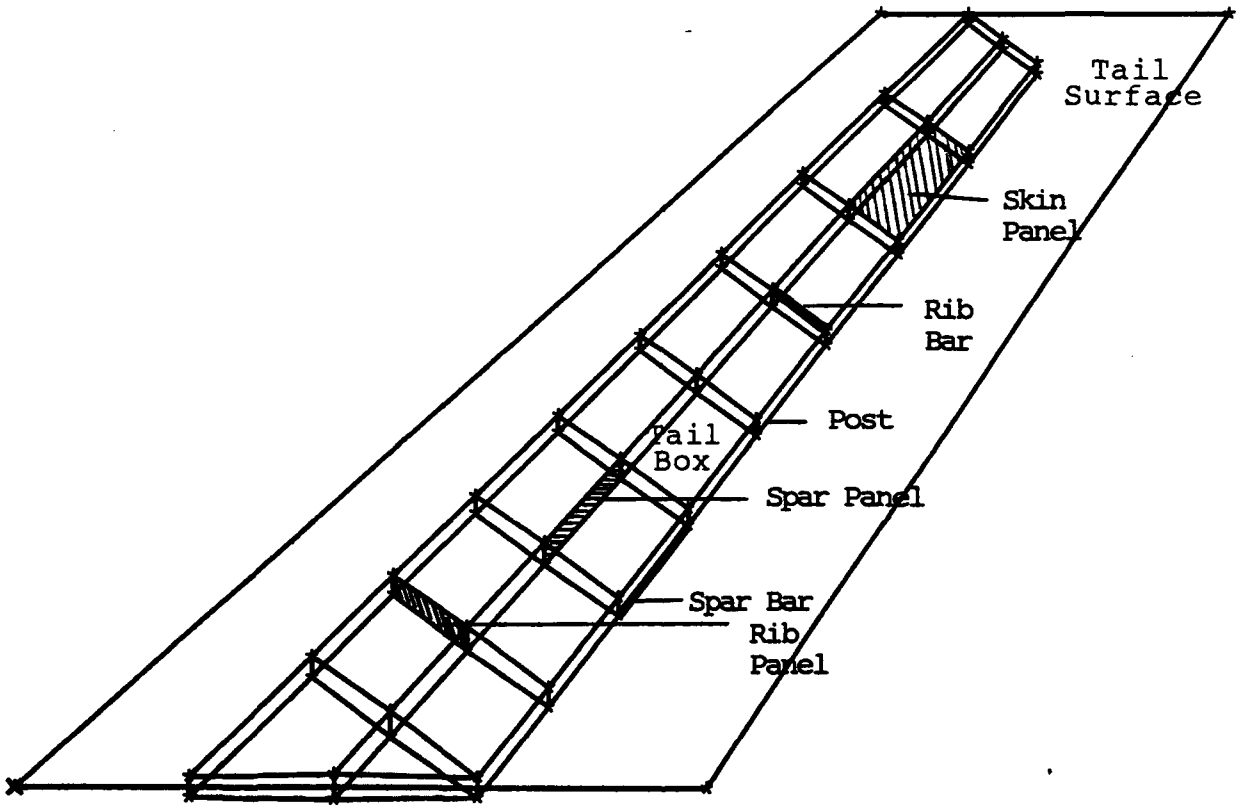

* = Node Point

Figure 3-3 : Description of location of each of the six groups of elements.

quadrilateral panel element. This element requires four nodal points. Only two elements use the second type of element which requires only three nodal points. This is referred to as a triangular panel element. There are 58 nodal points in the tail box design. The tail box is composed of 80 panel elements and 114 bar elements. (See figure 3-4)

The stiffness matrix (equation 2-22) for this problem can be calculated with the information known about the geometry of the tail box, and the properties of the bar and panel element. The mass matrix is formed by assuming the mass is evenly distributed throughout the element. This implies that the mass is evenly distributed among the nodal

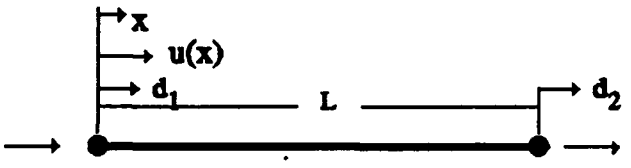

Bar Element

The unknown constants, c_p are determined from the displacements at u_j and v_j.

$$u(x) = c_1 + c_2 x$$

$$u(x,y) = c_1 + c_2 x + c_3 y + c_4 xy$$

$$v(x,y) = c_5 + c_6 x + c_7 y + c_8 xy$$

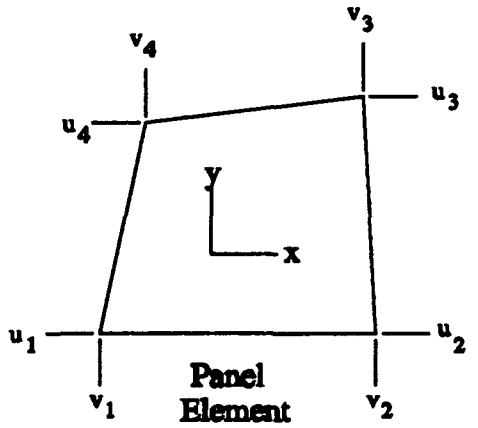

Panel Element

Figure 3-4 : Element Types used in design model.

points of each element. Since the dynamic response of the tail box is sensitive to the mass distribution, additional mass was added to various nodal points to represent the mass of the leading and trailing edges of the tail, and any other non-structural mass (electrical equipment, paint, etc.) that should be included to accurately model the dynamic behavior of the structure. The total mass added was 34 kg.

If the applied loads are given, then enough information is now available to solve the displacement-force equilibrium equation for the unknown displacements; from which the stress, strains, etc. can be obtained.

3.3 Optimization Model

Some additional information is required to define how the optimization process will progress. First, the optimization problem uses all the information from the structural model. In addition, the design variables, objective function, and constraint functions have to be defined. The objective and constraint equations must be declared, but they do not directly affect the model so further discussion is postponed until the next chapter. Note, however, that the objective of the design is to minimize the weight and the only constraints considered are structural constraints.

The cross-sectional area of the bar elements and the thickness of the panel elements are defined as the design variables. This implies that there are 194 design variables in the model. (Total number of panel and bar elements) The complexity and size of the problem increases rapidly as the number of design variables are increased. So,

to reduce the problem size, design variable groups are defined where the design variables in each group are forced to be equal in value (linked together). Three schemes for design variable linking are used. The first scheme reduces the problem to two design variables. All of the bar elements are linked together as one design variable and all of the panel elements are linked together as one design variable. The second scheme includes the variation of stiffness requirements between the six components of the tail box defined earlier by linking all of the posts together as one design variable, all of the spars as one design variable, etc. In all, there are 6 design variables. The last scheme subdivides each of the six components by location on the tail. The design variables are given as follows:

1. Post - Inboard (Bar Elements),
2. Post - MidSpan (" "),
3. Post - MidSpan (" "),
4. Post - Outboard (" "),
5. Spar - Inboard (" "),
6. Spar - MidSpan (" "),
7. Spar - MidSpan (" "),
8. Spar - Outboard (" "),
9. Ribs - Inboard (" "),
10. Ribs - MidSpan (" "),
11. Ribs - Outboard (" "),
12. Skin Panels-Inboard (Panel Elements),
13. Skin Panels-MidSpan (" "),
14. Skin Shear Panels-Outboard (" "),
15. Spar Shear Panels-Inboard (" "),
16. Spar Shear Panels-MidSpan (" "),
17. Spar Shear Panels-Outboard (" "),
18. Rib Shear Panels-Inboard (" "),
19. Rib Shear Panels-MidSpan (" "),
20. Rib Shear Panels-Outboard (" "),
21. Rib Shear Panels-Outboard (" "),

The location of the linked design variables is given in figures (3-5 through 3-10).

Now that the design variables are defined, the optimization code can use these

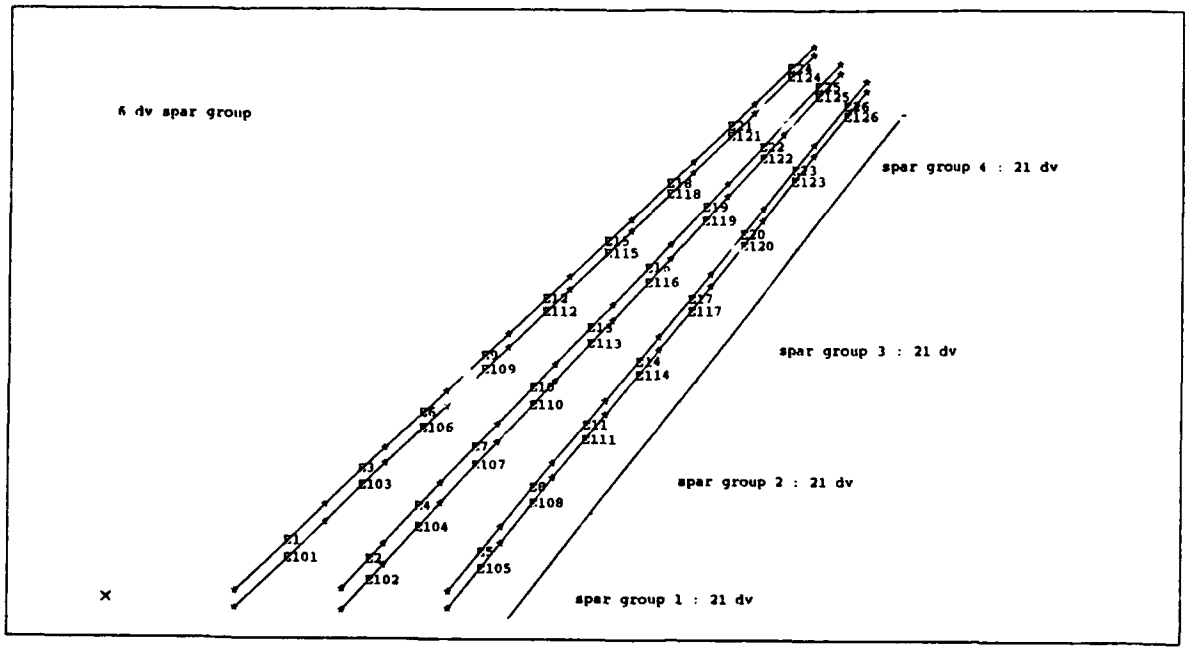

Figure 3-5 : Illustration of the six and twenty one design variable linking scheme for the spar (bar) elements.

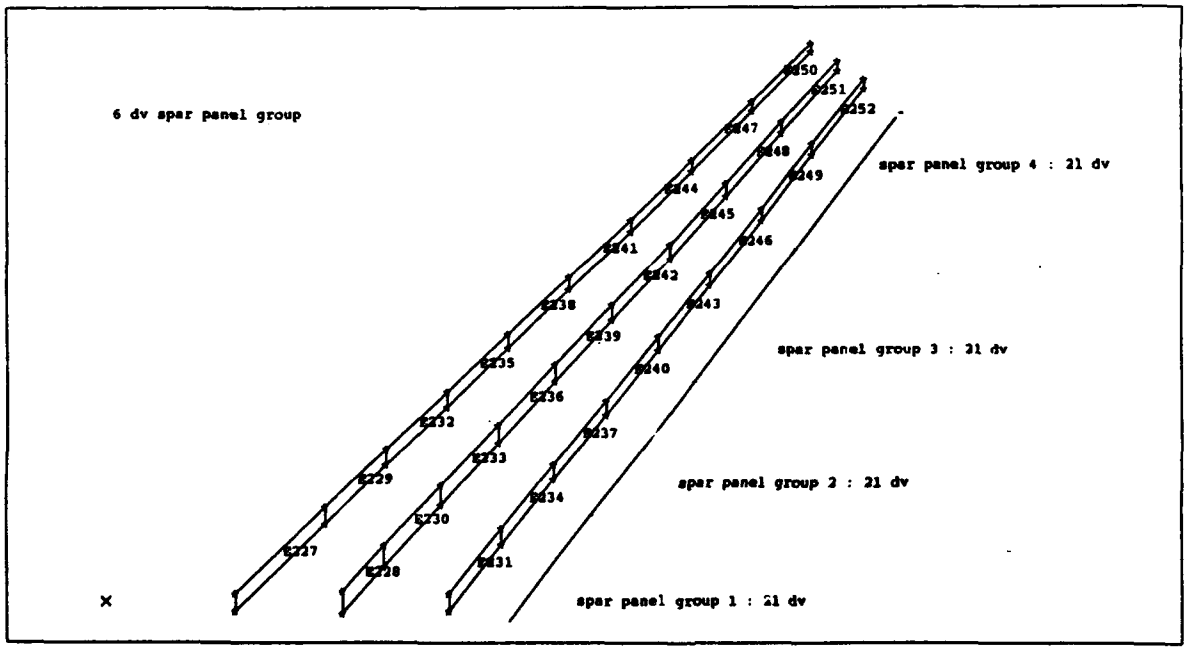

Figure 3-6 : Illustration of the six and twenty one design variable linking scheme for the spar panel elements.

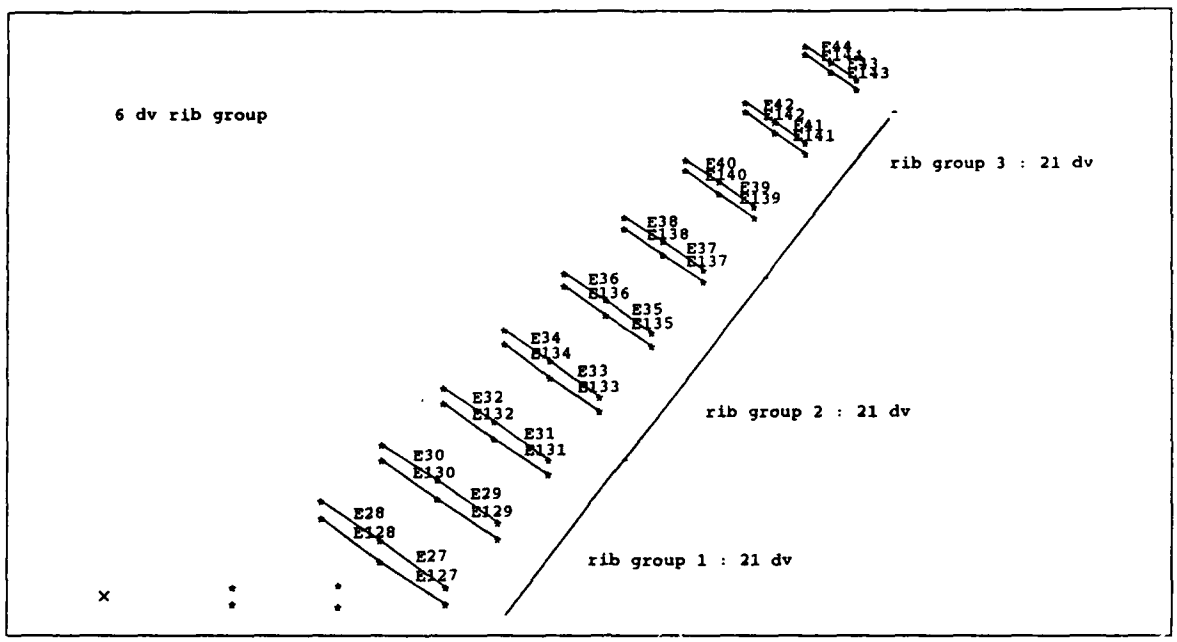

Figure 3-7 : Illustration of the six and twenty one design variable linking scheme for the rib (bar) elements.

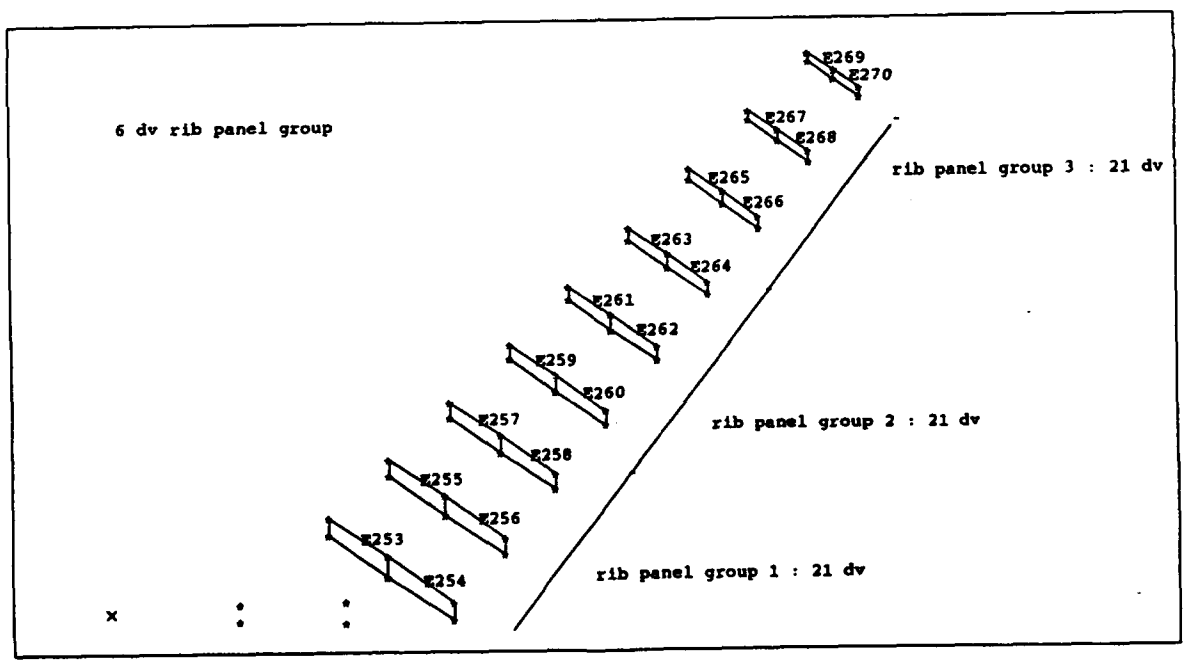

Figure 3-8 : Illustration of the six and twenty one design variable linking scheme for the rib panel elements.

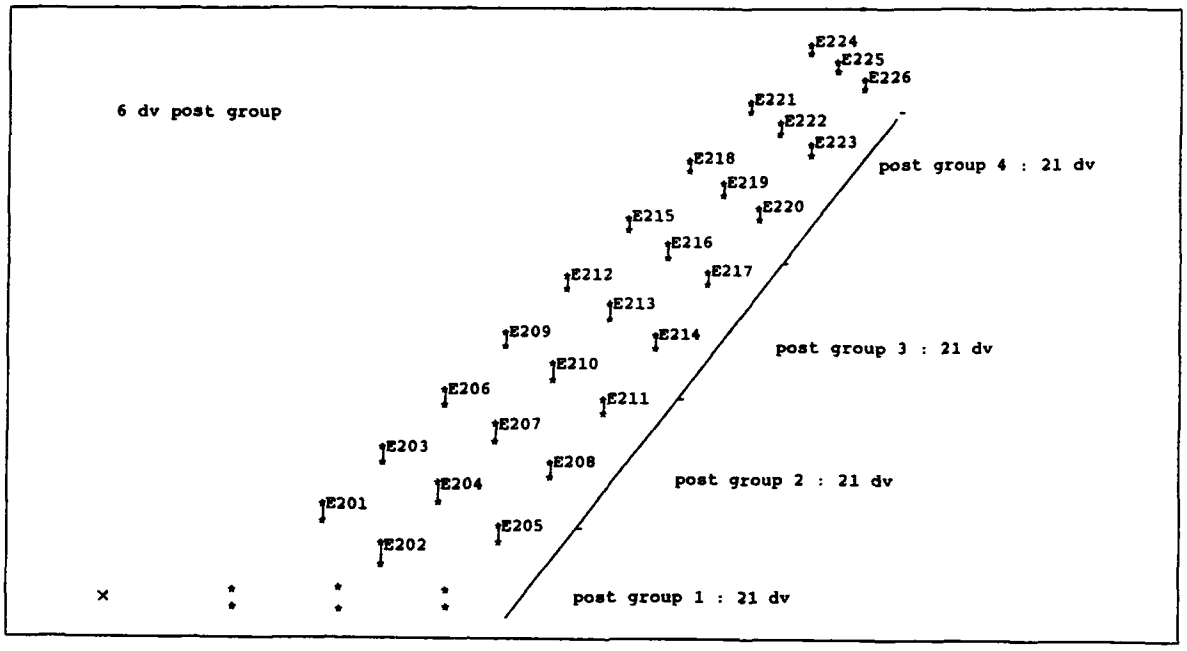

Figure 3-9 : Illustration of the six and twenty one design variable linking scheme for the post (bar) elements.

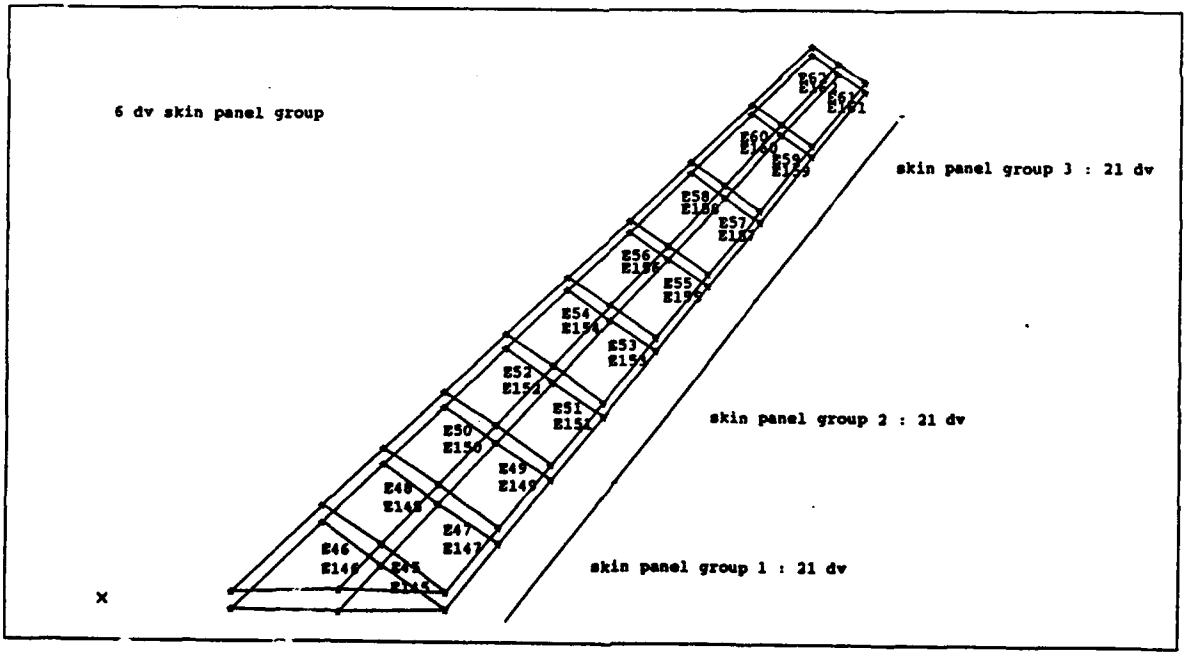

Figure 3-10 : Illustration of the six and twenty one design variable linking scheme for the skin panel elements.

variables in the objective function and enforce the constraint equations on the design. The last item that needs to be addressed is the applied forces. The optimization code can only use forces which are independent of displacement. This becomes a problem with aerodynamic loads which are dependent on structural displacement. To alleviate this coupling, the loads used with the optimization sequence were the rigid tail loads. Rigid tail loads are the aerodynamic loads that would be produced if the wing were infinitely stiff and did not deform. By not including the aeroelastic influence on the structural loading the accuracy of the optimization is decreased. The significance of the flexible aerodynamic loads on a optimal design based on rigid tail aerodynamics is addressed in chapter 4.

The iterative optimization algorithm assumes that an optimal solution has been attained when the objective function changes less than 0.1 percent between three iterations. The constraints are allowed to be violated by 0.5 percent, and the maximum number of allowed iterations before the program was terminated was set at 20. (The number of iterations never reached 20 during the analysis, however)

3.4 Aerodynamic Model

The tail is assumed to have a symmetrical surface with no camber or twist. This allows the tail to be treated as a flat plate. The surface is positioned at the mid-plane between the top and bottom surface of the tail box. To configure the tail in a manner which can use the doublet-lattice method of section 2.2, the tail is subdivided into a finite

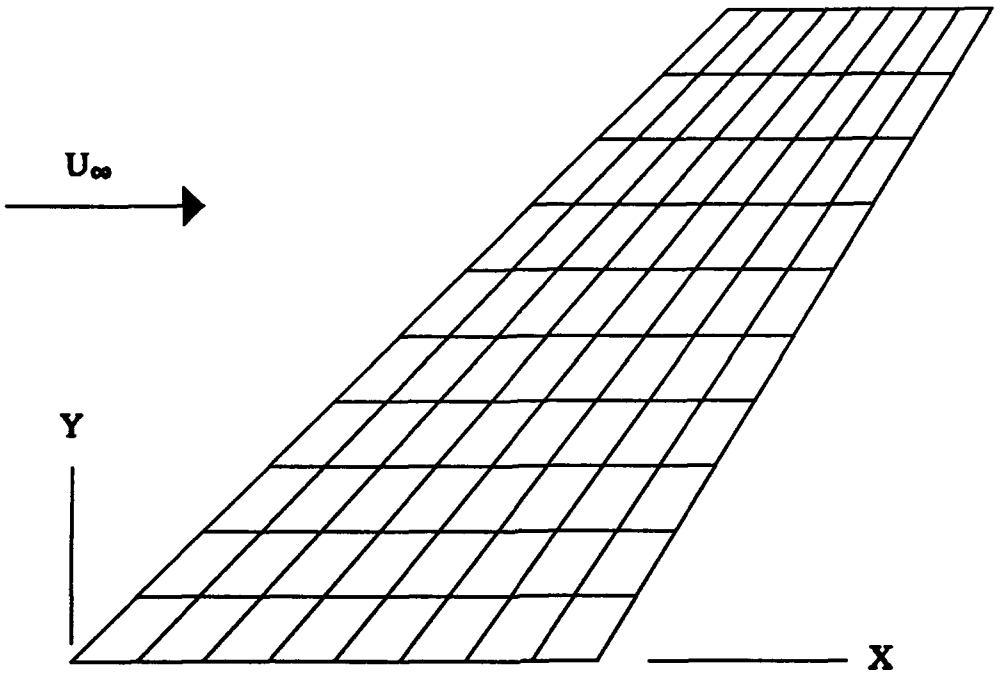

Figure 3-11 : Aerodynamic Panel Mesh.

number of panels. Reference 18 recommended at least six chordwise panels and that each of the panels maintains an aspect ratio near 1.0. This recommendation was taken at first, but it was found that by increasing the number of chordwise panels to seven, and adding the appropriate number of panels in the span wise direction to keep the aspect ratio near 1.0, that the lift values varied significantly. The large variation in lift tapered off to negligible differences for the case of eight and then nine chordwise panels, so the configuration of eight chordwise panels was chosen. To keep the aspect ratio near one, ten spanwise panels were required. This brought the total number of panels to eighty. The resulting mesh of aerodynamic panels is shown in figure 3-11. Each of the panels

has a doublet line at the quarter chord line and a control point at the mid-span of the three-quarter chord line, resulting in 80 control points from which to solve the downwash-pressure equation (equation (2-17).

Each of these panels is treated as a rigid flat plate with freedom to displace vertically and rotate about the control point. If an initial angle of attack is given, then the entire surface is rotated about a given point at the root of the tail and the initial downwash for each panel would be the slope of the individual panel with respect to the x-coordinate direction (see equation 2-4). As the tail box deforms under the applied loads, these structural deformations are then converted to appropriate aerodynamic deformations at the aerodynamic control points through the splining matrix, and appropriate changes are made to the relative vertical displacement and rotation of each panel.

3.5 Comments on MSC/NASTRAN

The theory discussed in chapter 3 is incorporated into a program marketed by the MacNeal-Schwendler Corporation (Reference 18). This program is called MSC/NASTRAN (Version 66-A). The program was used to produce the results given in this thesis. This program was chosen because of it's structural analysis, aeroelastic analysis, and optimal design capabilities. To accomplish each of these tasks, at least one of three major data decks had to be used. The first deck contains all of the structural information. For example, structural grid point information, element description, element connectivity, material type, etc. The second deck contained all of the structural

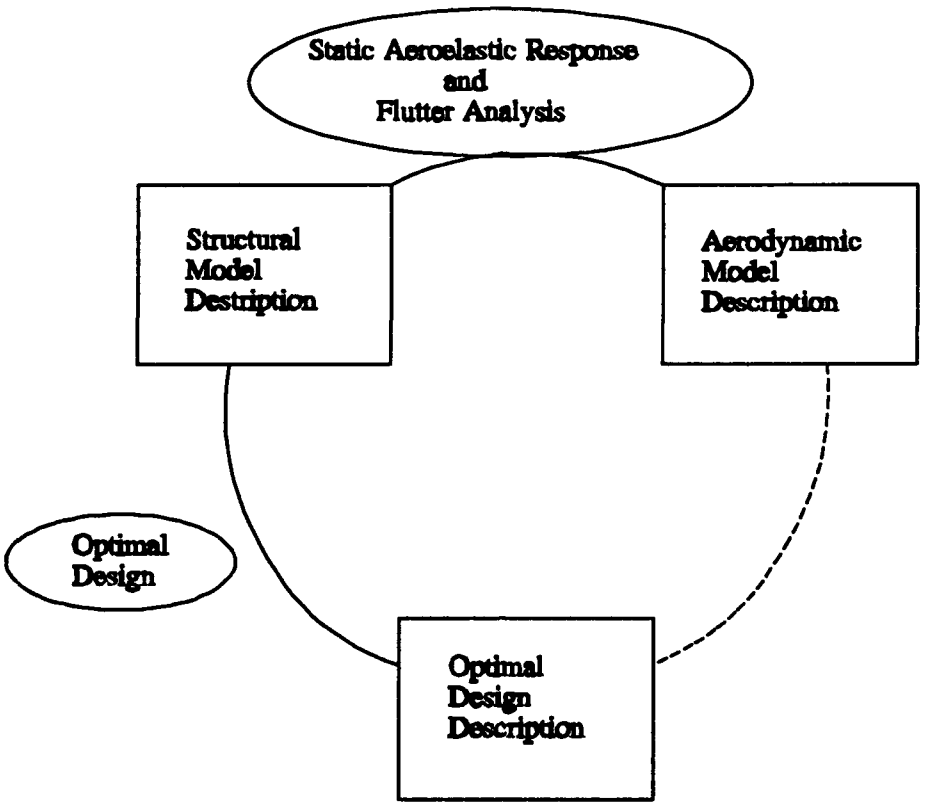

Figure 3-12 : The Three NASTRAN Modules utilized for the analysis of the vertical tail.

information and additionally aerodynamic information such as flight conditions, aerodynamic mesh description, planes of symmetry, etc. The last deck described the optimization design model. Therefore, the objective function, constraints, and design variables had to be defined. The optimization is based on the structural model so the structural information had to be included in the model. The modular structure of NASTRAN made the individual analysis simpler, which allowed the author to track the flow of information more effectively. Examples for each of the data decks is provided in appendix B, C, and D.

The loads used in the aeroelastic analysis are based on doublet-lattice

aerodynamics (1:279). Therefore, the flutter analysis uses a paneling method based on unsteady, potential aerodynamic flow. The loads calculated reflect the change in aerodynamic properties due to the flexible nature of the structure. This applies to both the static and dynamic response.

The downside of NASTRAN was that their is no "bridge" between optimal design and aerodynamic analysis. For example, the optimal design is based on the aerodynamic loads of a rigid tail. These loads are extracted from the output of the static aeroelastic analysis by segregating the loads due to flexibility from the loads due to initial conditions.and then inserted into the optimization analysis. This deficiency stems from the inability of the NASTRAN code to update the change in the aeroelastic loads ' structural deformations during the optimization procedure. Another restriction oı NASTRAN is that the constraint functions are restricted to structural properties. Thei no opportunity to constrain the values of the stability derivatives, local angle of attack, etc.

A program without these deficiencies would enhance the accuracy of the analysis, but unfortunately a program with these capabilities was not available to analyze a cantilevered lifting surface.

4. *Results*

4.1 Introduction

This chapter presents the results from the analysis of the vertical tail. The analysis focussed on the influence that design parameters have on the optimal size and weight of the tail box. These parameters include the choices of design variable linking scheme, critical design load, and design constraints. The influence of each factor is presented in the first three sections.

The aeroelastic properties of each of the designs are then evaluated. Comparisons of the aerodynamic properties of each of the designs are discussed. Section 4.5 focuses on the results of the static aeroelastic analysis while section 4.6 presents the flutter analysis results. A discussion and comparison of the optimization and aerodynamic results will follow in chapter five.

4.2 Effect of Design Variable Linking on Objective Function

Three design linking schemes are considered to illustrate the influence of design variable linking on the results of an optimization analysis. Design variable linking is valuable because of the savings in computer time. The three linking schemes described in section 3.3 are used. Recall the first scheme subdivided the model into 2 groups, the bar elements make up one design variable group and the panel elements made up the other group. The second

scheme further subdivided the bar elements and panel elements into 3 design variable groups respectively. (six groups total) The final scheme was yet a further subdivision of the second scheme, and is composed of 21 design variable groups. These groups will be periodically referred to as design variables themselves. (See Figures 3.3 - 3.8)

Each linking scheme is compared by observing the resulting objective weight, design variable size, and element stress values. Only one loading condition is considered for each case and the only constraint enforced on the design is maximum stress allowed. The tail load is calculated at Mach number 0.4 (sea level) and 30 degrees angle of attack (steady level flight).

The optimal weight for each case was obtained from the optimization output. The heaviest design was the two design variable case which had an optimal weight of 73.5 kg. By increasing the number of design variables to six, the weight of the design dropped considerably to 44.3 kg. The 21 design variable case subdivided each of the six design variables into three or four subgroups. By using the 21 design variable scheme, the optimal weight calculated dropped even further to 38.2 kg.

To illustrate where the structural mass is being used to create a feasible design, the values for each of the design variables (member sizes) are compared graphically. Since the 6 and 21 design variable case are subdivisions of the 2 design variable case, comparisons of member sizes are easily shown. These comparisons are shown in figures 4-1 through 4-6.

The stress values along three selected tail box regions are also graphically depicted to illustrate the dependence of element stress values on the design variable scheme chosen. Three groups of elements were chosen. The first group of elements is the middle spar

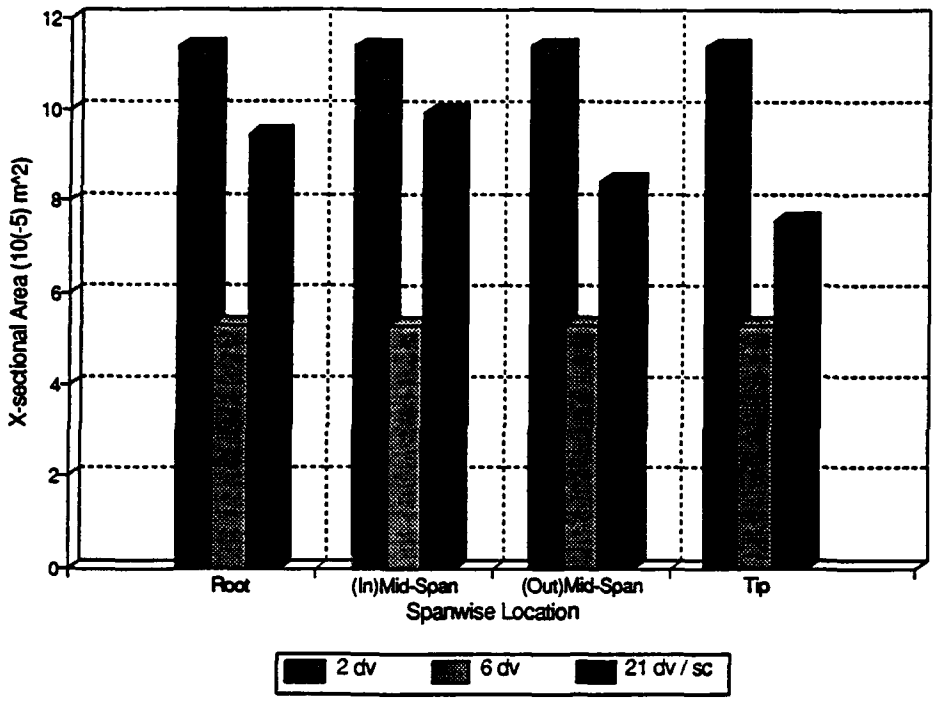

Figure 4-1 : Optimal design variable size - cross-sectional area of spar elements.

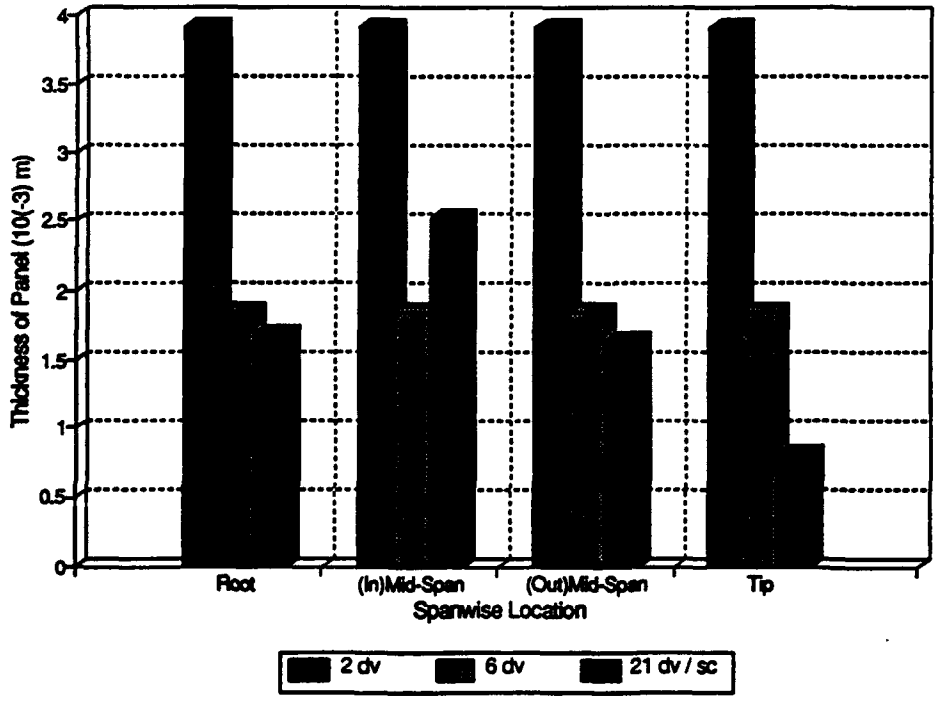

Figure 4-2 : Optimal design variable size - thickness of spar panel elements.

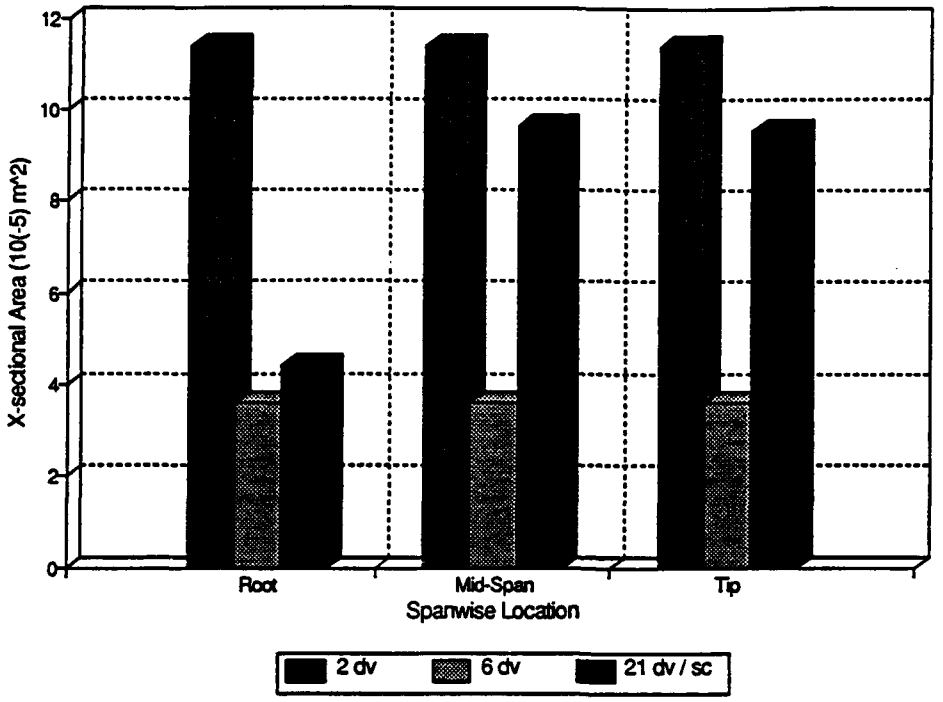

Figure 4-3 : Optimal design variable size - cross-sectional area of rib elements.

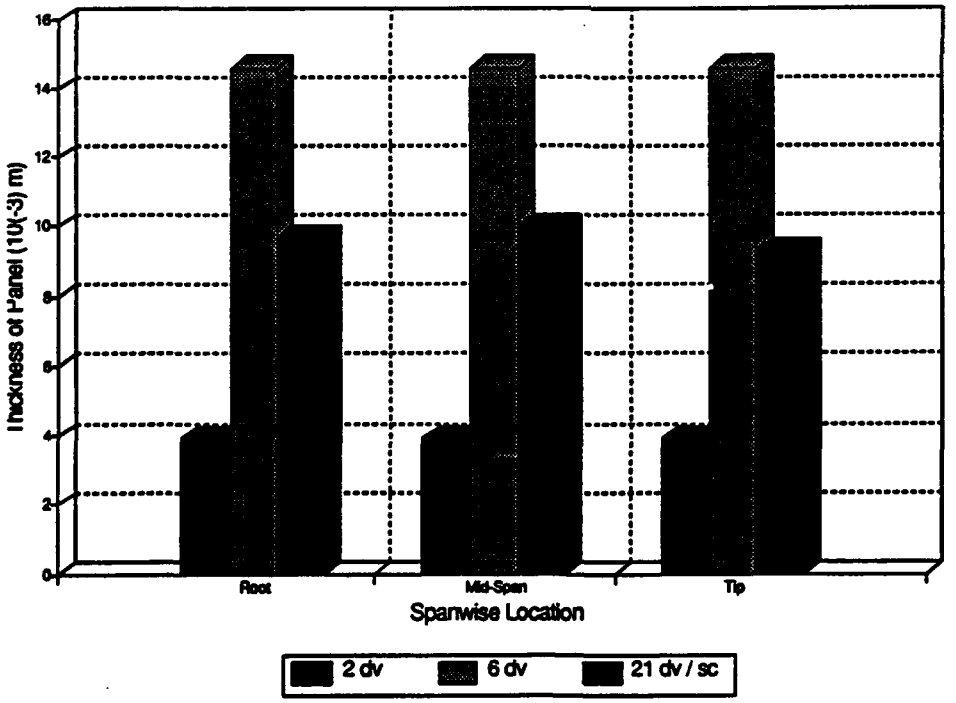

Figure 4-4 : Optimal design variable size - thickness of rib panel elements.

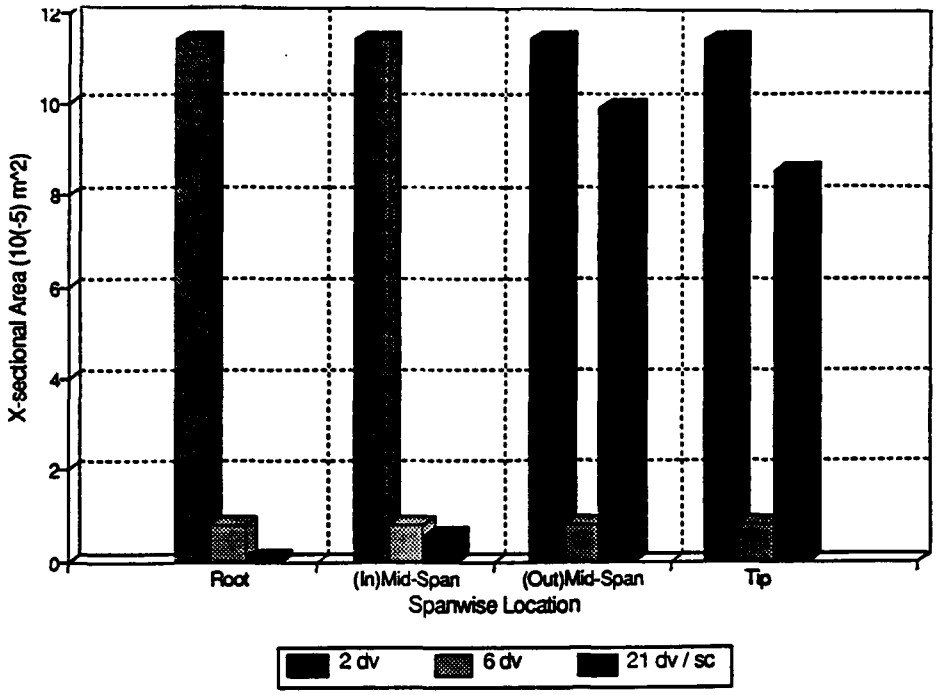

Figure 4-5 : Optimal design variable size - cross-sectional area of post elements.

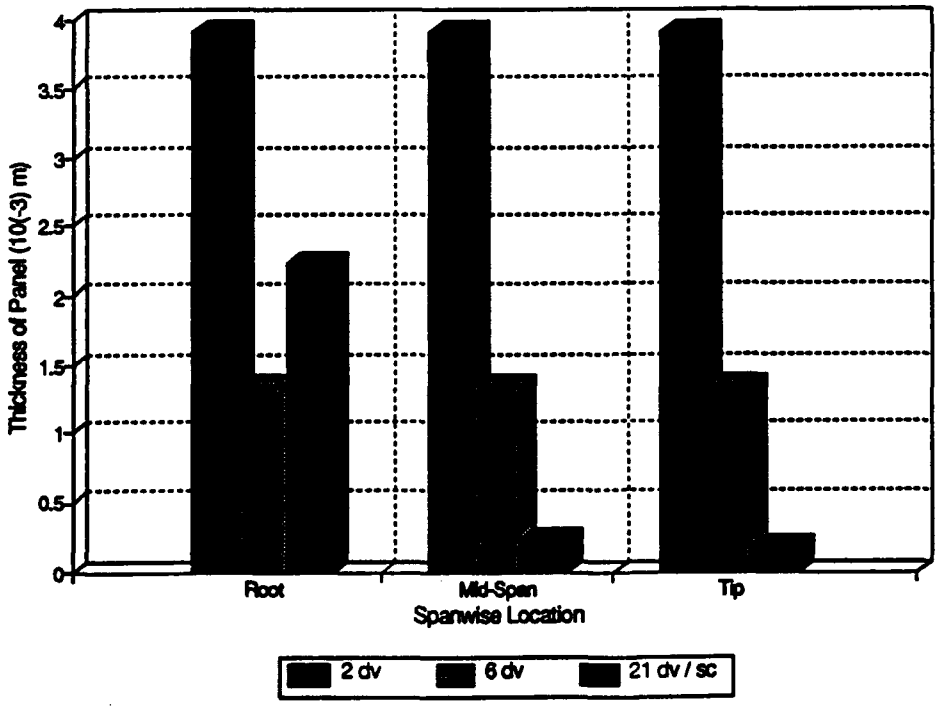

Figure 4-6 : Optimal design variable size - thickness of skin panel elements.

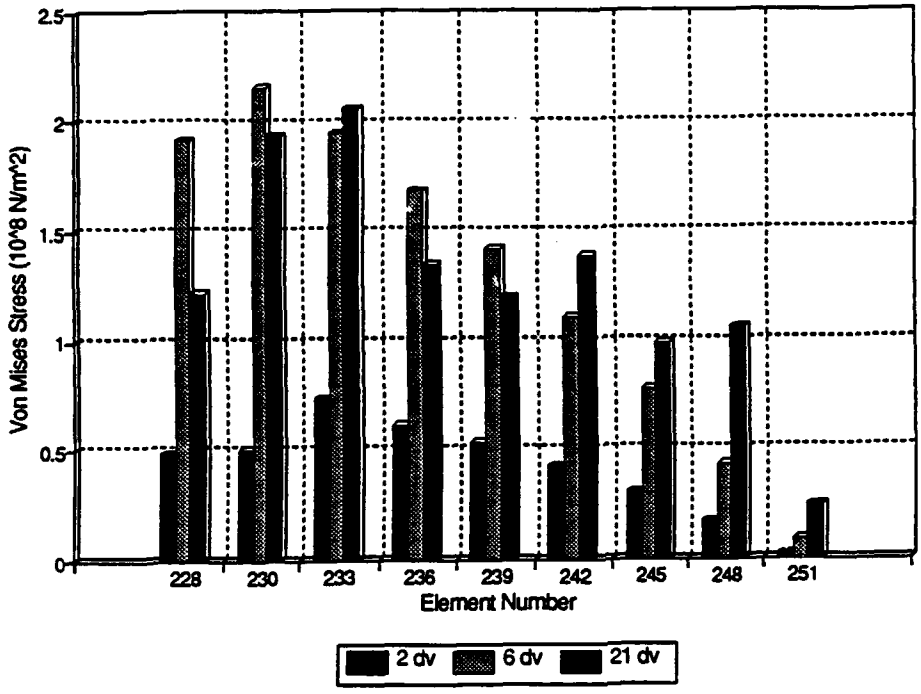

Figure 4-7 : Von Mises stress values - mid spar panel elements.

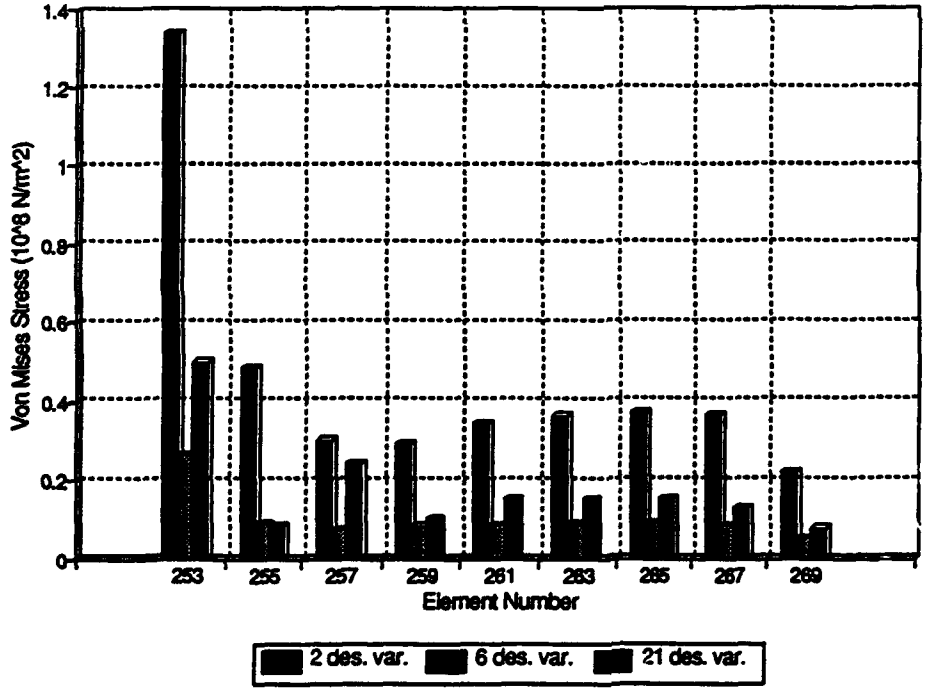

Figure 4-8 : Von Mises stress values - forward rib panel elements.

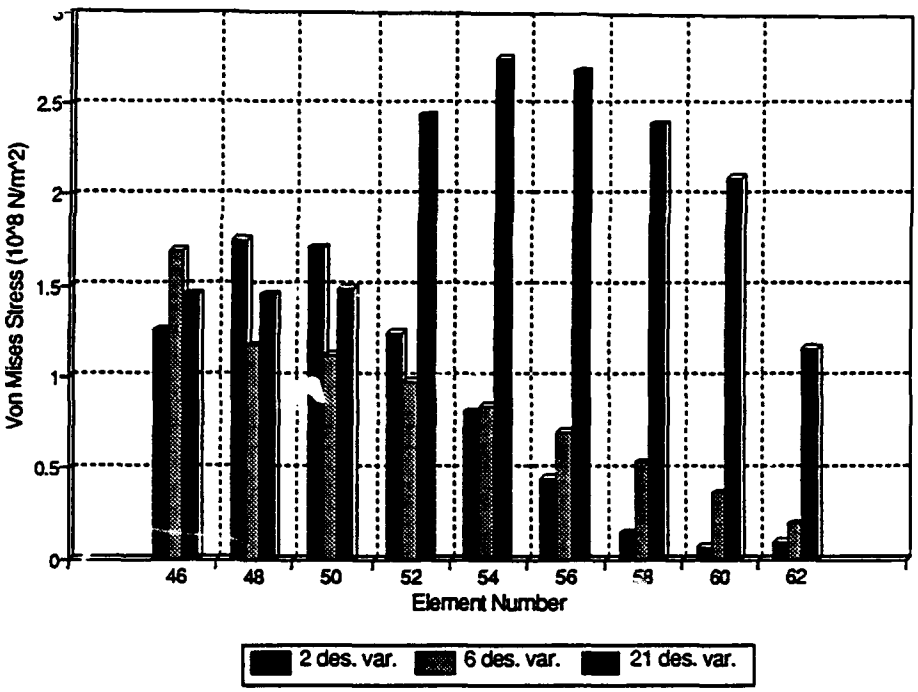

Figure 4-9 : Von Mises stress values - forward skin panel elements.

section. The Von Mises stress for the string of spar panel elements from the root chord to the tip chord (left to right) are depicted in Figure 4-7. Note that the stress values given are the stresses at the geometric centroid of the element. The second group is the forward section of rib panel elements. The elements are located along the span of the tail box from root to tip also (Figure 4-8). The last group is the forward section of the skin panels, these elements also are presented in Figure 4-9 ordered from root to tip section of the tail box.

4.3 Effect of Design Load Condition on Minimum Weight

A relationship between the design load and the required structural weight to sustain the load could be valuable in determining the weight penalty for an increased tail design load.

This relationship is examined by optimizing the tail for a variety of possible design load conditions.

Again, the tail loads are based on rigid tail aerodynamics and the optimization is based on the linking scheme of six design variables. The six design variable case is chosen since it represents a considerable improvement of the objective function value over the two design variable case yet does not require near the computer time that the 21 design variable case does. The structure is optimized for minimum weight and the design variables are constrained by maximum stress limits and minimum gauge limits. The minimum gauge limits are enforced to examine how the minimum sizes effect the optimal weight values.

The load cases were determined by providing the Mach number and angle of attack parameters. All cases assume the tail is at sea level in steady level flight. The cases vary from a Mach number of 0.2 to a Mach number of 0.8. The peak design angle of attack was 40 degrees for M = 0.2, but tapered to 6 degrees for M = 0.8. It is recognized that the results at high angles of attack are tainted since the aerodynamic assumption that the surface is at a small angle of attack is violated. This error is accepted and noted for this analysis. The design weight varied from 16.2 kg (all members minimum gauge) for the M=0.2 α = 10 deg, to 58.9 kg for the case of M=0.6, α=15 deg. The variation in weight is illustrated in figures 4-10 and 4-11. Figure 4-10 shows the linear variation of design weight with angle of attack for a given mach number. Figure 4-11 better depicts the linear relationship between tail aerodynamic load and design weight. The lines are not co-linear but definitely show a general linear relationship between design load and optimal design weight. The cause for the large deviation along the M=0.4 line cannot be explained.

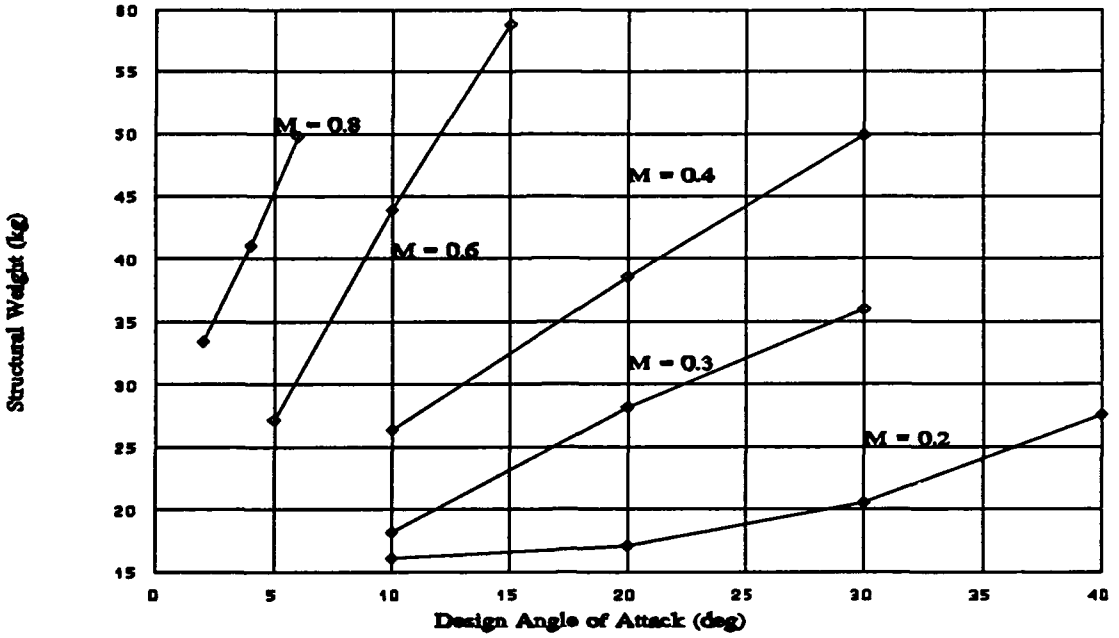

Figure 4-10 : Optimal structural weight versus design angle of attack for various flight conditions at sea level.

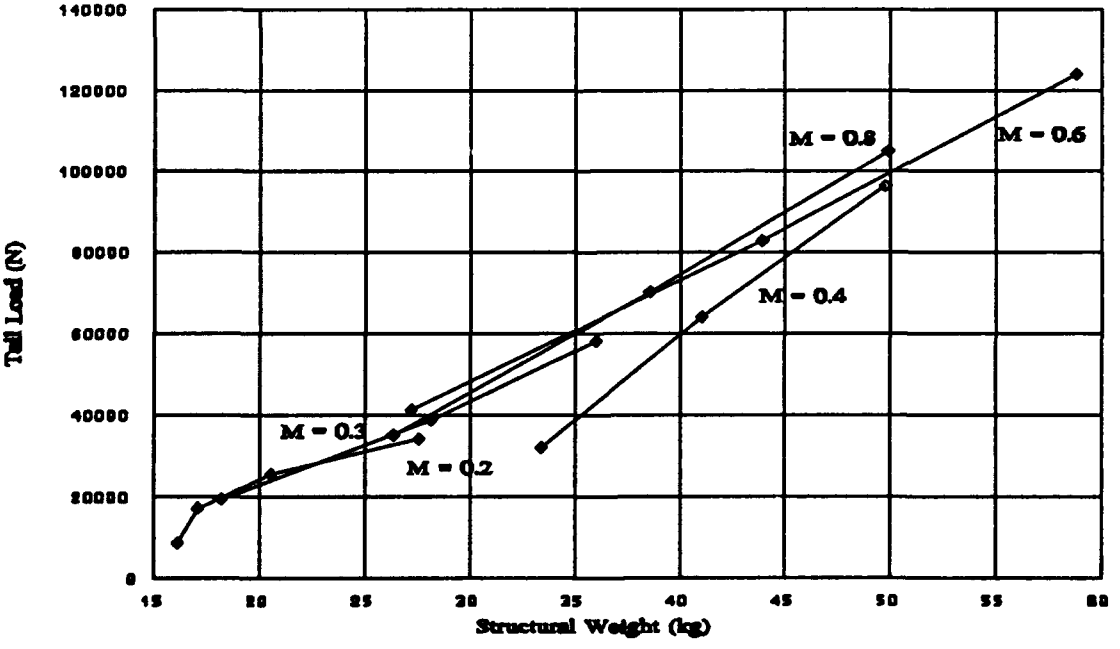

Figure 4-11 : Optimal weight of design compared to the applied aerodynamic load used for each of the optimization cases.

4.4 Effect of Constraints on Final Weight

To demonstrate the influence that design constraints have on an optimal design, the tail is optimized for three different cases. The first case constrained the values for the element sizes so that the maximum stress does not exceed the material yield stress. The second case adds an additional restriction that the member sizes can not decrease below a minimum value. The last case involves an attempt to drop the tip acceleration on the tail by constraining the tip deflection. Only one loading condition is used for each case; M = 0.4 at an angle of attack of 30 degrees (sea level, steady level flight, and rigid wing aerodynamics). In addition, to illuminate any spanwise differences between each of the designs, the linking scheme of 21 design variables is used.

The first case enforces internal stress limitations of the material. For the bar element, each bar cross-section is not allowed to exceed the yield stress of 2.76 (10^8) N/m^2. The panel element thickness values are not allowed to drop below a value which would cause the Von Mises' stress to exceed 2.76 (10^8) N/m^2. The stress constraint (sc) restricted the optimal weight from dropping below 38.2 kg. After completing the optimization, the stress values indeed remained below the maximum allowed. (See Figure 4-18)

The second constraint case enforced, in addition to maximum stress, a minimum gauge (mg) constraint to model a manufacturing limitation which might limit the size of the panel or bar from dropping below a given value. The minimum gauge (mg) values chosen for this analysis are 0.1 cm^2 (1. 10^{-5} m^2) cross-section for the bar elements and 1.0 mm (1. 10^{-3} m)

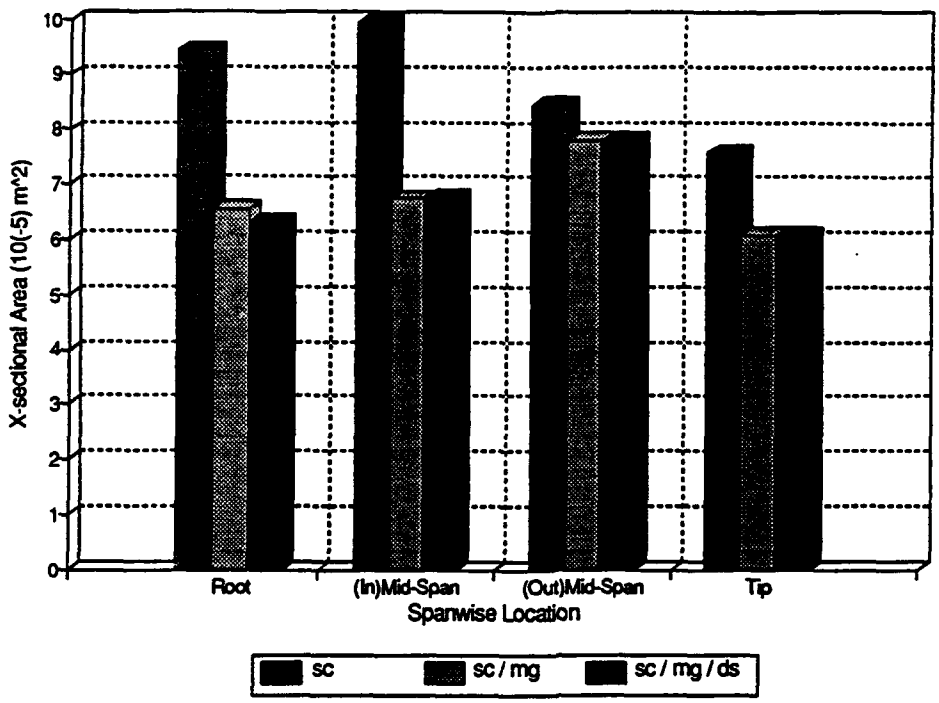

Figure 4-12 : Optimal design variable size - cross-sectional area of spar element.

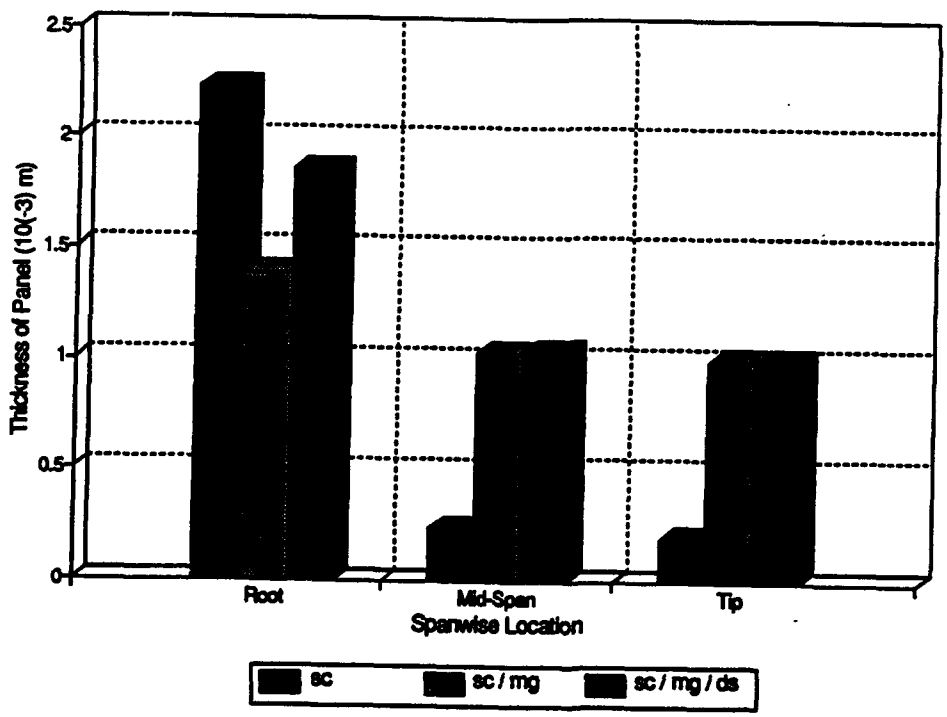

Figure 4-13 : Optimal design variable size - thickness of spar panel elements.

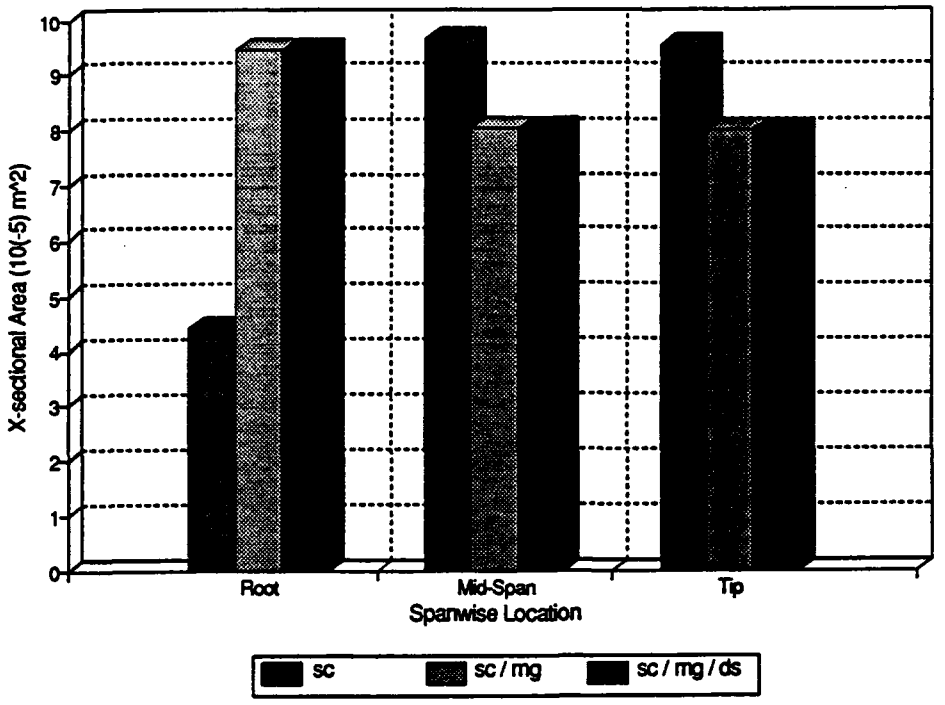

Figure 4-14 : Optimal design variable size - cross-sectional area of rib elements.

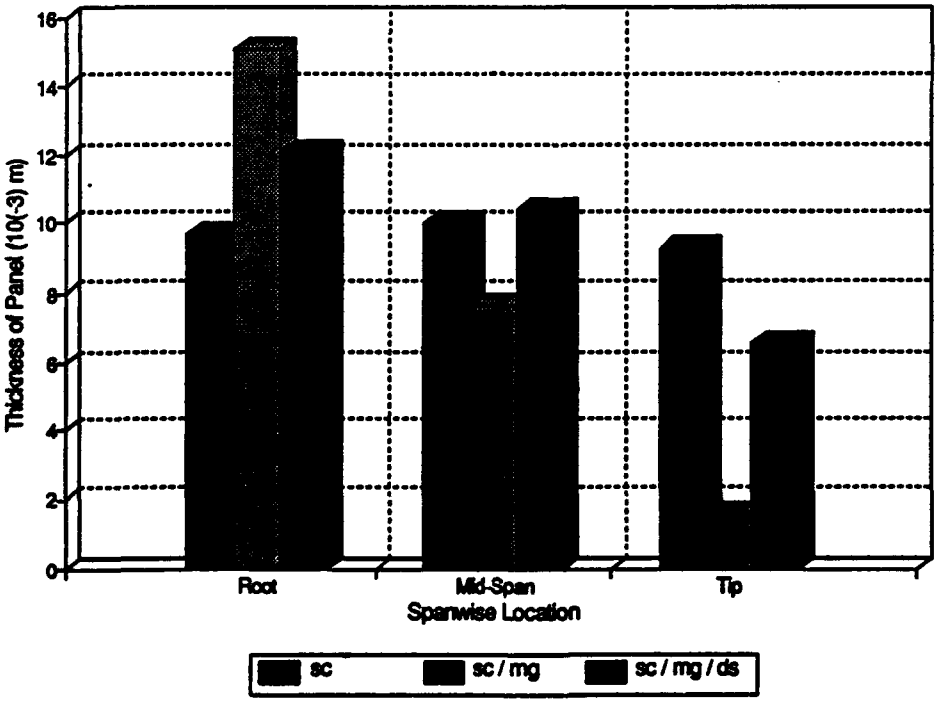

Figure 4-15 : Optimal design variable size - thickness of rib panel elements.

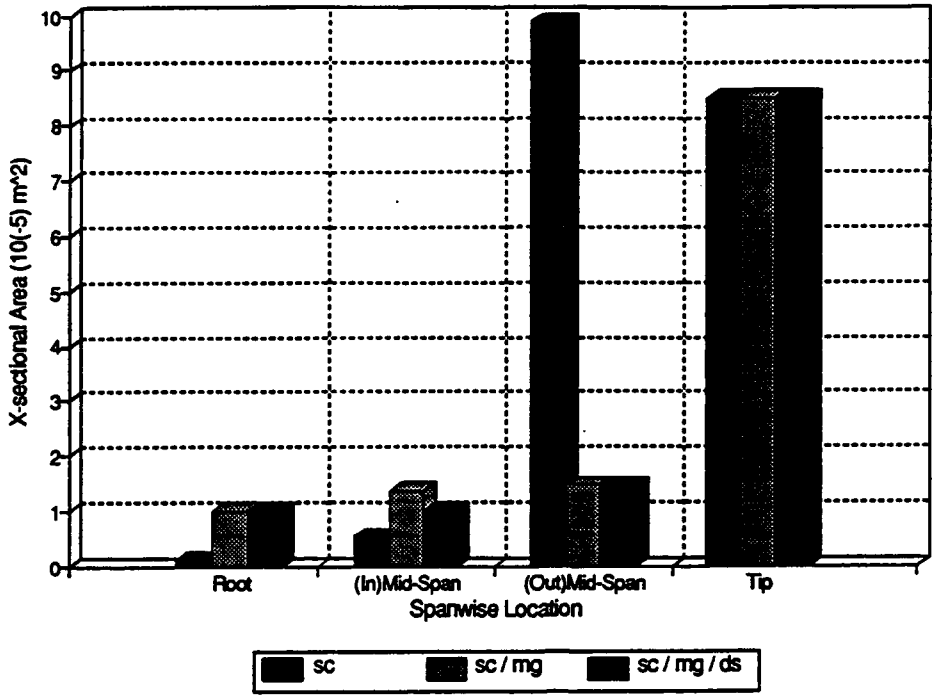

Figure 4-16 : Optimal design variable size - cross-sectional area of post elements.

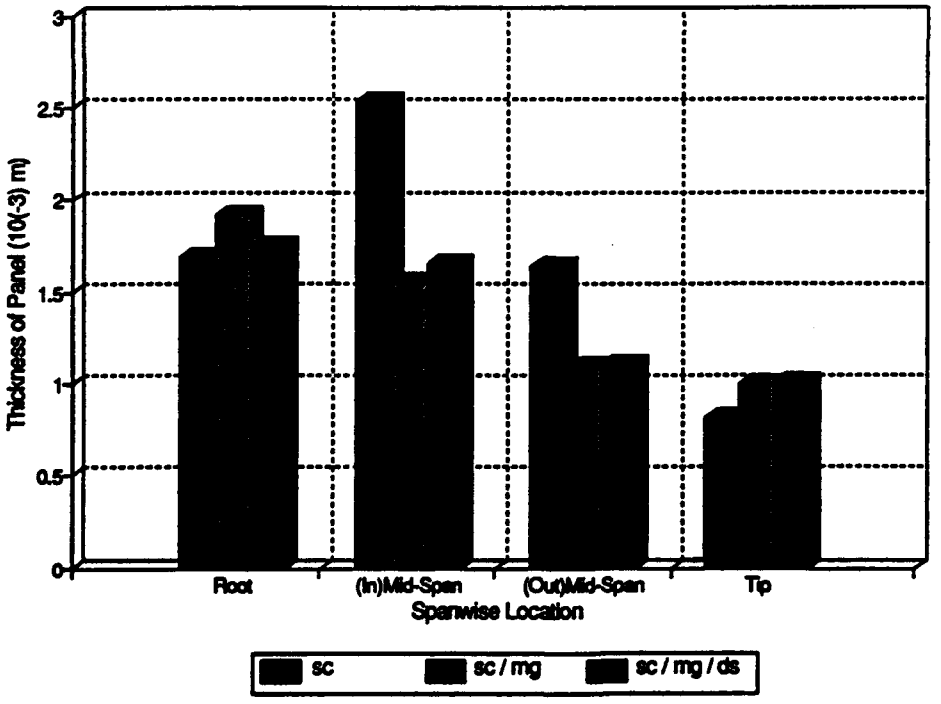

Figure 4-17 : Optimal design variable size - thickness of skin panel elements.

thickness for the panel elements. This constraint increased the size of the post elements (Figure 4-13) and skin panels (Figure 4-16). Because of the increase in size, the stress level in some of the elements which are near the minimum limit in the stress constrained case decreased, as is seen for the mid-spar elements of figure 4-18. The weight penalty for this constraint is minor, however, as the weight only increased to 38.4 kg.

The third constraint case additionally restricted the tail tip (nodal point 28) from deflecting more than 10 cm. For the minimum gauge case (case two), the deflection was 19.6 cm. Why would a reduction in tip displacement be necessary? Electronic equipment which is often placed at the tail tip is sensitive to accelerations. If a piece of equipment (navigational or electronic countermeasure for example) must not 'see' accelerations greater

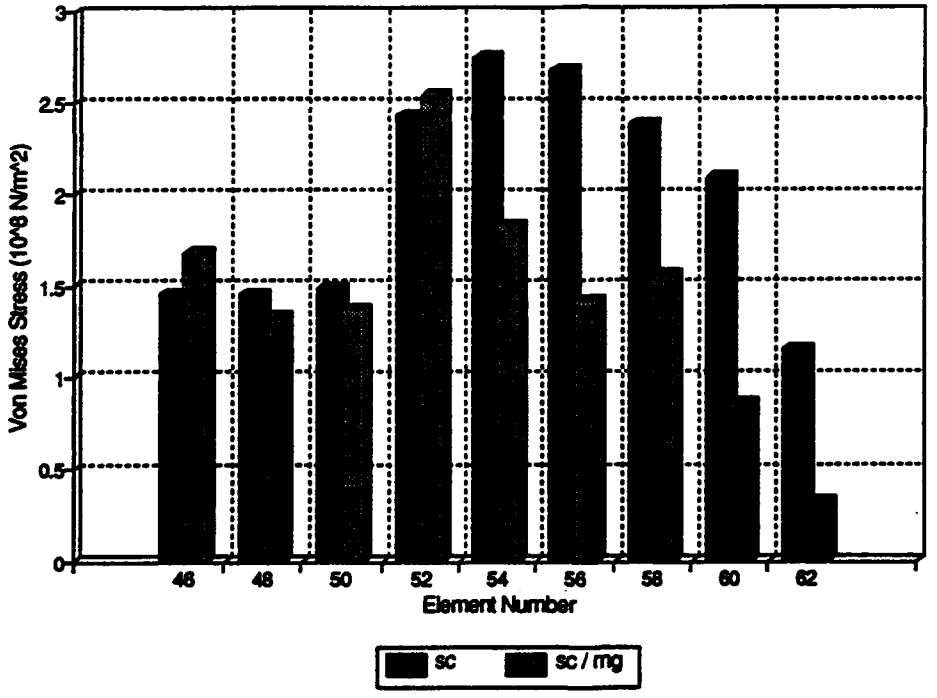

Figure 4-18 : Comparison of stress values in identical skin panel elements for stress constrained case (sc) and stress constrained/ minimum gauge (mg) case.

than a given value, then the structure must be redesigned to insure that the maximum allowed acceleration is not exceeded. The accelerations at the tail tip are assumed to be proportional to the displacement at the tip. (acceleration = (frequency)^2 x vertical displacement) This is true for harmonic motion. If the tail can be redesigned to reduce this deflection then the maximum acceleration should decrease linearly. This assumption turned out to be incorrect because as the wing is stiffened to reduce the tip deflection, the added stiffness also increases the first bending frequency. The displacement constraint dropped the deflection from 19.6 cm to 10.0 cm, however, this constraint increased the first frequency (a first bending mode) from 11.30 Hz (sc/mg) to 16.91 Hz. The result was a net gain in tip acceleration from 988.03 m/s^2 for the minimum gauge case to 1128.9 m/s^2 for the displacement constraint (dc) case. Therefore, this type of constraint was not successful in reducing the tip acceleration and, therefore, a relationship between the tip acceleration and the design variables will need to be developed to reduce the tip acceleration.

It is interesting to note where the optimization code increased the sizes of the members to reduce the tip deflection. The members which were affected most were the spar panels, rib panels, and skin panels. The displacement constraint (dc) also increased the optimal weight to 40.5 kg.

Now after examining the structural behavior of these different designs, the data which is most important to the performance of the aircraft is examined next. This data is the aeroelastic response, static and dynamic, of the tail to given aerodynamic loads.

4.5 The Static Aeroelastic Properties of Constrained Designs.

The aerodynamic properties of a lifting surface are closely related to the structural response to applied aerodynamic loads. To illustrate this, the structural displacements of each of the constrained designs of section 4.4 are related to three basic static stability derivatives C_{L_α}, C_{M_α}, C_{N_α}, where α is the angle of attack of the tail. The symbol C_{L_α} is the lift coefficient which relates angle of attack to the lift on the tail (Lift = q S C_{L_α} α). The symbols, C_{M_α} and C_{N_α}, relate the pitch moment about the ¼ chord line and roll moment about the tail root span to angle of attack (Pitch Moment = q S c C_{M_α} α and Roll Moment = q S b C_{N_α} α), where c is the root chord length and b is the full span of the tail. Recall that the structure was optimized with respect to the rigid tail loads. The true aerodynamic loads (tail flexibility accounted for) differ from the loads used to optimize the structural members. The difference in loads affect the displacement and member stresses of each design.

TABLE 4-1 : Aerodynamic Stability Derivatives.

Case				Load (N)
Rigid Tail	3.269	-1.002	0.7386	104892.1
Stress Constraint	3.498	-1.1168	0.7992	112229.5
Minimum Gauge	3.269	-1.005	0.7408	104874.1
Displacement Constraint	3.370	-1.0514	0.7648	108129.1

An aeroelastic analysis is conducted for the three constraint design cases of the previous section. (stress constrained (sc), minimum gauge (mg), and displacement constraint (dc) designs). The flexible static stability derivatives for each of these cases are presented in table 4-1. For each of the cases, however, the change was less than 7 percent. The stress constrained case exhibited the greatest variation of lift coefficient compared to the rigid tail aerodynamics lift coefficient (increase from 3.269 to 3.498) The moment and rolling coefficients increased proportionaly more for each case as compared to the overall lift, suggesting that the majority of the added lift came from the outboard section of the tail.

Since the aerodynamic loads change, it is expected that the structural properties also change. The displacement of the tail due to the flexible aerodynamic loads changed very little as compared to the rigid load displacements for each of the cases. As an example, figures 4-19 through 4-24 show the small difference in displacement for the different design cases. For the stress constrained case, since the lift coefficient increased when flexibility was accounted for, it is intuitive that the total lift increased and, therefore, the stresses must have increased in the tail box. The result of this increase is illustrated by comparing the rigid load stresses against the flexible load stresses for the rib panel elements and the skin panel elements in figures 4-25 and 4-26.

The static aeroelastic properties of the tail are important, but equally important is the maximum speed the tail can operate without encountering dynamic instabilities or flutter. The next section addresses the flutter characteristics of each of the constraint designs.

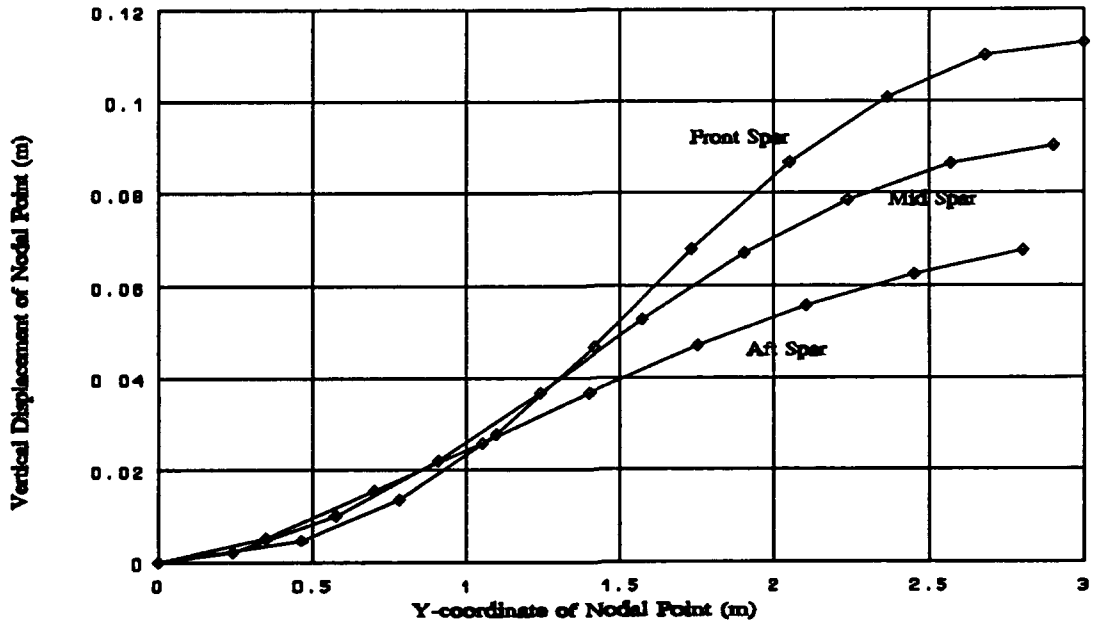

Figure 4-19 : The stress constrained (sc) case displacements at nodal points along the three spars due to rigid tail loads.

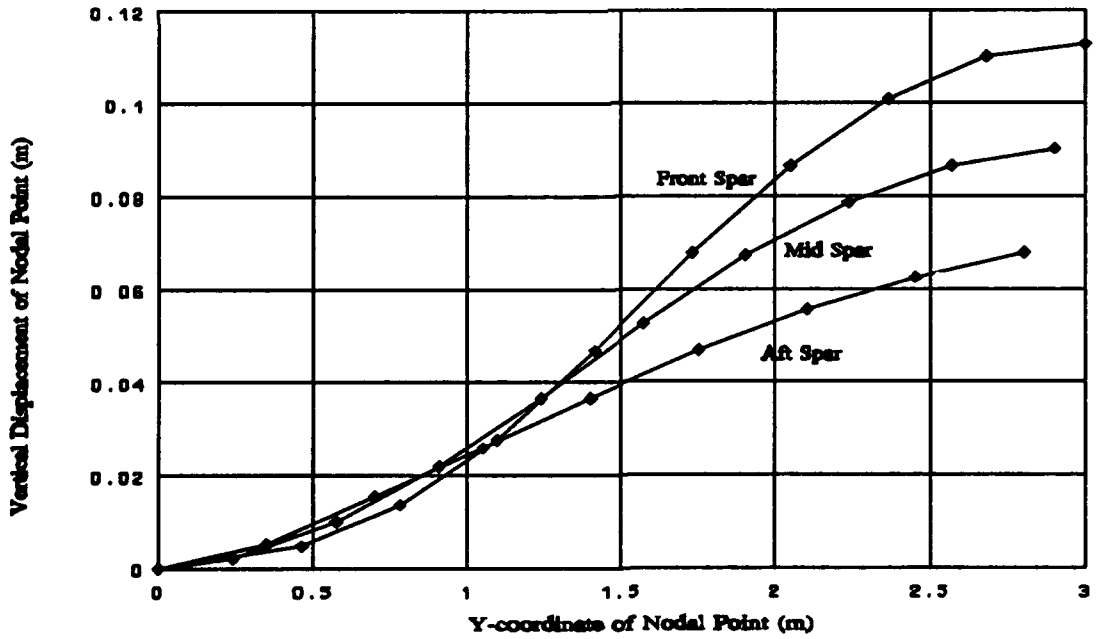

Figure 4-20 : the stress constrained case displacements at nodal points along the three spars due to aeroelastically corrected tail loads.

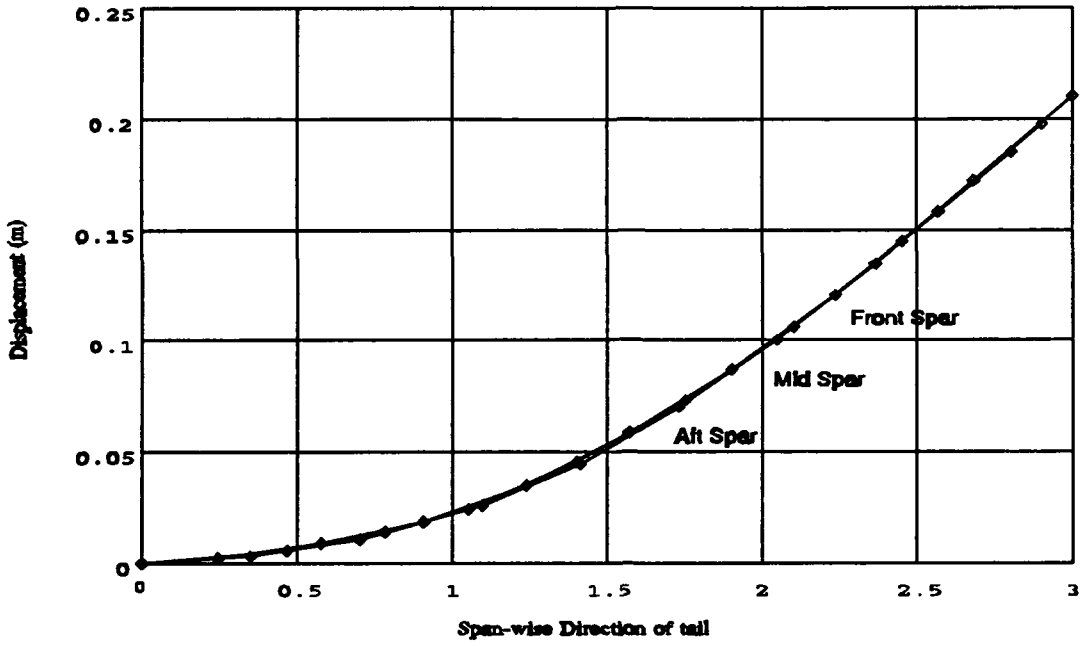

Figure 4-21 : The minimum gauge case displacements at nodal points along the three spars due to rigid tail loads.

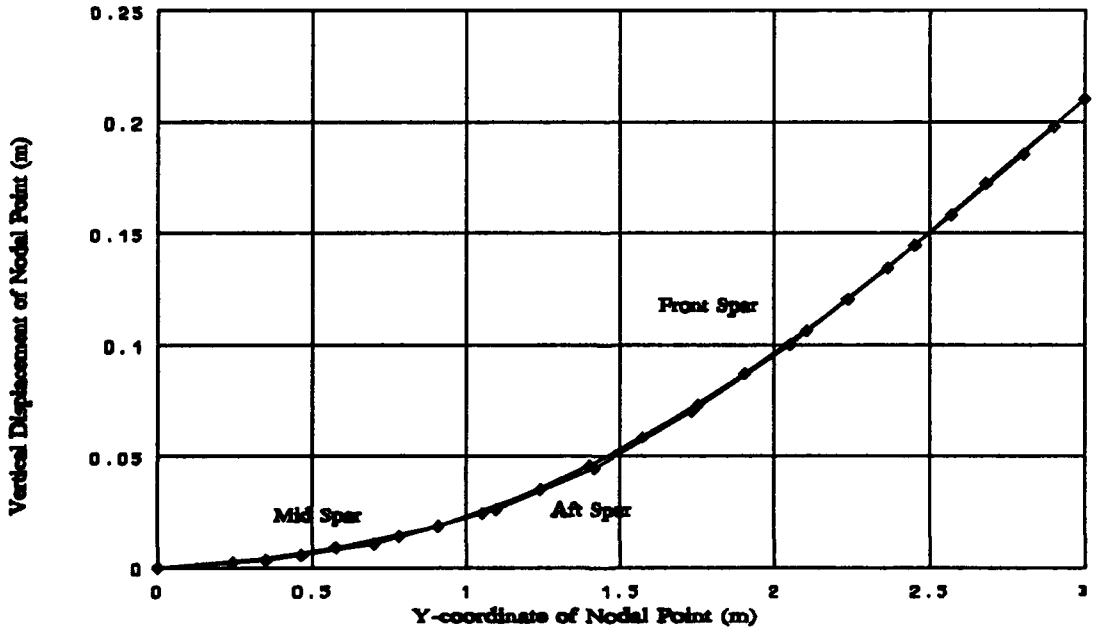

Figure 4-22 : The minimum gauge case displacements at nodal points along the three spars due to aeroelastically corrected tail loads.

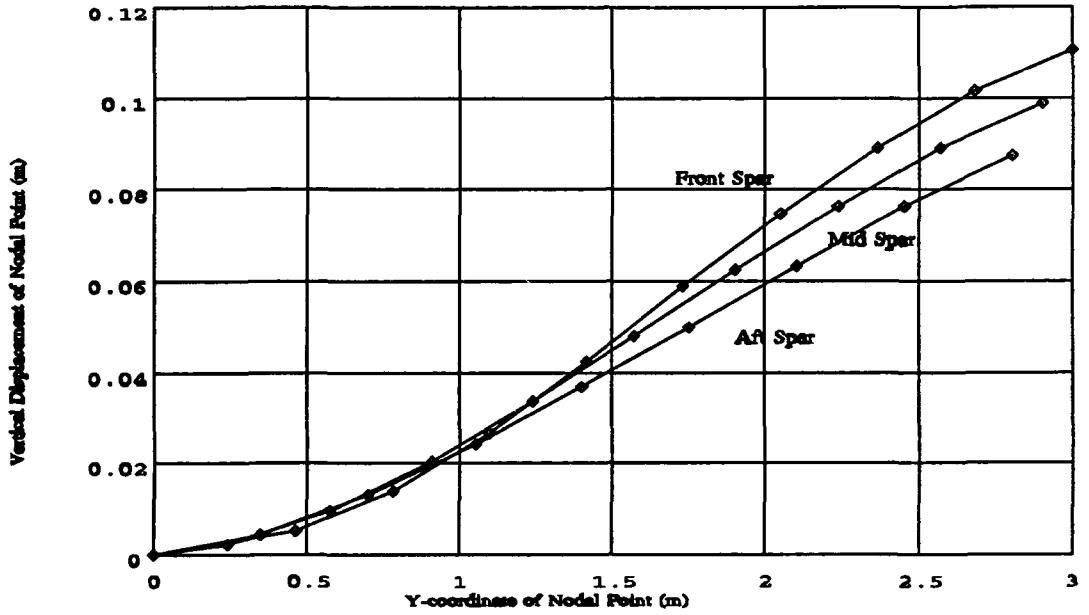

Figure 4-23 : The displacement constraint case - displacements at nodal points along the three spars due to rigid tail loads.

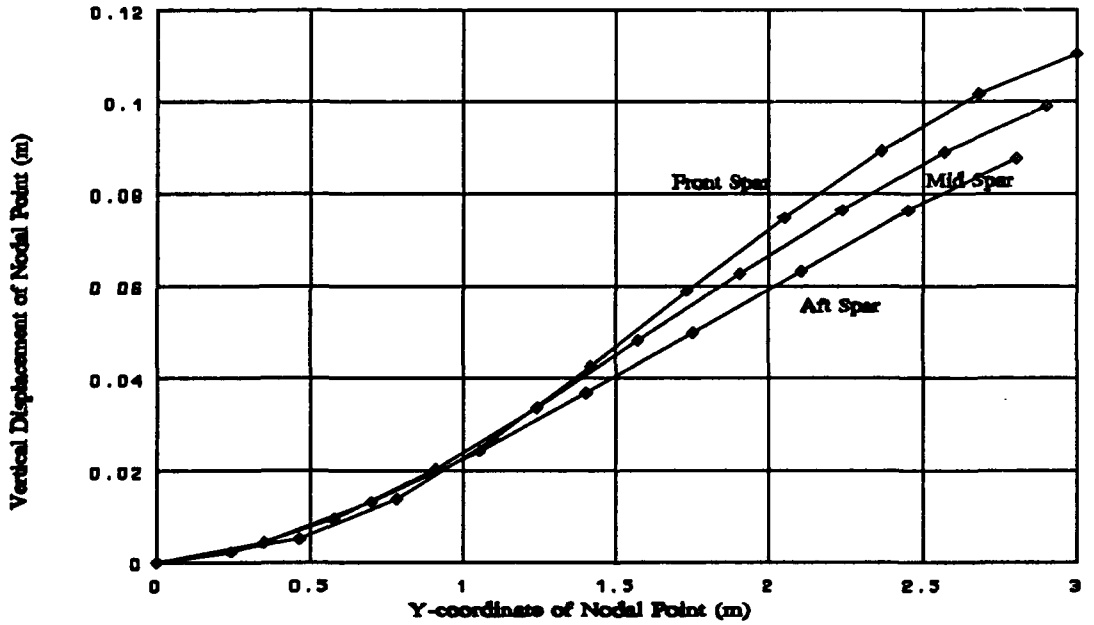

Figure 4-24 : The displacement constraint case - displacements at nodal points along the three spars due to aeroelastically corrected tail loads.

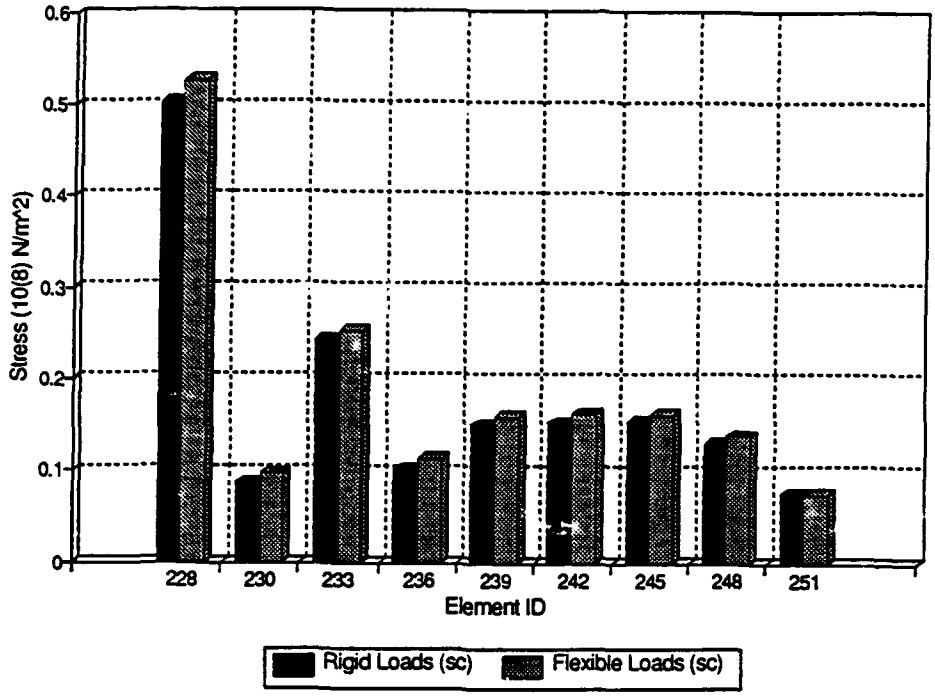

Figure 4-25: Comparison of Von Mises stress values in mid spar panels with rigid aerodynamic loads and aeroelastically corrected flexible lc

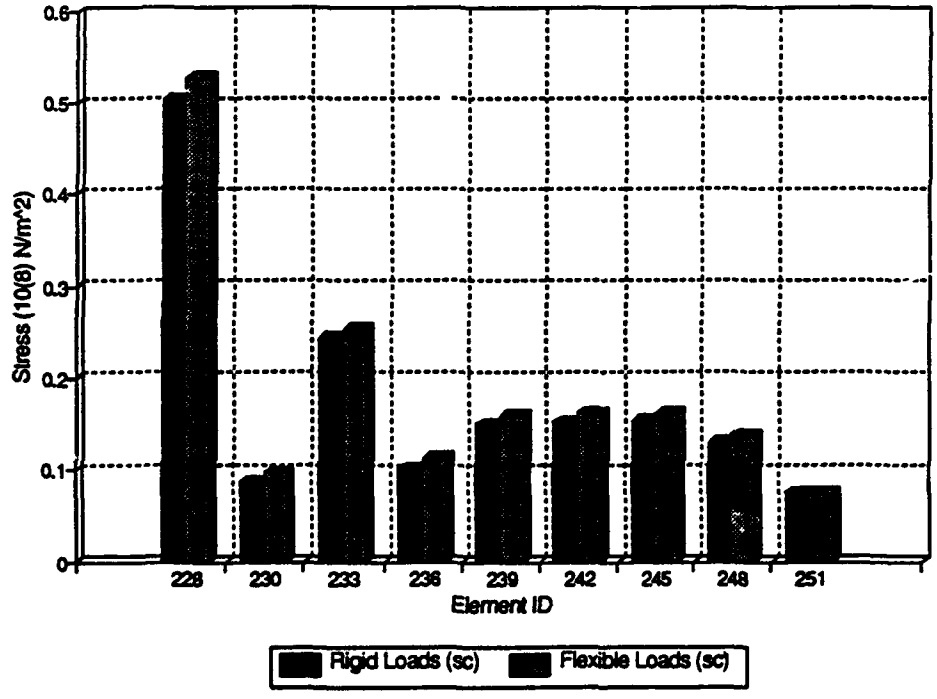

Figure 4-26: Comparison of Von Mises stress values in forward rib panels with rigid aerodyanamic loads and aeroelastically corrected flexible loads.

4.5 Effect of Design Constraints on Flutter Speed

The dynamic characteristics of each of the three design are now examined. Since dynamic response is closely tied to the structural mass, additional mass is evenly distributed to selected tail box nodal points to account for the sections of the tail which are not included in the finite element model and to include the mass of any equipment which may be stored in the tail. The location of the added mass is shown in figure 4-27. The total mass added was 34 kg. (2 kg at each node) To further examine the dependence of the dynamic response to the mass distribution, the location of the concentrated mass was varied in the minimum gauge design. The modified mass distributions are noted as (1) the mass forward and (2) the mass aft case. (See Figures 4-28 and 4-29)

The first four natural frequencies and mode shapes were calculated for each design. The frequencies are given in table 4-2 and the mode shapes are given in appendix A. The first two modes of each design case are predominantly bending modes for each of the cases except for the stress constrained case whose second mode is predominantly a torsion mode. The dominant bending modes are expected for a swept tail (wing) (Reference 8) The first frequency varies from 10.2 Hz for the stress constrained design to 16.9 Hz for the displacement constraint design. This compares well with the frequency of the F-16 vertical tail ($\approx$ 12.7 Hz) and the F-15 fighter aircraft ($\approx$ 9.1 Hz). The higher frequencies of the vertical tail model grow much more rapidly than the values for the two fighter aircraft used as a benchmark, however. For example, the second frequency of the stress constrained design (sc) is 41.28 Hz whereas the F-16 fighter aircraft vertical tail has a second frequency of $\approx$ 32

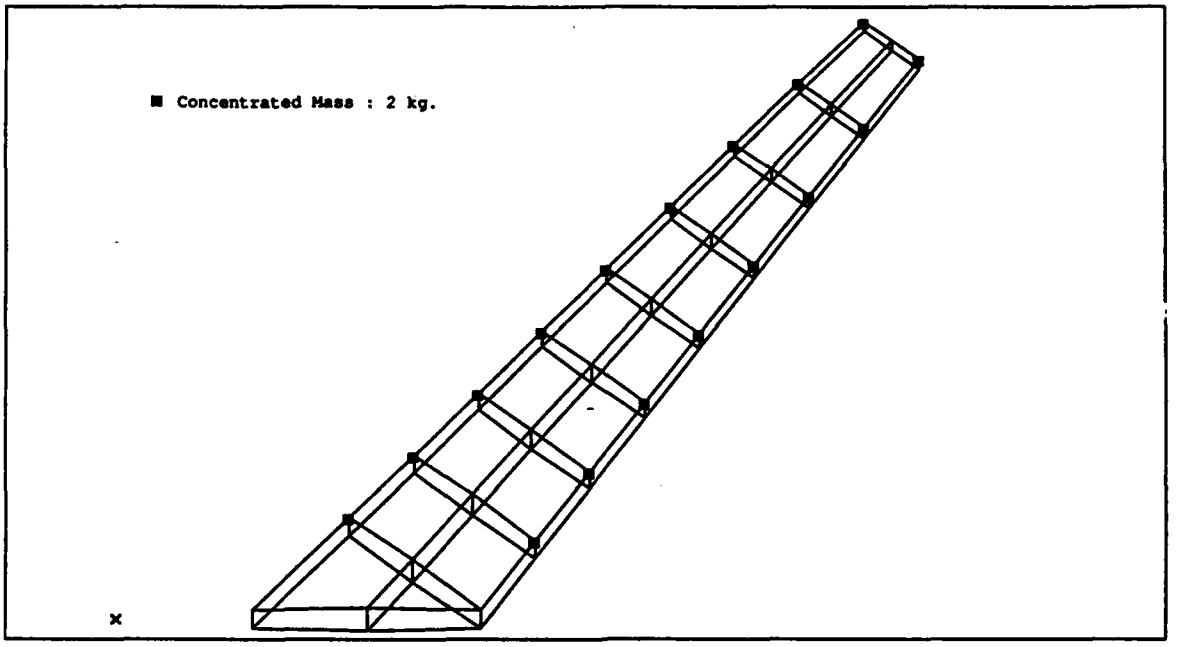

Figure 4-27: Normal distribution of concentrated mass.

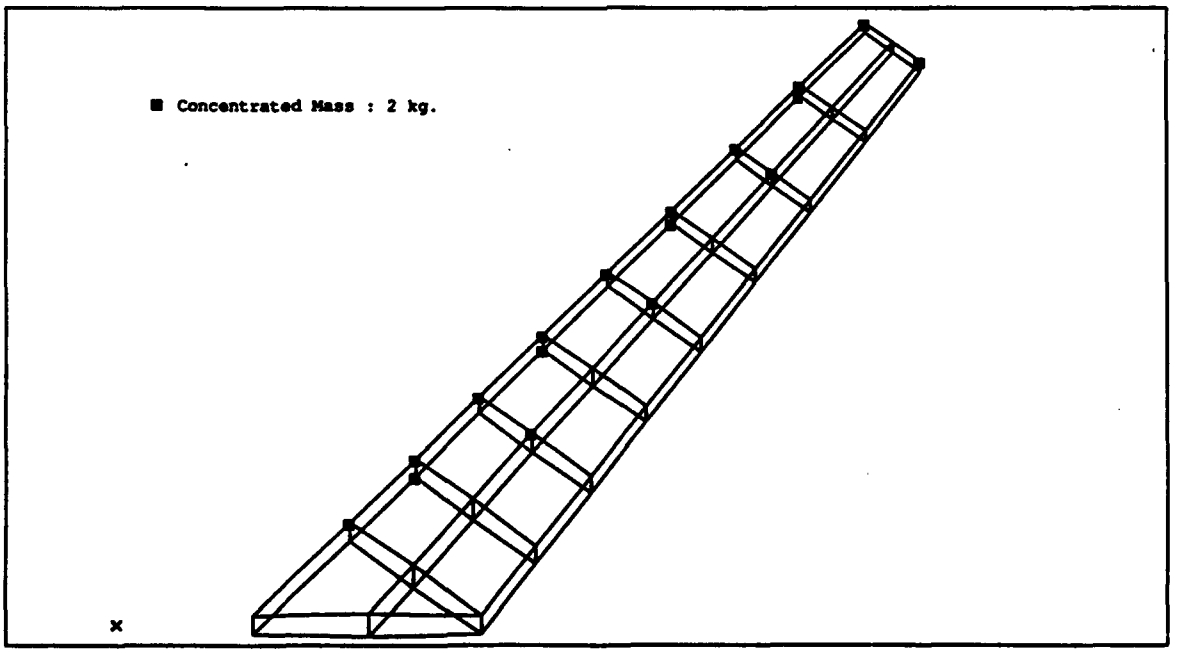

Figure 4-28: Mass forward distribution of concentrated mass.

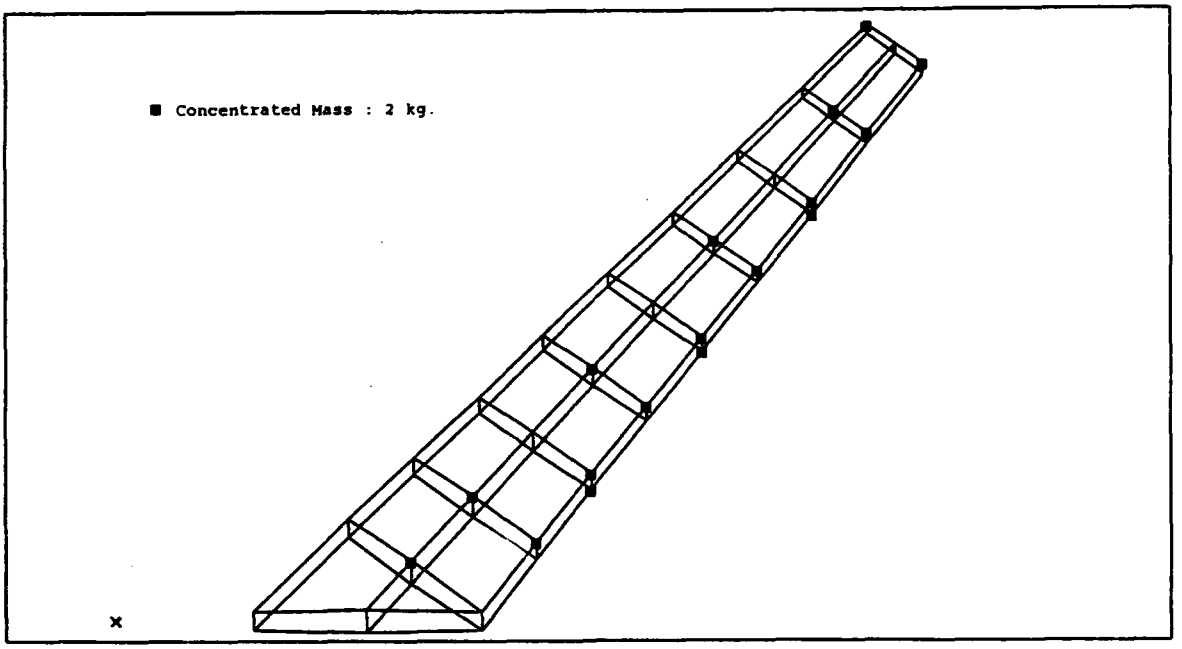

Figure 4-29: Mass aft distribution of concentrated mass.

Hz.

Table 4-2 : Natural Frequencies of the Different Designs.

Design Condition	1st Frequency (Hz)	2nd Frequency (Hz)	3rd Frequency (Hz)	4th Frequency (Hz)
Stress Constrained (sc)	10.20	41.28	53.94	89.49
Minimum Gauge (mg)	11.30	43.01	55.23	97.70
Node 28 < 10 cm (dc)	16.91	50.55	56.79	106.26
Weight Forward (mg)	12.65	42.78	75.41	90.58
Weight Aft (mg)	13.59	43.42	72.80	100.8

The fundamental flutter speed in each of the design cases is predominantly affected by

the second mode (bending mode). Equation 2-47 was used to determine the flutter speed. The aerodynamic matrix, [A], is calculated for a series of reduced frequencies at Mach number of 0.8. (sea level) The reduced frequency, k, was varied to determine the value at which the artificial damping term, g, crossed zero along with the corresponding velocity. Graphs of g for different values of velocity and the forced frequencies of vibration for different values of k are shown in figures 4-30 through 4-39. The lowest value of velocity for which g was zero was defined to be the flutter speed. A linear interpolation was used between data points to determine the flutter speed. The smallest flutter speed calculated was for the stress constraint design (417.17 m/s). The minimum gauge, mass forward case recorded the highest flutter speed of 737.14 m/s. (See Table 4-3) These flutter speeds are well above the speed of sound (M = 1.0). To solve equation 2-47 exactly, a Mach number - velocity match should be found. In other words, the Mach number at which the aerodynamic matrices were calculated should match the Mach number at which flutter instability is predicted. It is assumed in this analysis that the accuracy of the doublet-lattice method falls off sharply as the Mach numbers become transonic and the calculations for flutter speed loose credibility above M = 0.8. Therefore, no attempt was made to match the flutter speed to the aerodynamic Mach number. Instead, it is assumed that flutter is not important to the defined mission of the vertical tail. To examine the flutter mechanism for each design, velocity-damping (v-g), reduced frequency - frequency (k-ω) plots are given for each design in figures 4-30 to 4-39.

Table 4-3 : Flutter Speeds for the Different Designs.		
Case Description	Flutter Speed (m/s)	Flutter Frequency (Hz)
Stress Constraint (sc)	417.17	22.5
Minimum Gauge (mg)	500.17	18.73
Node 28 < 10 cm (dc)	467.64	22.85
Mass Forward (mg)	737.14	45.40
Mass Aft (mg)	479.99	25.81

Through this chapter the characteristics and properties of several designs have been presented. A minimum weight structure was obtained for each design case by reducing the sizes of the structural members. Constraints on the design limited the minimum member size which would be allowed. The structural analysis was based on a computer model which assumed that the tail structure was cantilevered at the base and deformed elastically in response to the applied aerodynamic loads. The aerodynamic loads were calculated based on the doublet-lattice harmonic flow theory.

Several designs have been evaluated and subtle differences have been found between each of the designs. The next chapter will now compare and contrast these differences and identify the properties which would be used when considering which design would integrate best into an aircraft system.

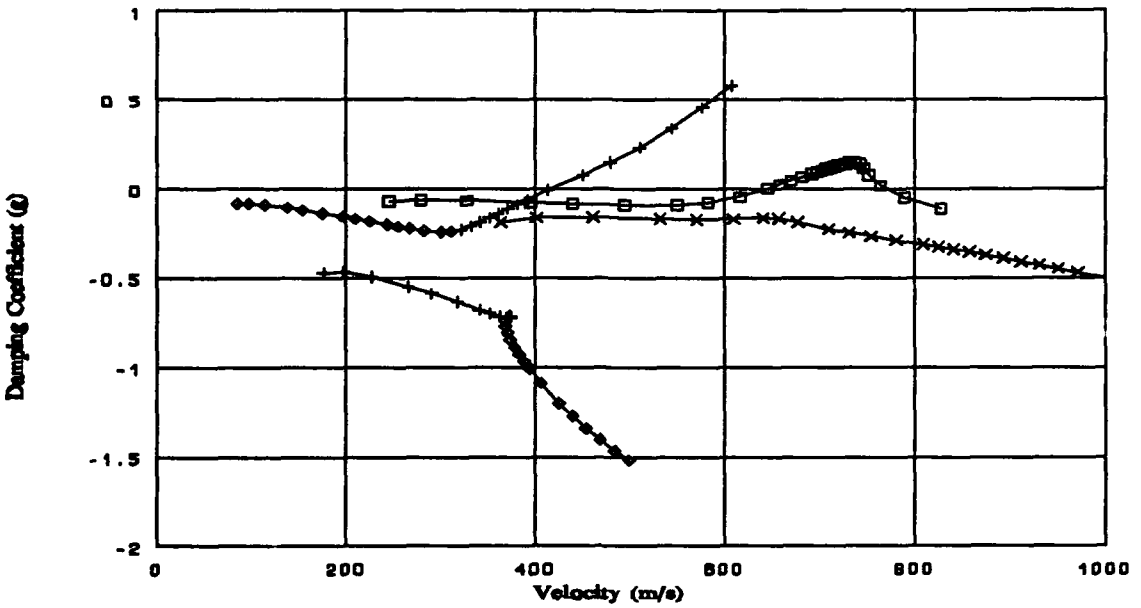

Figure 4-30 : Velocity - artificial damping (V-g) curve for the first four modes of the stress constrained (sc) case.

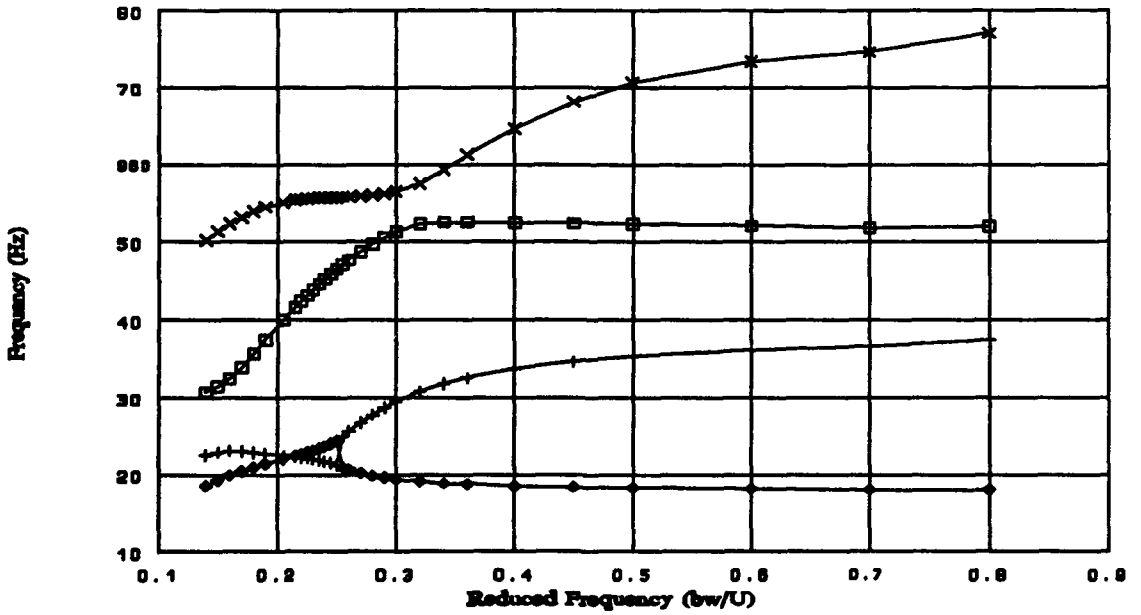

Figure 4-31: Reduced frequency - frequency (K-$\bar{\omega}$) curves for the first 4 modes in the stress constrained (sc) case.

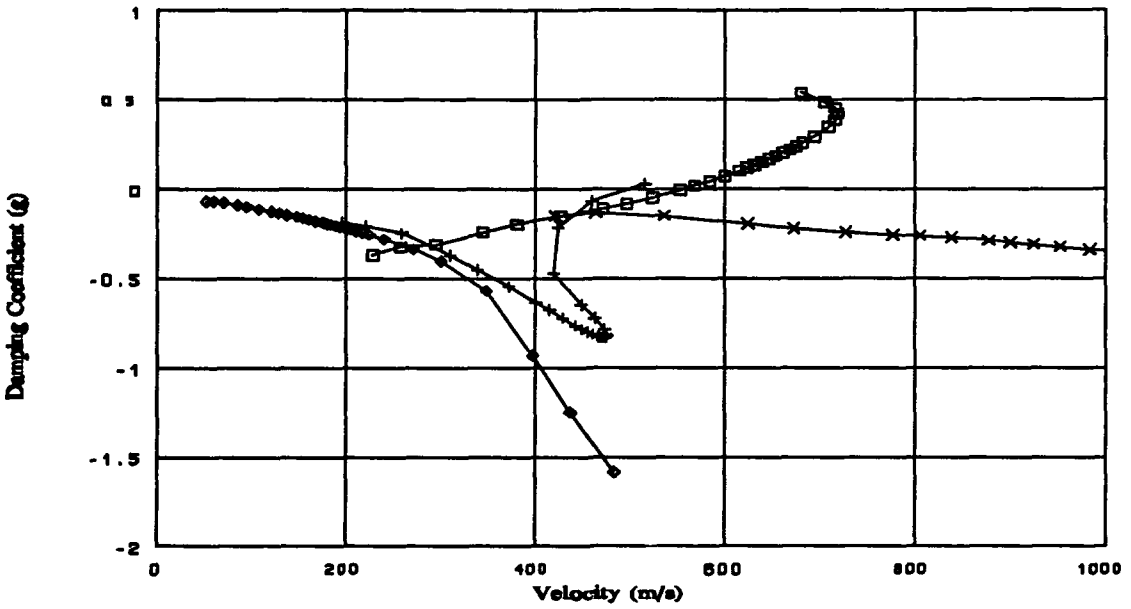

Figure 4-32: Velocity - artificial damping (V-g) curves for the first 4 modes in the minimum gauge (mg) case.

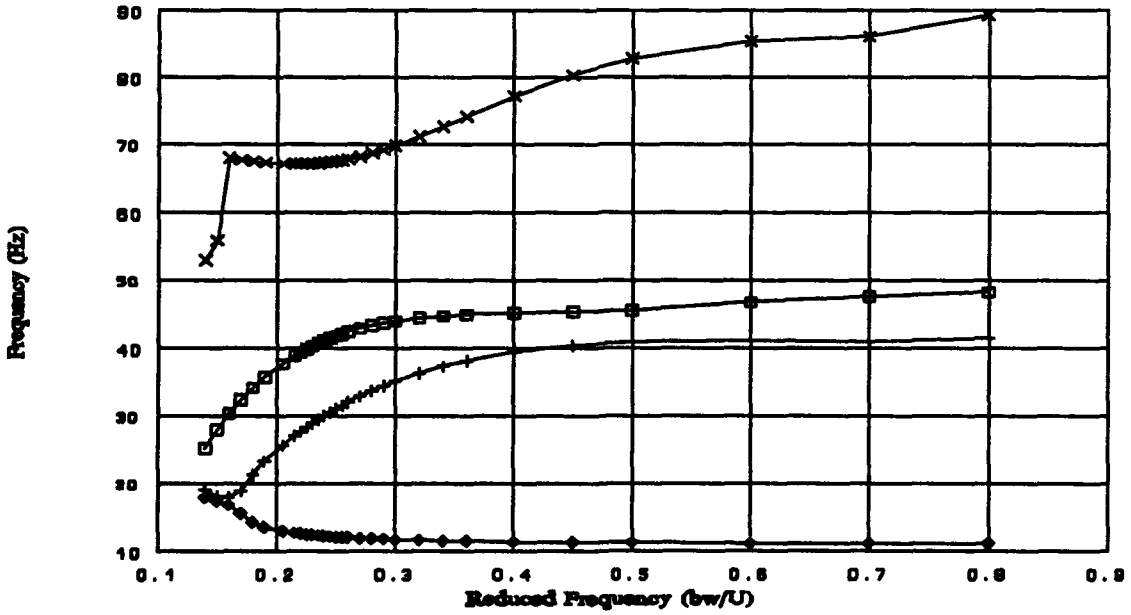

Figure 4-33: Reduced frequency - frequency (k-ϖ) curves for the first 4 modes in the minimum gauge constraint (mg) case.

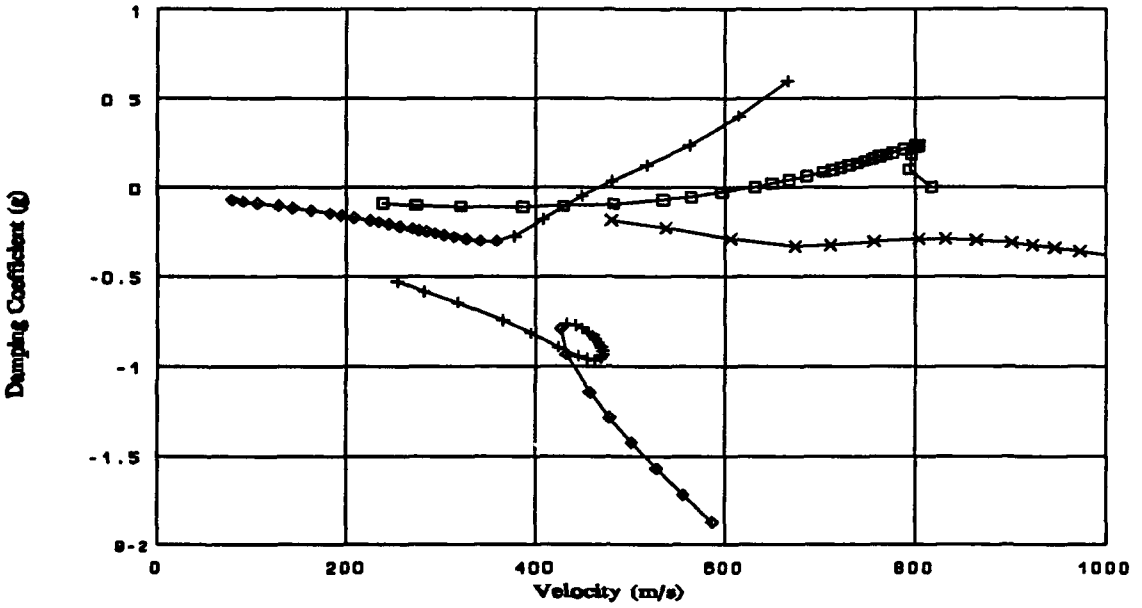

Figure 4-34: Velocity - artificial damping (V-g) curves for the first 4 modes in the displacement constraint case.

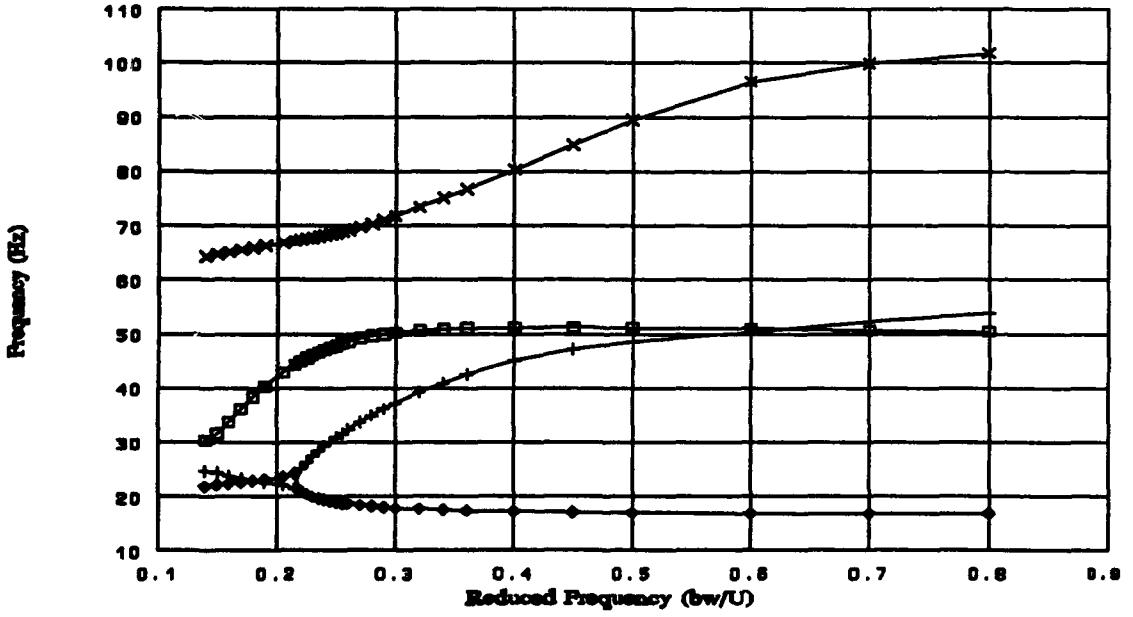

Figure 4-35: Reduced frequency - frequency (k-ϖ) curves for the first 4 modes in the displacement constraint (dc) case.

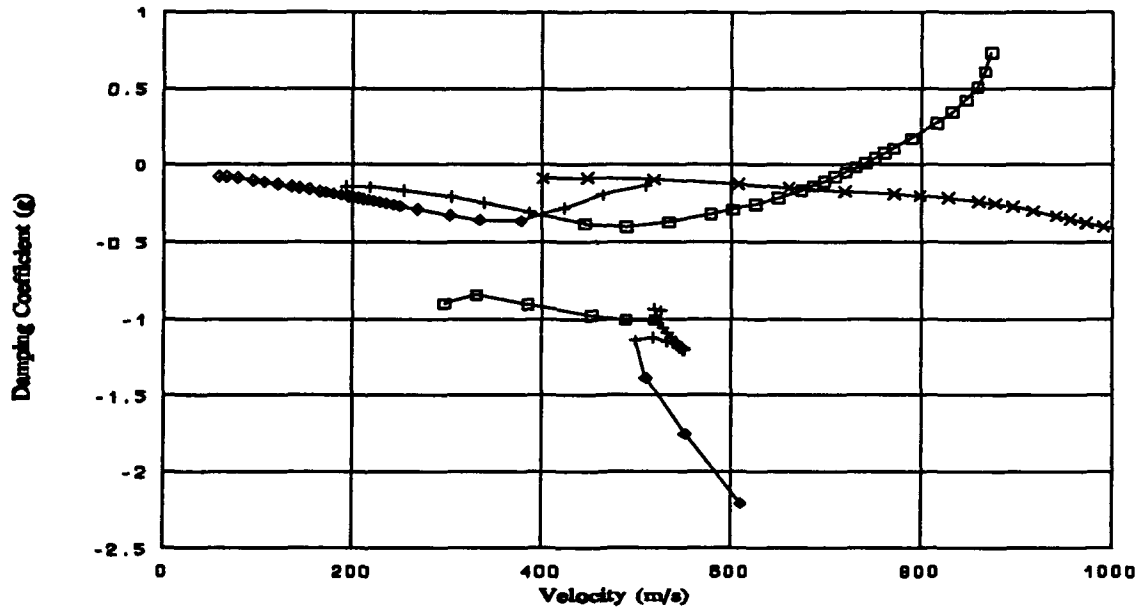

Figure 4-36: Velocity - artifical damping (V-g) curves for the first 4 modes in the mass forward (mg) case.

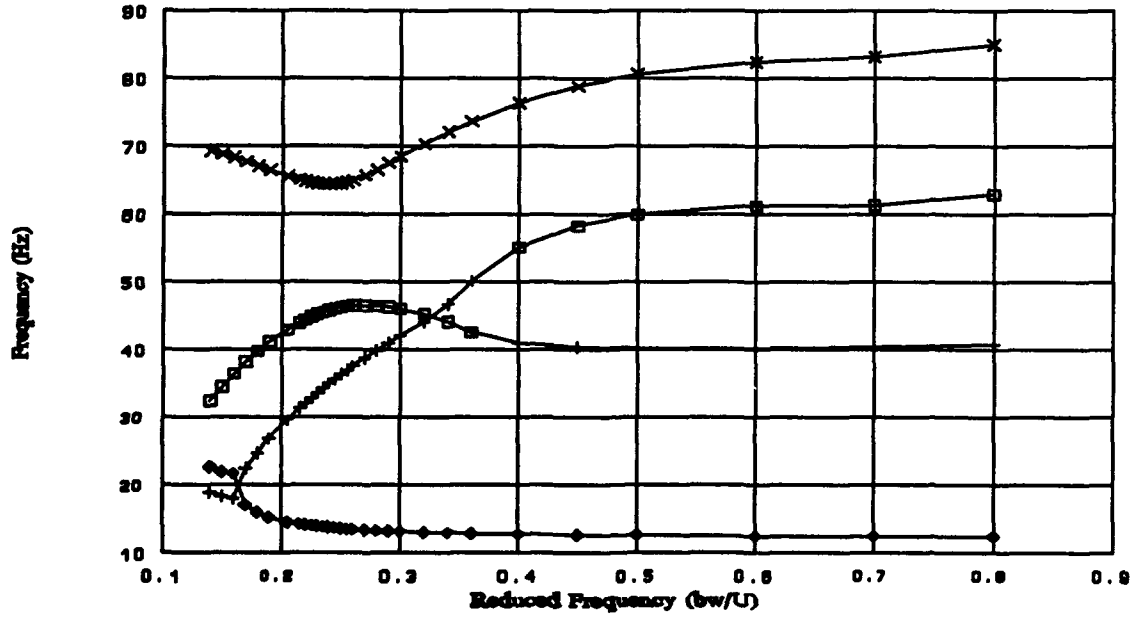

Figure 4-37: Reduced frequency - frequency (k-ϖ) curves for the first 4 modes in the mass forward (mg) case.

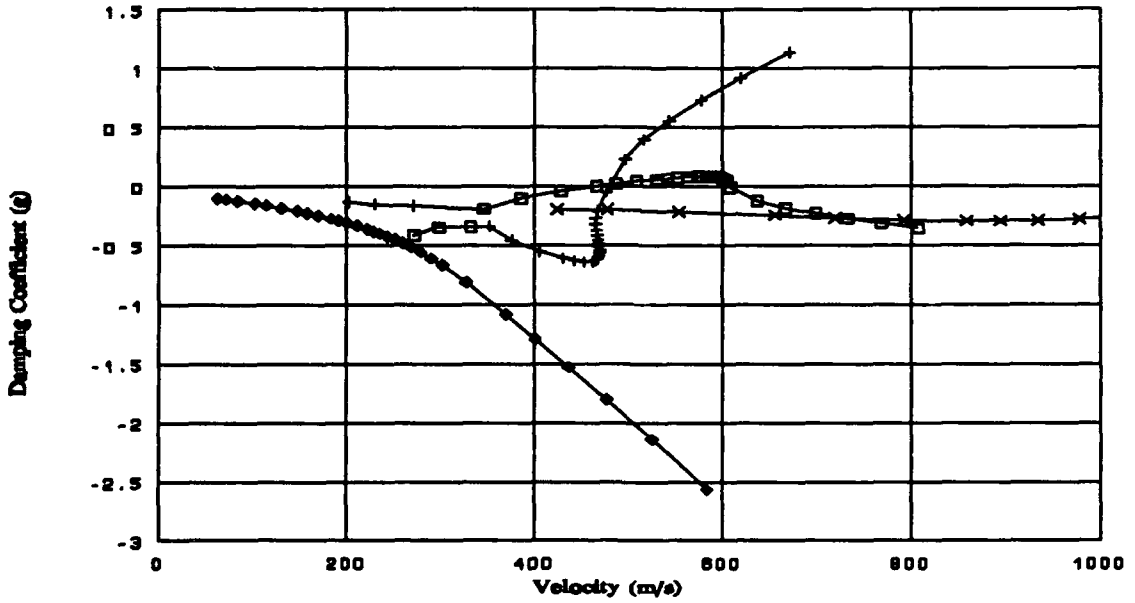

Figure 4-38: Velocity - artificial damping (V-g) curves for the first 4 modes in the mass aft (mg) case.

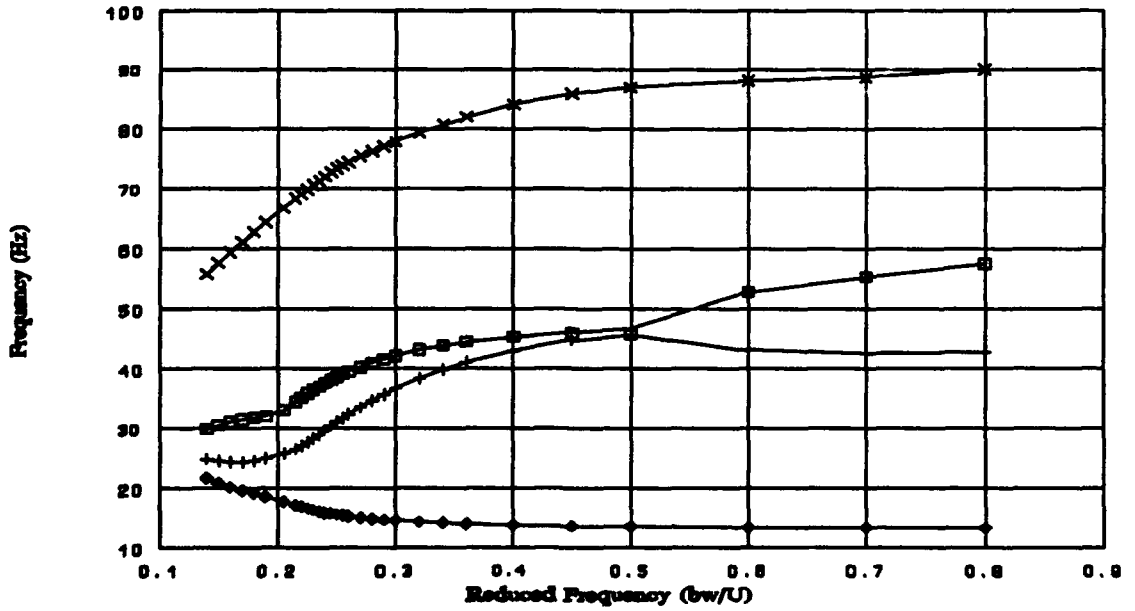

Figure 4-39: Reduced frequency - frequency (k-ϖ) curves for the first 4 modes in the mass aft (mg) case.

5. *Discussion and Conclusions*

5.1 Introduction

The previous three chapters have been devoted to developing and applying structural optimization to the design of the vertical tail. A considerable amount of theoretical work had to be covered in chapter two to describe the process of numeric optimization. Chapter three showed how the paper design was transformed into the finite element analysis model and then modified to incorporate the optimization techniques of chapter two. After considering the manhours required to develop these models, and the large amounts of computer time required for the analysis and reanalysis, the question has to be raised whether optimization is worth the effort. The results of chapter four clearly demonstrate that structural optimization is worth the initial cost. This belief is echoed in many papers (39:56 and 34:16).

Although this thesis is limited to structural optimization, the development of the aeroelastic theory reveals the opportunity to expand the optimization techniques so as to include aeroelastic tailoring. This capability is in development today with programs such as ASTROS (30:1021). More discussion on further research is saved for the final section of this chapter. The attention is first directed toward the significant results of chapter 4.

5.2 Structural Optimization

Recall that optimization works by calculating a value or series of values for the design variables which minimize the objective of the design. The objective could be anything that is a function of the design variables. The objective chosen for the tail design was to minimize the structural weight. Because of the matrix formulation chosen to automate the optimization process (FEM), the size of the matrices grew considerably as the number of design variables increased. Therefore, the computer time required to solve the problem also increased rapidly with matrix size. To keep the problem size manageable, the idea of design variable linking was introduced in chapter 3. Three different linking schemes were used on the tail design to document the effect that linking had on the optimal weight. By linking the elements together, the number of design variables could be reduced from 197 design variables to (1) 2 design variables, (2) 6 design variables, and (3) 21 design variables.

There was a large difference in optimal weight between the two design variable and six design variable linking scheme (73 kg -> 44 kg). The large difference in weight was due to, for the bar elements, the highly stressed spar elements at the root of the tail which prevented the optimization algorithm from reducing the size of the lesser stressed bars. When the spar elements were subdivided into their own group, the other elements then were allowed to reduce in size. (See Figures 4-1 through 4-3) The obvious question to ask after examining these figures is, why is not one of the

sizes in the six design variable scheme equal to the size of the two design variable scheme. The answer lies in the complex stress distribution throughout the tail box. If any of the element sizes in the design is changed then the stress distribution can change drastically.

A more subtle decrease in the optimal weight occurred between the six and twenty-one design variable linking scheme (44 kg -> 38 kg) suggesting that the required sizes differ little at the wing tip versus the wing root. The small change between the six and twenty-one design variable case was surprising since it was believed that the spanwise variation in internal forces would allow a large drop in required structural weight. It might then be concluded that if minor variations were

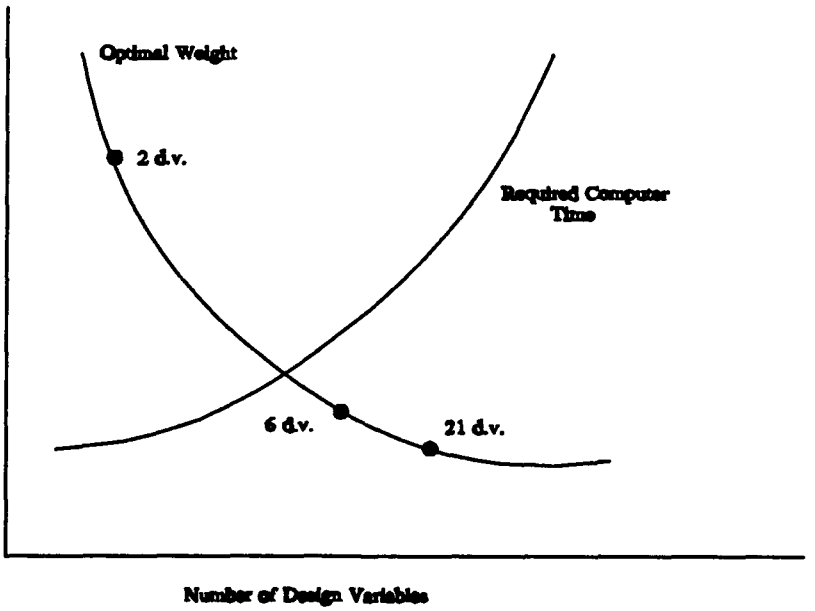

Figure 5-1 : Qualitative view of the effect of linking together design variables.

made to the design, the six design variable linking scheme would give accurate results for a fraction of computer time.

The effectiveness of the optimization was verified by checking the stress values of different sections of the tail box. The direct relationship between element stress values and element weight allows this to be true. The fully optimized tail structure with only stress constraints would have stress values at the yield stress values. This could not be realized because of the design variable linking that was utilized.

Table 5-1: Stress value of the element with maximum stress from each of the twenty one design variable groups. The design was stress constrained only.

Element Number (Bar Element)	Axial Stress (10^9 N/m^2)	Element Number (Panel Element)	Von Mises Stress (10^9 N/m^2)
Spar 4	1.42	Skin 47	1.94
Spar 9	1.15	Skin 54	2.74
Spar 15	0.64	Skin 57	2.22
Spar 21	0.86	Spar 232	2.26
Rib 27	0.82	Spar 235	1.96
Rib 35	0.20	Spar 241	2.04
Rib 39	0.23	Spar 247	2.03
Post 201	0.10	Rib 254	0.75
Post 206	0.04	Rib 263	0.15
Post 215	0.05	Rib 265	0.15
Post 226	0.06		

However, at least one element out of every design variable group should be fully stressed. For reasons unknown the algorithm would halt and declare that the design had been optimized before one of the elements inside of each group would reach maximum stress of $2.76(10^8)$ N/m^2 (see figure 5-1). Because of the large range of numbers used during the analysis, it is suspected that loss in significant figures during calculations may be one source of error. This belief is supported by the fact that the bar elements did not optimize as well as the panel elements. The bar elements had values three orders of magnitude less than the panel elements.

A relationship was developed between the optimal weight and the design load by optimizing the structure for a variety of design loads. The linear relationship is shown in figure 4-11. The linear relationship was expected since the stiffness properties of the structure are linear (linear stress-strain relationship). The slope of the curve, 3000 N/ kg, was calculated from the tabulated data using a least squares fit. The slope of the curve is the estimated load capability per kg of structural mass. As the load decreased under 20000 N the minimum gauge restraint influence began to dominate the minimum weight design. The minimum gauge constraint was enforced in this design section. With the minimum gauge restraint active, the minimum design weight was 16.2 kg (all members at minimum size). As long as the design load is well above 20000 N, however, a good guide for estimating the required structural weight for a given design load is to divide the design load by the slope (3000 N/kg) of the design load/ design weight curve. The reader is reminded that this curve is based on rigid loads for the given Mach number/ angle of attack pair. The effect that

flexibility would have on the optimization process could not be determined with the capabilities available. It would be interesting to know how the flexible design curve would compare to this curve.

The next relationship that was explored was the influence that design constraints had on the optimization problem. The stress constraint case provided the lowest objective weight (38.2 kg). After an additional minimum gauge constraint was added the weight increased only from 38.2 kg to 38.4 kg. One of the reasons for such a small weight penalty is the ability of the optimization code to compensate for the size limitation by reducing the sizes of other elements which were not fully stressed nor at the minimum gauge value. This reduction increased the forces on the elements which were at the minimum gauge, therefore, utilizing the potential load bearing capability of the elements at a minimum gauge value (see figures 4-14 through 4-18).

The last constraint was the tip deflection constraint. This constraint was aimed at reducing the expected tip acceleration. This could not be achieved by merely constraining the displacement, unfortunately, because the square of the first frequency of vibration increased more rapidly than the tip deflection decreased. (See figure 5-2) This is not a complete surprise since frequency increases with additional stiffness (see equations 2-40 through 2-42) and displacement decreases with additional stiffness (equation 2-33). If, unlike figure 5-2, a feasible solution does exist then a constraint formula would have to be formulated by producing a sensitivity equation similar to equations 2-33 and 2-42 except the sensitivity equation would be concerned with

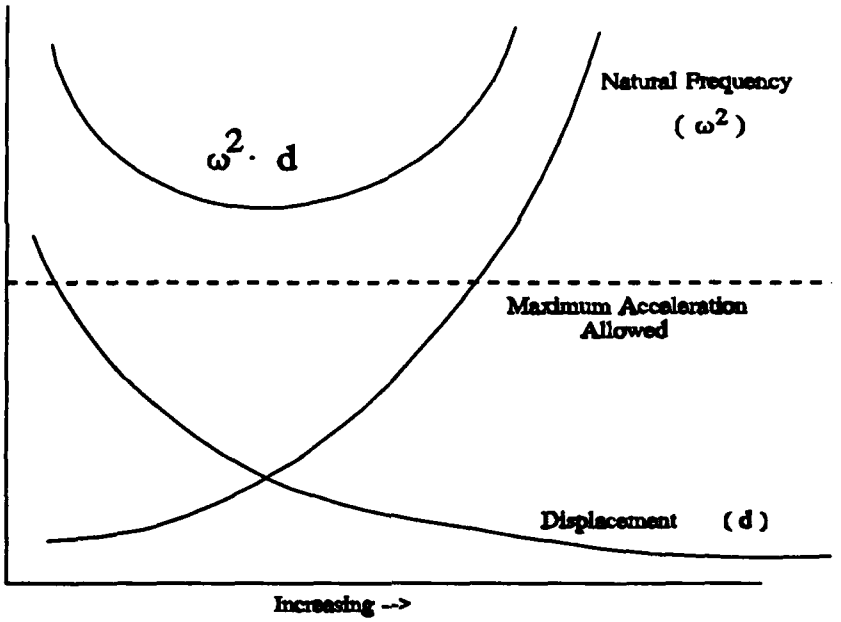

Figure 5-2: Example of possible displacement and natural frequency curves as a function of structural stiffness.

$\frac{\partial}{\partial X_i}(\omega^2 d)$=..... This was not incorporated into this design. The difficulty with this type of constraint is the requirement to utilize both the strength analysis equations and the frequency analysis equations (NASTRAN can not perform both of these simultaneously).

The displacement constraint increased the weight of the design by approximately 6 kg. The biggest increases in design variable size was to the rib panels, followed by smaller increases to the spar and skin panels. So if tip displacement becomes an issue in the tail design, the structural members which would

most effect the displacement are the rib panels, followed by the skin and spar panels.

5.3 Aeroelastic Analysis

The static aeroelastic response of the three constrained designs showed that the added load from the flexibility affected the structural response less than three percent except with the stress constrained design with which the lift coefficient, C_{L_a}, increased over seven percent. (See Table 4-1) In each case, however, the lift coefficient did increase. The larger increases in the rolling moment, C_{M_a} and C_{N_a}, suggest that most of the increase in lift is due to a positive rotation near the tip of the tail. There were no stress concentrations in any of the elements near the tip, however, instead there was a general increase in stress values throughout the members. All member stresses remained under the yield stress limit.

A dynamic analysis of each of the designs showed that the first mode was a bending mode for each of the designs. Only in the stress constrained design was the second mode a torsion mode. For each of the other designs the second mode was a bending mode. It is interesting to note that the largest aeroelastic influence came from the stress constrained design. It appears that the modal shapes might influence the magnitude to which the aeroelastic loads influence the overall loads.

Two relationships were determined from the flutter analysis; the variation in flutter speed between the different constraint designs, and the variation in flutter speed

with respect to mass distribution. The largest flutter speed for the three design cases was with the minimum gauge case. By shifting the mass distribution of the minimum gauge design so that much of the mass was in the forward section of the tail, there was a large gain in flutter speed. (500 m/s --> 737 m/s) By shifting the mass aft, the flutter speed decreased to 480 m/s. The flutter speeds are based on the aerodynamic influence matrix at M=0.8. None of the flutter speeds are in the defined flight envelope (M < 0.8 sea level or 270 m/s). An important fact to notice is that the flutter phenomenon appears to be most influenced by the first and second mode of each design. These modes are bending modes, except in the stress constraint design in which the second mode is a torsion mode.

5.4 Closing Comments

This thesis provides a base for additional research to build. The analysis of the tail utilized structural optimization to improve the design. The design environment was predicted with doublet-lattice aerodynamics. There are three major areas from which the tail design can be modified

(1) Structural Model,

(2) Optimization Parameters,

(3) Aerodynamic theory.

The structural model can be modified to include the effect of topics such as control

surfaces, a flexible fuselage, or an all-movable tail design. How would the aeroelastic response vary for each of these designs?

The area with the most attention in todays literature (35:982) is optimization. To be more exact, multi-disciplinary optimization. An example from this thesis is the inability to optimize the tail members with respect to flexible aerodynamic loads. The aerodynamic force equation (Eqn 2-18) needs to be tied into the influence equations of section 2-5. Two new areas which are gaining a lot of attention in the engineering community are shape sensitivities where the influence of the geometry of the design is incorporated into the optimization, and the ability to insert or remove structural members depending on whether they improve or degrade the objective of the optimization. With respect to aeroelasticity, computer code has been developed which allows the user to include as constraints, or an objective, stability derivatives, flutter speed, divergence speed, etc. More and more relationships are being implemented constantly. As researchers and programmers incorporate these relationships into their computer codes, the vertical tail model could be used as a test bed for evaluation.

The last area is the area of aerodynamic modeling. The aerodynamic model used in this thesis uses linear potential flow theory. The non-linear influence of high angles of attack, transonic flow, and the viscous effects of turbulence were ignored in the current aerodynamic model. The influence that these effects might be significant, therefore, a new approach to predicting aerodynamic loads might be warranted.

Bibliography

1. Albano, Edward and William P. Rodden. "A doublet-Lattice Method for Calculating Lift Distributions on Oscillating Surfaces in Subsonic Flows," *AIAA Journal*, Vol. 7, No 2, Feb 1969, pp.279-285.

2. Ashley, Holt and Marten Landahl. *Aerodynamics of Wings and Bodies*. New York: Dover Publications 1965.

3. Bellinger, Dean. MSC/NASTRAN Technical Representative. May 5.1992.

4. Bismarck-Nasr, Maher N. "Kernel Function Occurring in Subsonic Unsteady Potential Flow," *AIAA Journal*, 29:878-879 (June 1991)

5. Bisplinghoff, R. L. and Holt Ashley. *Principles of Aeroelasticity*. New York: John Wiley & Sons, 1962.

6. Cook, Robert D. and others. *Concepts and Applications of Finite Element Analysis*. New York: John Wiley & Sons, 1989.

7. Dowell, Earl H. *A Modern Course in Aeroelasticity-2nd Edition*. Boston: Kluwer Academic Publishers, 1989.

8. Eastep, Frank. Class notes, AERO 538, Introduction to Aeroelasticity, University of Dayton, Dayton, OH, Fall 1991.

9. Fletcher, Dennis A. *Effects of Concentrated Masses on the Flutter of a Uniform Cantilever Wing*. MS Theses, AFIT/GAE/ENY/76-D. School of Engineering, Air Force Institute of Technology, WPAFB, 1976.

10. Gallagher, R.H. and O.C. Zienkiewicz. *Optimum Structural Design*. New York: John Wiley & Sons, 1982.

11. Giesing, J. P., "Basic Principles and Doublet Lattice Applications in Potential Aerodynamics," McDonnell Douglas Corporation, Long Beach, Ca., no further reference available.

12. Grossman, B. and others. "Integrated Aerodynamic-Structural Design of a Transport Wing," *Journal of Aircraft*, 27:1050-1057 (December 1990).

13. Haftka, Raphael T. and Manohar P. Kamat, *Elements of Structural*

Optimization, Kuwer Academic Publishers, 1985.

14. Haftka, R.T. "Structural optimization with aeroelastic constraints: A survey of US applications," *Int. J. of Vehicle Design*, 7: 381-392 (1986).

15. Harder, R. L. , and Desmarais, R. N., "Interpolation Using Surface Splines," *Journal of Aircraft*, 9: 869-871 (December 1972).

16. Haug, Edward J. *Applied Optimal Design for Mechanical and Structural Systems*, New York: John Wiley & Sons, 1979.

17. Higdon, Archie and other authors. *Mechanics of Materials : Fourth Edition*, New York: John Wiley and Sons, 1985.

18. Johnson, E. H. and Michael Reymond. "Multidisciplinary Aeroelastic Analysis and Design Using MSC/NASTRAN,"*AIAA Paper* 91-1097-CP, 1991.

19. Kirsch, Uri. *Optimum Structural Design*, New York: McGraw-Hill, 1981.

20. Kussner, H. G. "General Airfoil Theory," *NACA TM 979*, 1941.

21. Landahl, Marten T. and Valter J. E. Stark. "Numerical Lifting-Surface Theory - Problems and Progress," *AIAA Journal*, 11:2049-2061 (November 1968).

22. Lottati, I. and E. Nissim. "Nonplanar, Subsonic, Three-Dimensional Oscillatory Piecewise Continuous Kernel Function Method," *Journal of Aircraft*, 22:1043-1048 (December 1985).

23. MacNeal-Schwendler Corporation. *Handbook for Aeroelastic Analysis for MSC/Nastran Version 65: Volume 1 and 2*. 1987.

24. MacNeal-Schwendler Corporation. *The NASTRAN Programmer's Manual*, December 1972.

25. MacNeal-Schwendler Corporation. *The NASTRAN Theoretical Manual.* December 1972.

26. MacNeal Schwendler Corporation. *Handbook for Structural Optimization for MSC/NASTRAN Version 66*. December 1988.

27. McCormick, Barnes W. *Aerodynmaics of V/STOL Flight*, Academic Press. New York. 1967.

28. Maple, Raymond C. *An Iterative Solution to Aeroelastic Effects in Potential Flow*. MS Thesis, AFIT/GAE/ENY/89D-22. School of Engineering, Air Force Institute of Technology, Wright-Patterson AFB OH, December 1989.

29. Morris, A. J. *Foundations of Structural Optimization: A Unified Approach*. New York: John Wiley & Sons, 1982.

30. Neill, D.J. and others. "ASTROS- A Multidisciplinary Automated Structural Design Tool," *Journal of Aircraft*, 27: 1021 - 1027 (December 1990).

31. Niekerk, Becker Van. "Integration of Singular Functions Associated with Lifting Surface Theory," *AIAA Journal*, 24:1194-1196 (July 1986).

32. Ryder, John K. *Modelling and Analysis of Kernel Function and Development of Equivalent Theodorsen Function for Three-Dimensional Aeroelastic Analysis*. MS Thesis, AFIT/GAE/ENY/90D-25. School of Engineering, Air Force Institute of Technology, Wright-Patterson AFB OH, December 1990.

33. Shelton, William L. Jr. *Flutter Prediction in Forward-Swept Wings by Assumed Modes and Strip Theory*, MS Thesis, AFIT/GAE/ENY/82D. School of Engineering, Air Force Institute of Technology, Wright-Patterson AFB OH, December 1982.

34. Shirk, Michael H. and Terrence J. Hertz. "Aeroelastic Tailoring - Theory, Practice, and Promise," *J. Aircraft*, 23: 6-16 (January 1986).

35. Sobieszczanski-Sobieski, Jaroslaw and Inderjit Chopra. "Multidisciplinary Optimization of Aeronautical Systems," *Journal of Aircraft*, 27:977-980 (December 1990).

36. Spunt, Leonard. *Optimum Structural Design*, New York: Prentice-Hall Inc, 1971.

37. Theodorsen, Theodore. "General Theory of Aerodynamic Instability and the Mechanism of Flutter," *NACA Report No. 496*, 1934.

38. Watkins, Charles E., D. S. Woolston, and H. J. Cunningham. "A Systematic Kernel Function Procedure for Determining Aerodynamic Forces on Oscillating or Steady Finite Wings at Subsonic Speeds," *NASA Technical Report R-48*, 1959.

39. Vanderplaats, Garret N. " The Best and The Lightest," *Mechanical Engineering*, 32: 56-62, February 1989.

Appendix A : Design Modal Shapes

The first four modal shapes of the five designs described in chapter four are given in the following pages. Each graph displays three lines which depict the spars of the tail box design as seen from a point in the x-y plane looking in the x-direction. The front most spar is labeled (FS), the mid-spar is labeled (MS), and the aft spar is labeled (AS). The frequency of vibration is included in each of the figure titles as "(ω= ..)". These drawings should illustrate the dominance of bending or torsion in each mode.

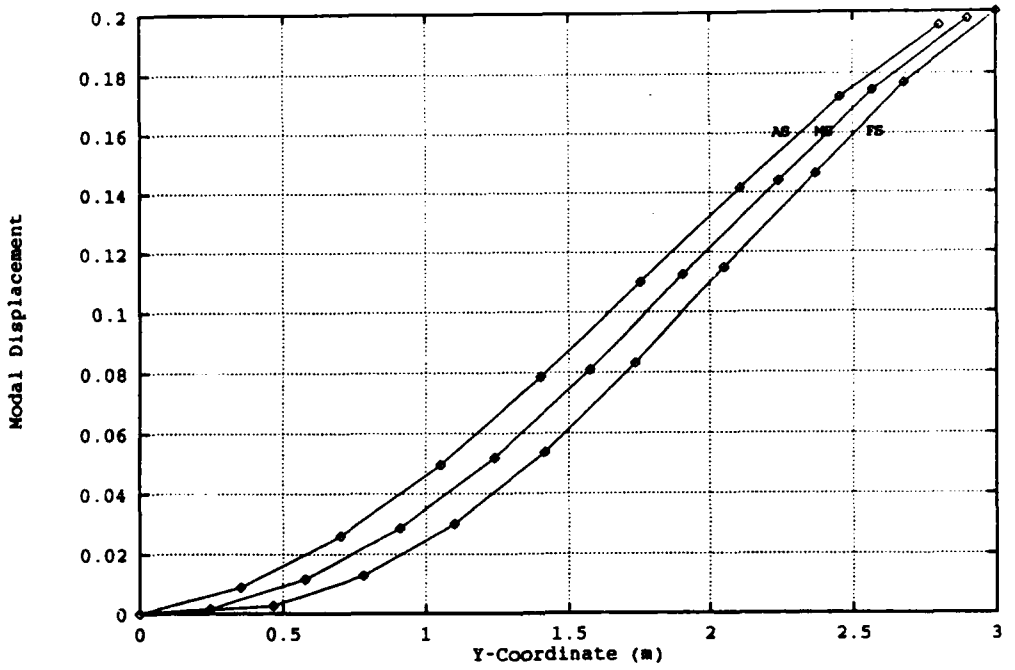

Figure A-1: First mode of vibration (ω = 10.2 hz) - stress constrained case

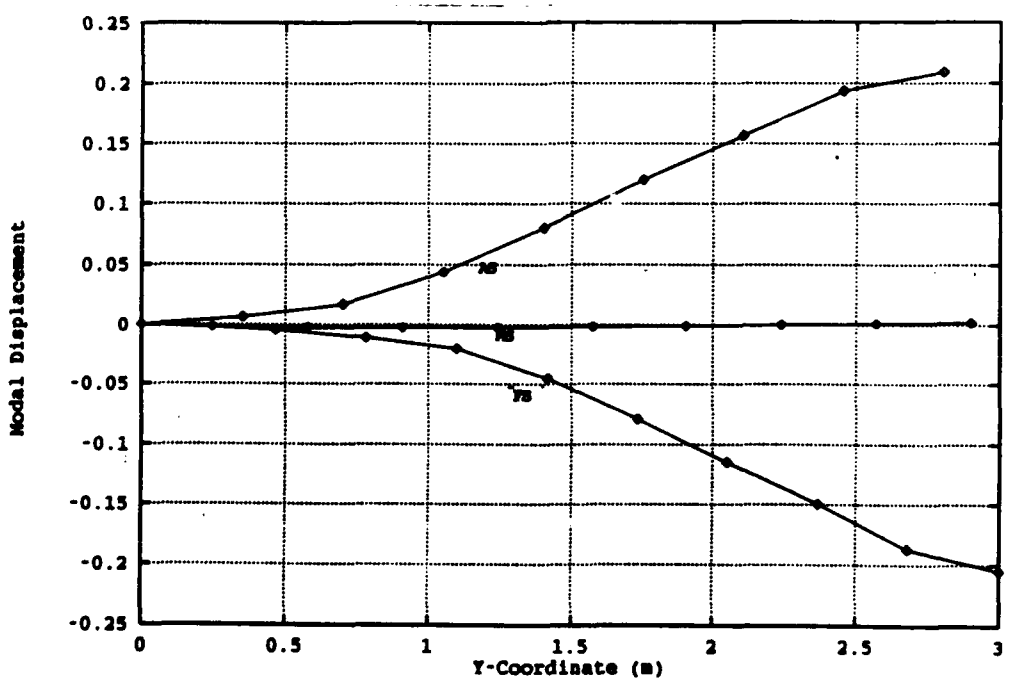

Figure A-2: Second mode of vibration (ω=41.3 hz) - stress constrained case

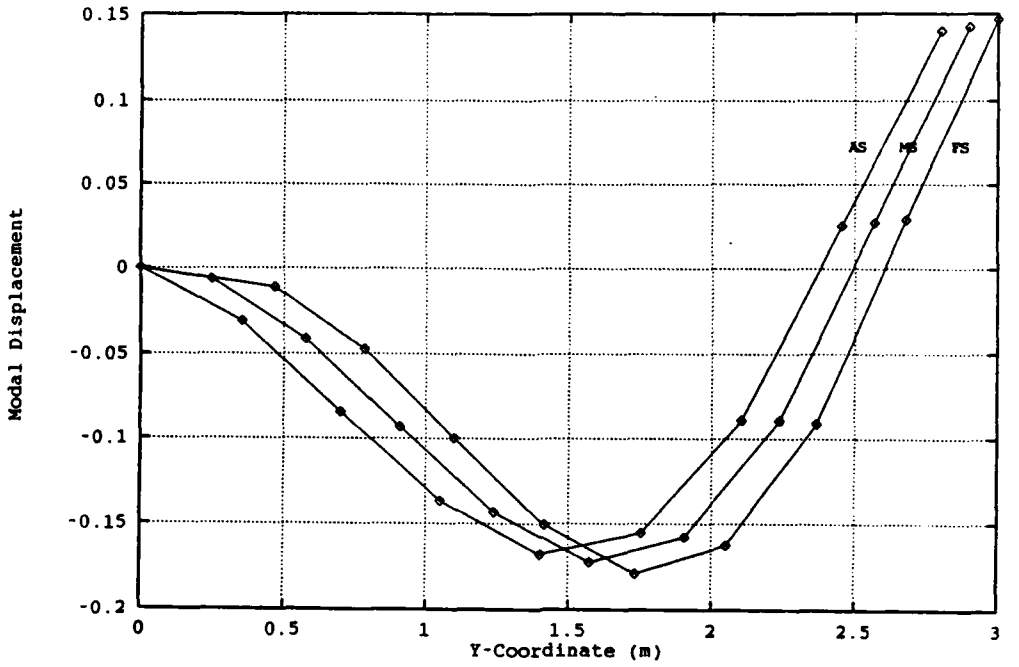

Figure A-3: Third mode of vibration (ω=53.9 hz) - stress constrained case.

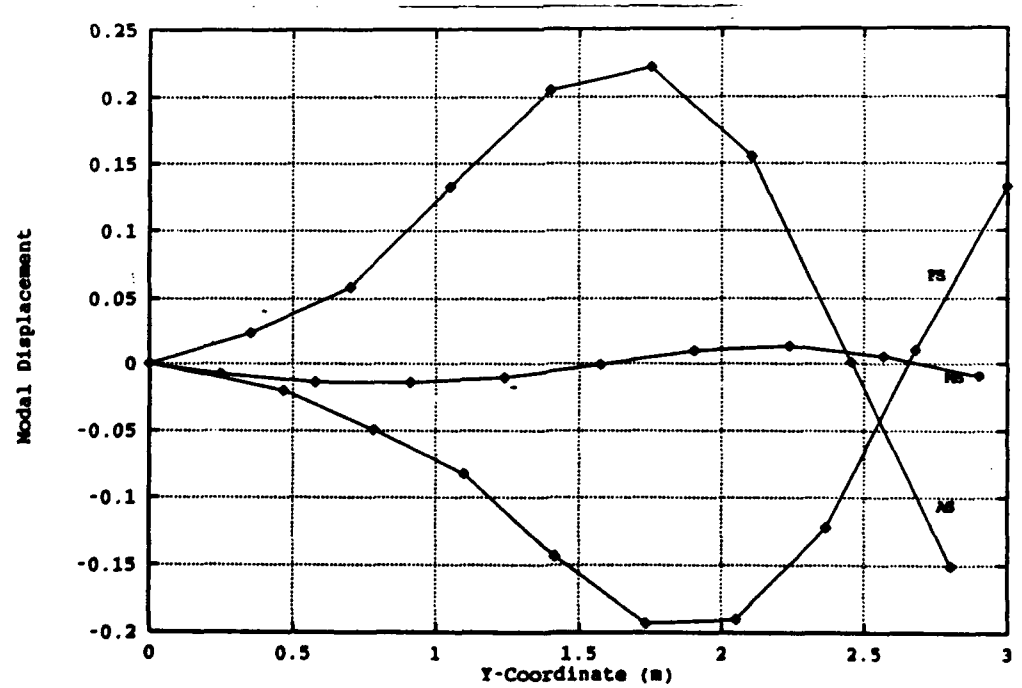

Figure A-4: Fourth mode of vibration (ω=89.5 hz) - stress constrained case.

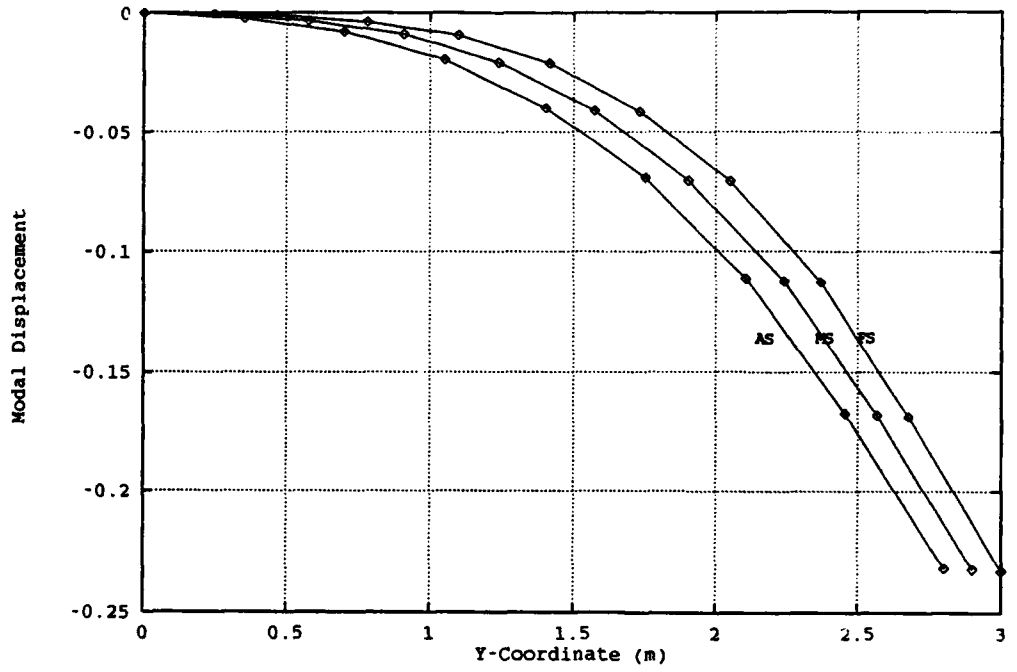

Figure A-5: First mode of vibration (ω=11.3 hz) - minimum gauge case.

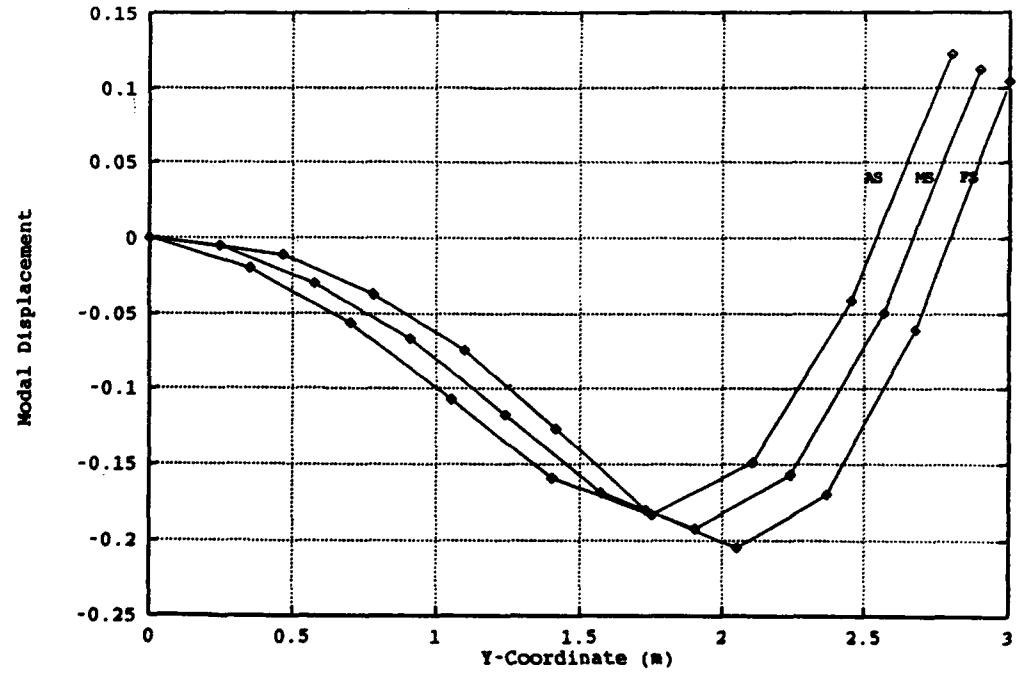

Figure A-6: Second mode of vibration (ω = 43.01 hz) - minimum gauge case.

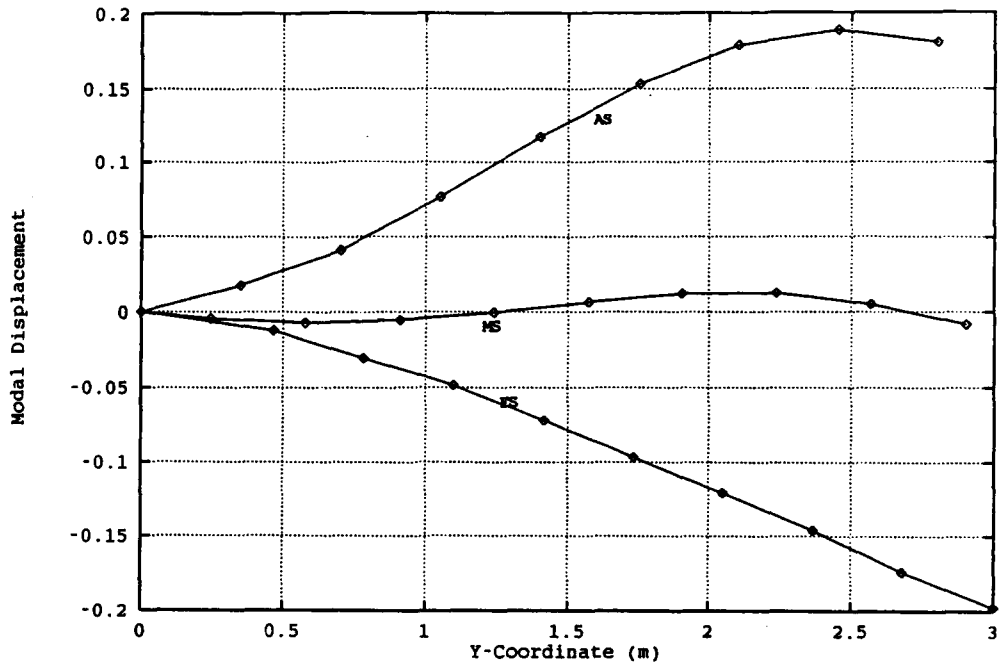

Figure A-7: Third mode of vibration (ω=55.23 hz) - minimum gauge case.

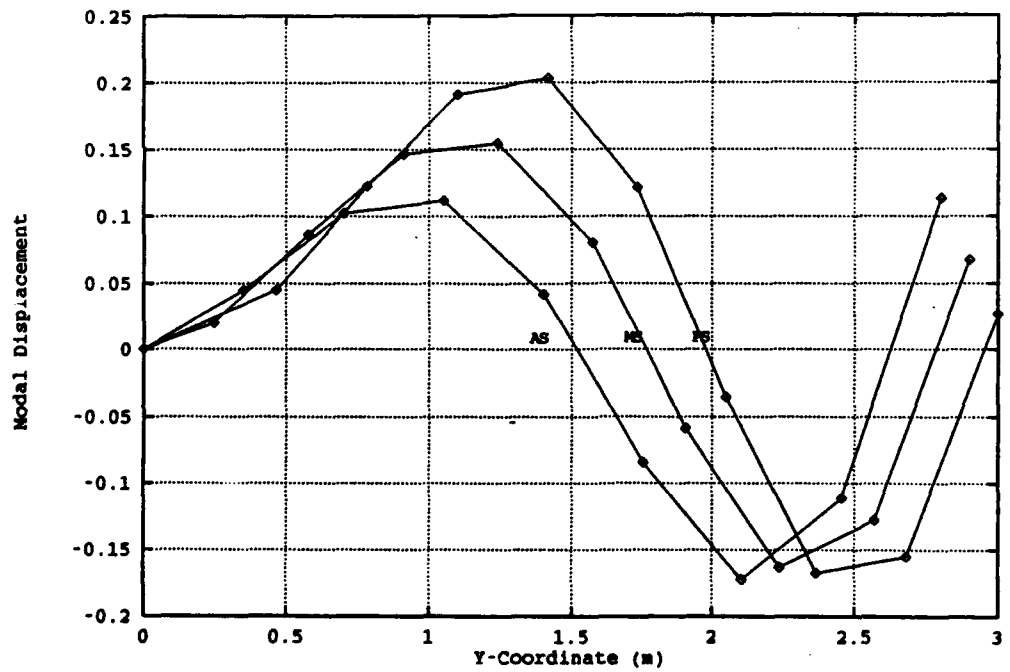

Figure A-8: Fourth mode of vibration (ω=97.7 hz) - minimum gauge case.

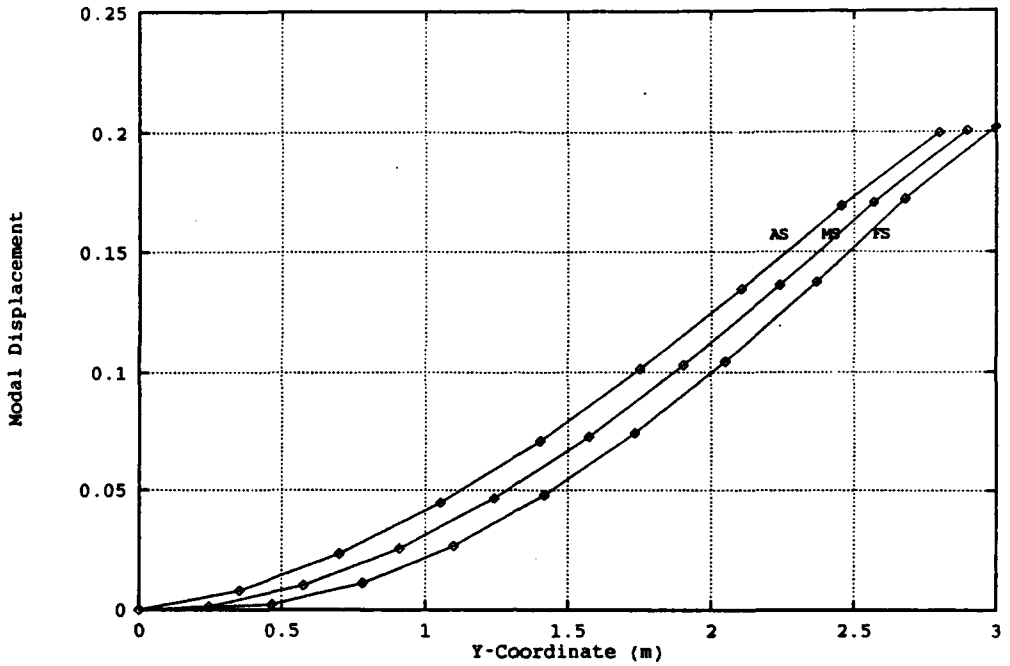

Figure A-9: First mode of vibration (ω=16.91 hz) - displacement constraint case.

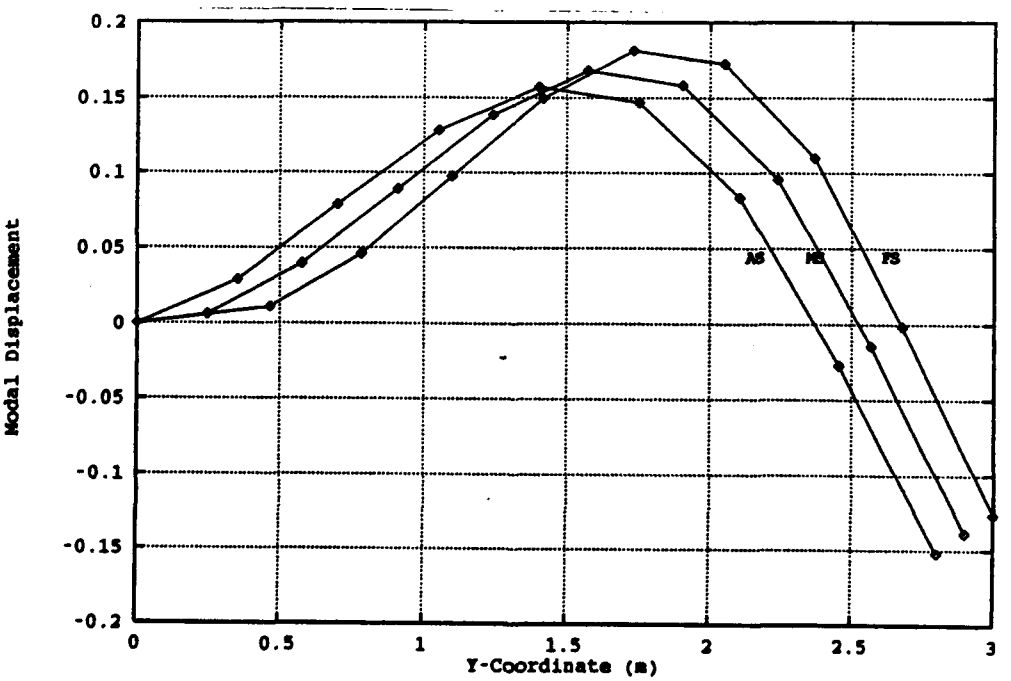

Figure A-10: Second mode of vibration (ω=50.6 hz) - displacement constraint case.

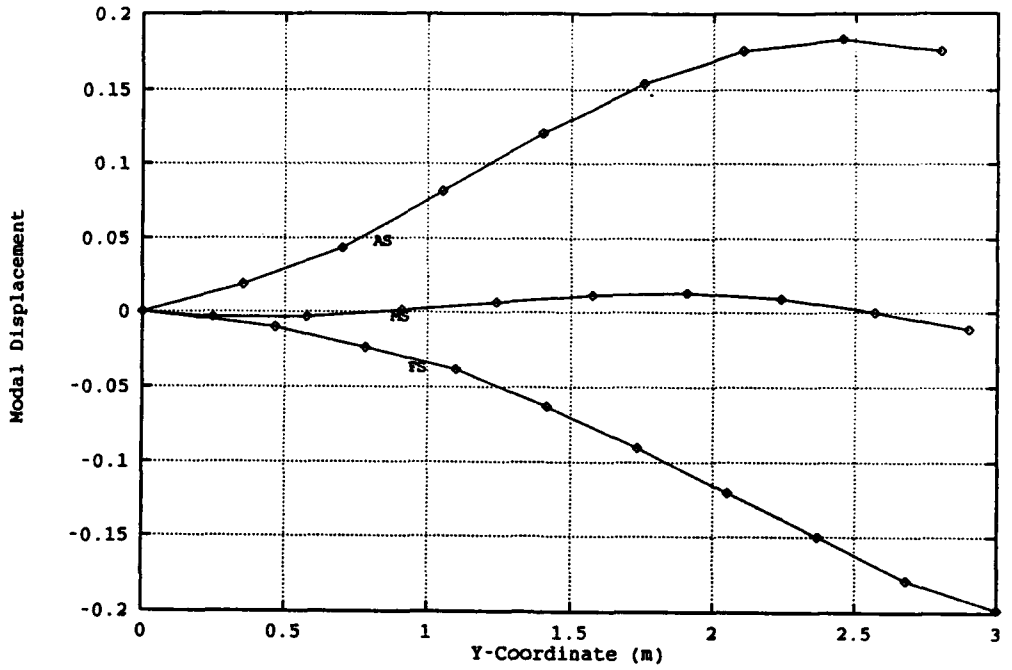

Figure A-11: Third mode of vibration (ω=56.8 hz) - displacement constraint case.

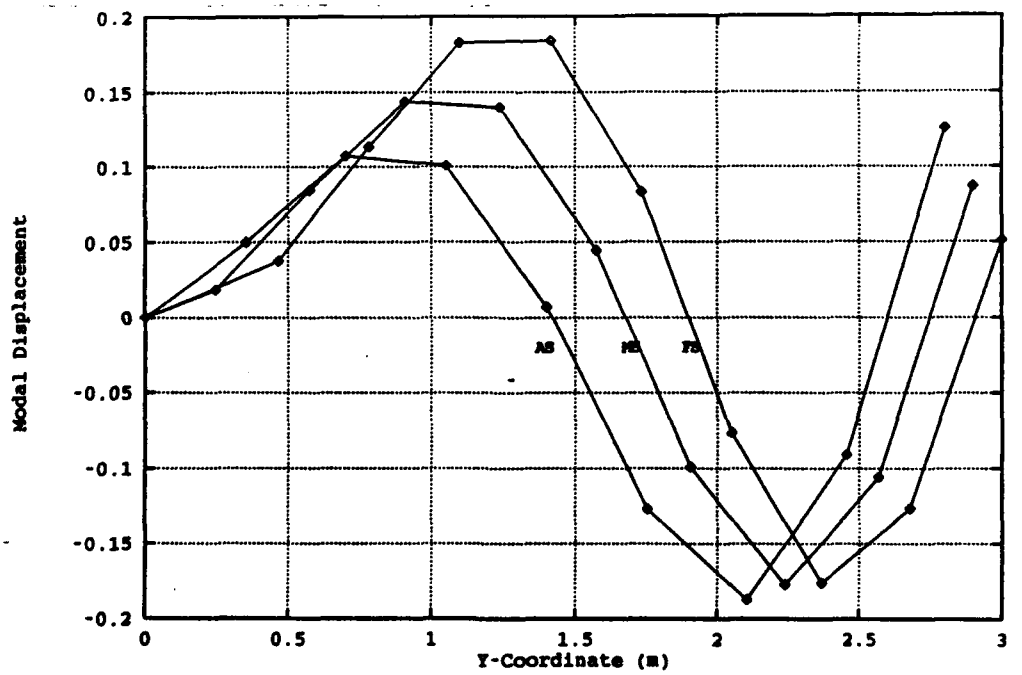

Figure A-12: Fourth mode of vibration (ω=106.3 hz) - displacement constraint case.

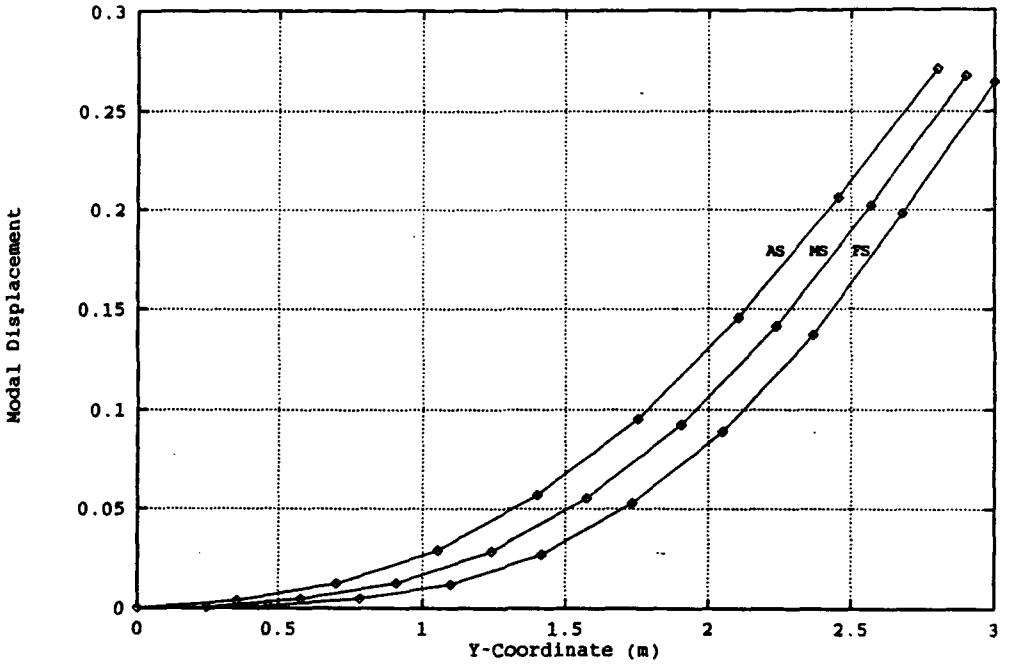

Figure A-13: First mode of vibration (ω=12.65 hz) - mass forward (minimum gauge) case.

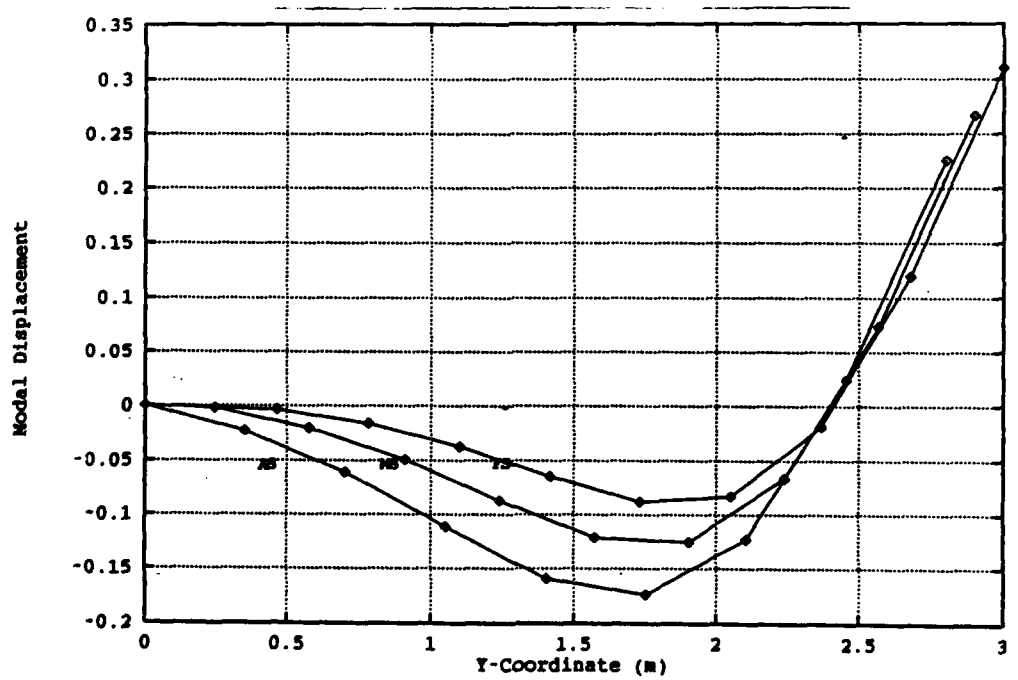

Figure A-14: Second mode of vibration (ω=42.8 hz) - mass forward (minimum gauge) case.

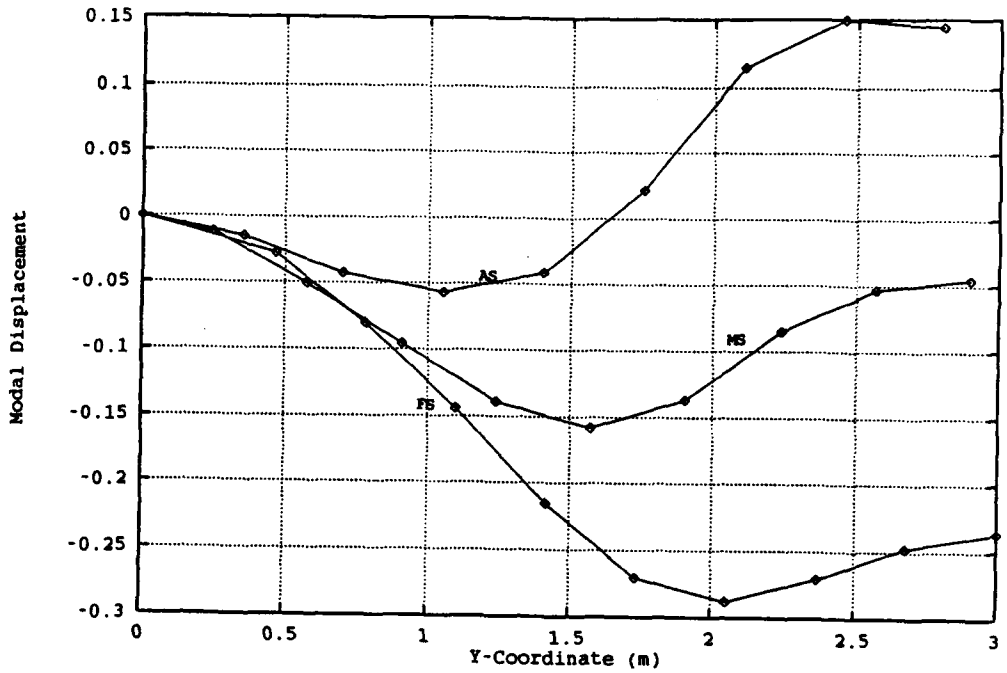

Figure A-15: Third mode of vibration (ω=75.41 hz) - mass forward (minimum gauge) case.

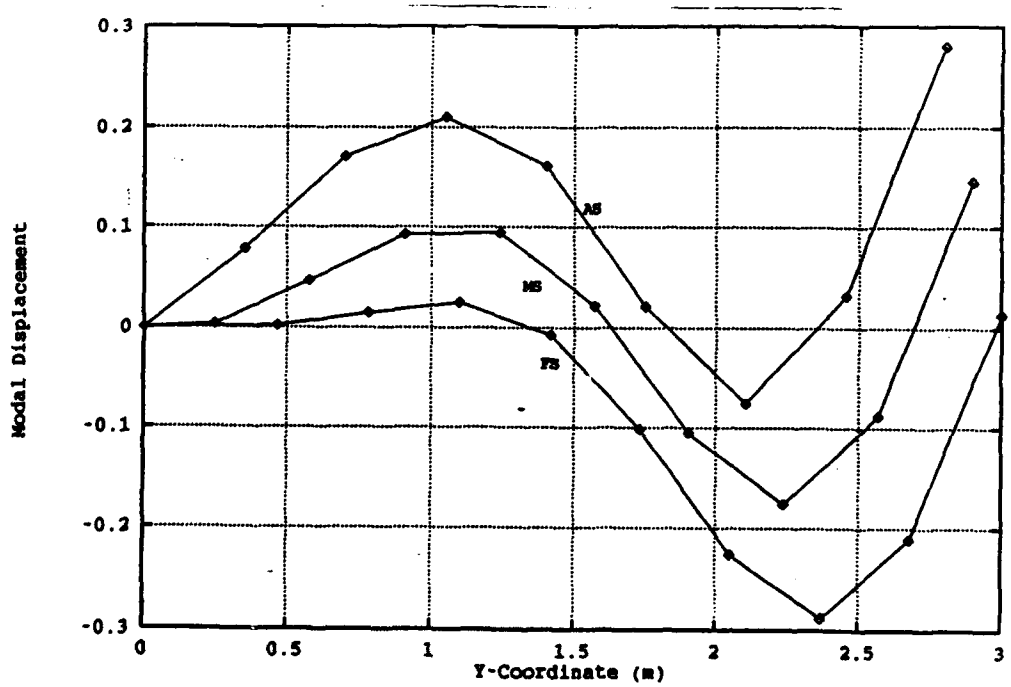

Figure A-16: Fourth mode of vibration (ω=90.58 hz) - mass forward (minimum gauge) case.

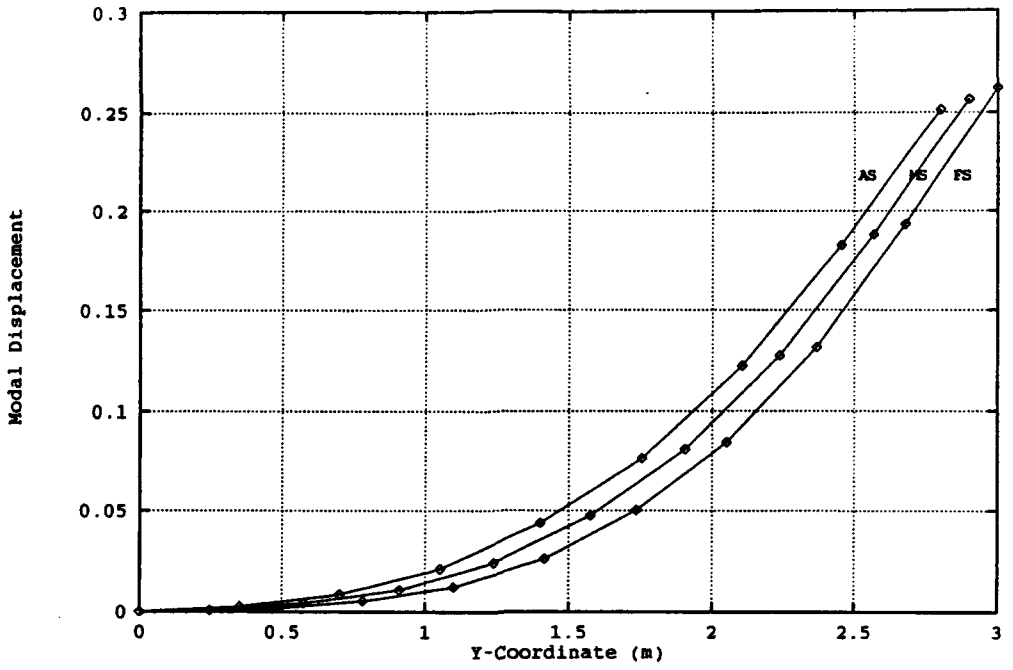

Figure A-17: First mode of vibration (ω=13.59 hz) - mass aft (minimum gauge) case.

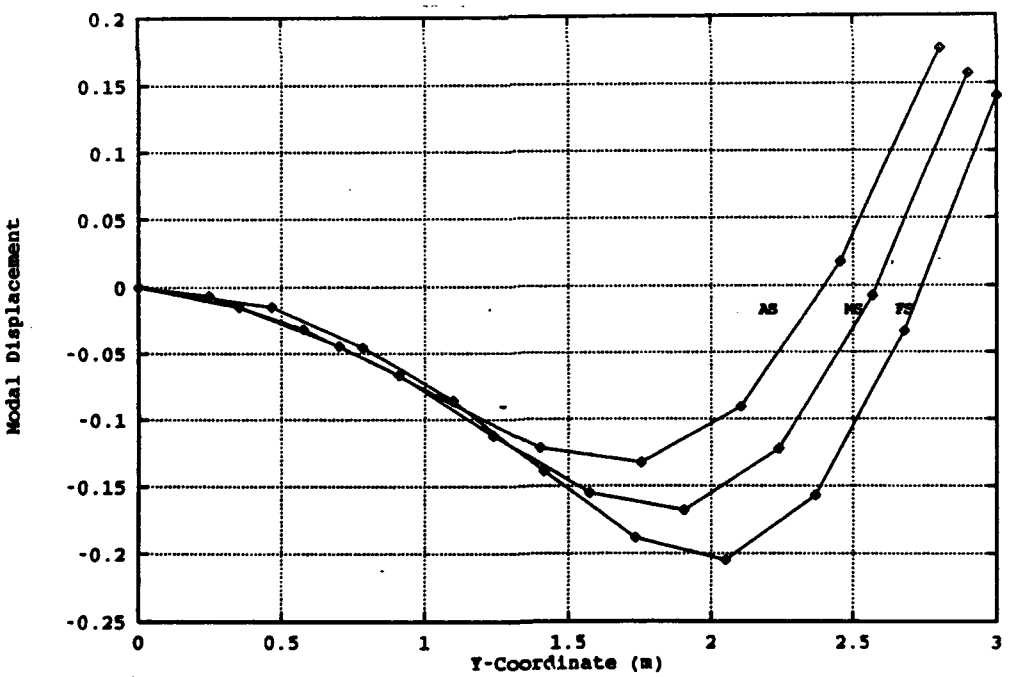

Figure A-18: Second mode of vibration (ω=43.42 hz) - mass aft (minimum gauge) case.

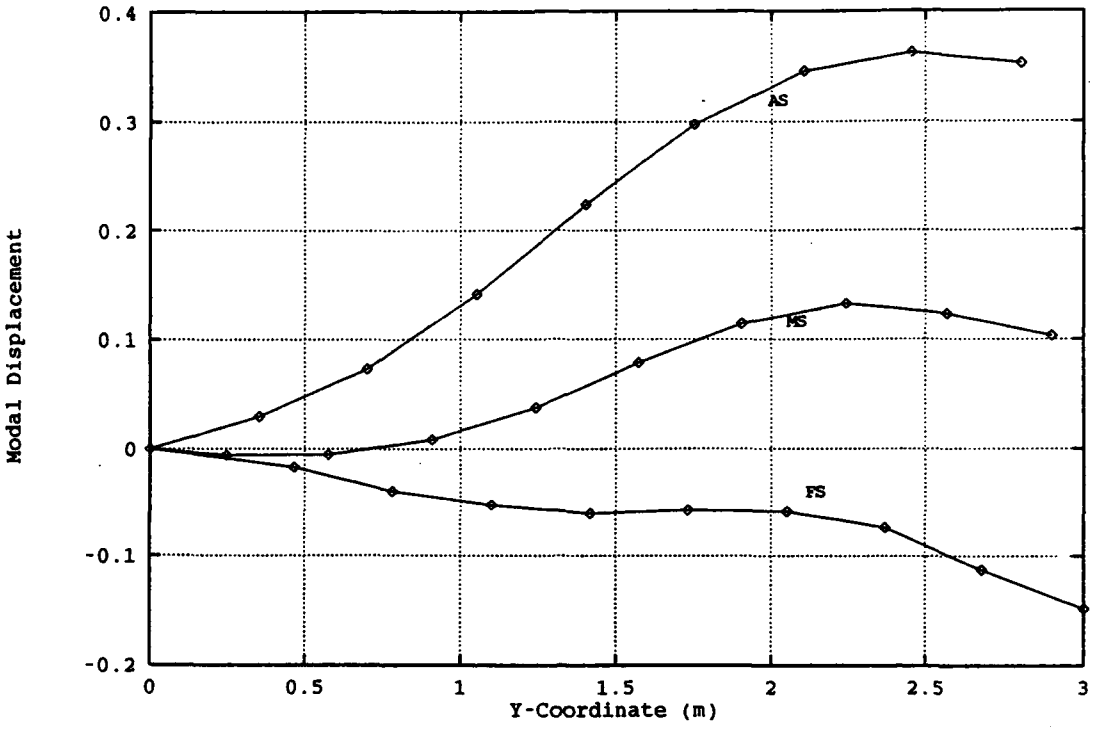

Figure A-19: Third mode of vibration (ω=72.8 hz) - mass aft (minimum gauge) case.

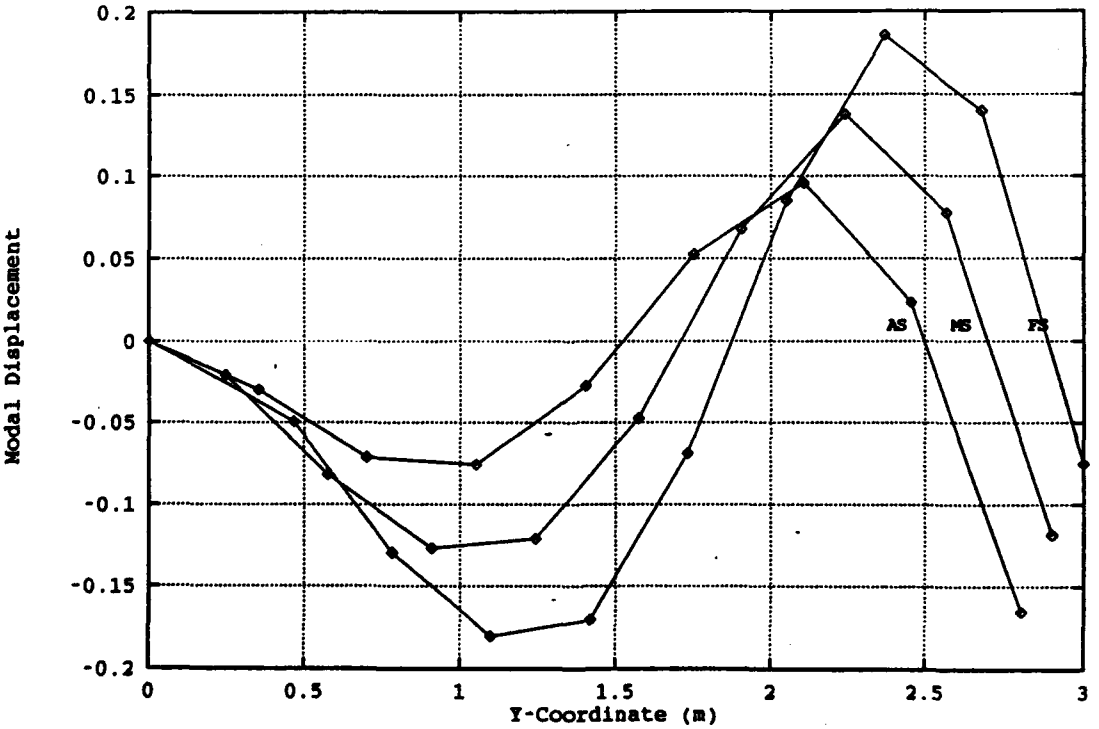

Figure A-20: Fourth mode of vibration (ω=100.84 hz) - mass aft (minimum gauge) case.

Appendix B : Input Data Decks

Four sample data decks are provided to demonstrate the procedure and to indicate the type of information that is required to submit the

(a) Structural Optimization Analysis,

(b) Static Aeroelastic Analysis,

(c) Flutter Analysis.

To reduce the amount of repetition, the first input data set is the structural definition. This definition is common among all three analysis. The lines beginning with a '$' are comment lines.

Tail Structural Definition

```
$    *     *     *     *     *     *     *     *     *
$ The SPC card enforces the boundary conditions necessary to cantilever
$ the root of the tail.
$
SPC1          1  123456      1      2      3     31     32     33
$
$ The MAT1 card defines the material properties of the aluminum.
$
MAT1            1 7.24e10            0.33   2800.                    +MAT
+MAT      2.76E8  2.76E8  1.89E8
$
$ Property Cards are Identified as follows...
$  PROD(1,2,3,4)  = Posts
$  PROD(5,6,7,8)  = Spars
$  PROD(9,10,11)  = Ribs
$  PSHELL(4) = Skin
$  PSHELL(5) = SparShear
$  PSHELL(6) = RibShear
$
```

```
$       The property cards give the cross-sectional area of the bar elements
$   and the thickness of panel elements.
$
PROD        1     1   0.01    1.0     1.0
PROD        2     1   0.01    1.0     1.0
PROD        3     1   0.01    1.0     1.0
PROD        4     1   0.01    1.0     1.0
PROD        5     1   0.01    1.0     1.0
PROD        6     1   0.01    1.0     1.0
PROD        7     1   0.01    1.0     1.0
PROD        8     1   0.01    1.0     1.0
PROD        9     1   0.01    1.0     1.0
PROD       10     1   0.01    1.0     1.0
PROD       11     1   0.01    1.0     1.0
$
PSHELL     12     1  0.001      1     1.     1          0.0
PSHELL     13     1  0.001      1     1.     1          0.0
PSHELL     14     1  0.001      1     1.     1          0.0
PSHELL     15     1  0.001      1     1.     1          0.0
PSHELL     16     1  0.001      1     1.     1          0.0
PSHELL     17     1  0.001      1     1.     1          0.0
PSHELL     18     1  0.001      1     1.     1          0.0
PSHELL     19     1  0.001      1     1.     1          0.0
PSHELL     20     1  0.001      1     1.     1          0.0
PSHELL     21     1  0.001      1     1.     1          0.0
$
GRDSET                                      456
$
$  GRID :  Nodal Point Definition.
$  CROD :  Nodal connectivity of the bar element.
$  QUAD4:  Nodal Connectivity of the Panel element.
$
GRID        1     0 0.60000 0.000000.060000     0
GRID        2     0 1.10000 0.000000.080000     0
GRID        3     0 1.60000 0.000000.060000     0
GRID        4     0 1.29550 0.244000.076747     0
GRID        5     0 1.01900 0.465400.055346     0
GRID        6     0 1.30413 0.782230.052178     0
GRID        7     0 1.56129 0.576250.072309     0
GRID        8     0 1.84296 0.350610.056494     0
GRID        9     0 1.58925 1.099050.049009     0
GRID       10     0 1.82708 0.908500.067887     0
GRID       11     0 2.08593 0.701220.052988     0
GRID       12     0 1.87438 1.415880.045841     0
GRID       13     0 2.09286 1.240750.063457     0
GRID       14     0 2.32889 1.051840.049482     0
GRID       15     0 2.15950 1.732700.042673     0
GRID       16     0 2.35865 1.573000.059027     0
GRID       17     0 2.57185 1.402450.045976     0
GRID       18     0 2.44463 2.049530.039505     0
```

```
GRID      19      0 2.62444 1.905250.054597      0
GRID      20      0 2.81481 1.753060.042469      0
GRID      21      0 2.72975 2.366350.036337      0
GRID      22      0 2.89023 2.237500.050167      0
GRID      23      0 3.05778 2.103670.038963      0
GRID      24      0 3.01488 2.683170.033168      0
GRID      25      0 3.15601 2.569750.045737      0
GRID      26      0 3.30074 2.454290.035471      0
GRID      27      0 3.30000 3.000000.030000      0
GRID      28      0 3.42180 2.902000.041307      0
GRID      29      0 3.54370 2.804900.031951      0
GRID      31      0 0.60000 0.00000-.060000      0
GRID      32      0 1.10000 0.00000-.080000      0
GRID      33      0 1.60000 0.00000-.060000      0
GRID      34      0 1.29550 0.24400-.076747      0
GRID      35      0 1.01900 0.46540-.055346      0
GRID      36      0 1.30413 0.78223-.052178      0
GRID      37      0 1.56129 0.57625-.072309      0
GRID      38      0 1.84296 0.35061-.056494      0
GRID      39      0 1.58925 1.09905-.049009      0
GRID      40      0 1.82708 0.90850-.067887      0
GRID      41      0 2.08593 0.70122-.052988      0
GRID      42      0 1.87438 1.41588-.045841      0
GRID      43      0 2.09286 1.24075-.063457      0
GRID      44      0 2.32889 1.05184-.049482      0
GRID      45      0 2.15950 1.73270-.042673      0
GRID      46      0 2.35865 1.57300-.059027      0
GRID      47      0 2.57185 1.40245-.045976      0
GRID      48      0 2.44463 2.04953-.039505      0
GRID      49      0 2.62444 1.90525-.054597      0
GRID      50      0 2.81481 1.75306-.042469      0
GRID      51      0 2.72975 2.36635-.036337      0
GRID      52      0 2.89023 2.23750-.050167      0
GRID      53      0 3.05778 2.10367-.038963      0
GRID      54      0 3.01488 2.68317-.033168      0
GRID      55      0 3.15601 2.56975-.045737      0
GRID      56      0 3.30074 2.45429-.035471      0
GRID      57      0 3.30000 3.00000-.030000      0
GRID      58      0 3.42180 2.90200-.041307      0
GRID      59      0 3.54370 2.80490-.031951      0
CROD      1       5       1       5
CROD      2       5       2       4
CROD      3       5       5       6
CROD      4       5       4       7
CROD      5       5       3       8
CROD      6       5       6       9
CROD      7       5       7       10
CROD      8       5       8       11
CROD      9       6       9       12
CROD      10      6       10      13
```

CROD	11	6	11	14			
CROD	12	6	12	15			
CROD	13	6	13	16			
CROD	14	6	14	17			
CROD	15	7	15	18			
CROD	16	7	16	19			
CROD	17	7	17	20			
CROD	18	7	18	21			
CROD	19	7	19	22			
CROD	20	7	20	23			
CROD	21	8	21	24			
CROD	22	8	22	25			
CROD	23	8	23	26			
CROD	24	8	24	27			
CROD	25	8	25	28			
CROD	26	8	26	29			
CROD	27	9	3	4			
CROD	28	9	4	5			
CROD	29	9	8	7			
CROD	30	9	7	6			
CROD	31	9	11	10			
CROD	32	9	10	9			
CROD	33	10	14	13			
CROD	34	10	13	12			
CROD	35	10	17	16			
CROD	36	10	16	15			
CROD	37	10	20	19			
CROD	38	10	19	18			
CROD	39	11	23	22			
CROD	40	11	22	21			
CROD	41	11	26	25			
CROD	42	11	25	24			
CROD	43	11	29	28			
CROD	44	11	28	27			
CTRIA3	45	12	3	4	2	0.0	
CQUAD4	46	12	2	4	5	1	0.0
CQUAD4	47	12	3	8	7	4	0.0
CQUAD4	48	12	4	7	6	5	0.0
CQUAD4	49	12	8	11	10	7	0.0
CQUAD4	50	12	7	10	9	6	0.0
CQUAD4	51	13	11	14	13	10	0.0
CQUAD4	52	13	10	13	12	9	0.0
CQUAD4	53	13	14	17	16	13	0.0
CQUAD4	54	13	13	16	15	12	0.0
CQUAD4	55	13	17	20	19	16	0.0
CQUAD4	56	13	16	19	18	15	0.0
CQUAD4	57	14	20	23	22	19	0.0
CQUAD4	58	14	19	22	21	18	0.0
CQUAD4	59	14	23	26	25	22	0.0
CQUAD4	60	14	22	25	24	21	0.0

```
CQUAD4     61     14     26     29     28     25     0.0
CQUAD4     62     14     25     28     27     24     0.0
CROD      101      5     31     35
CROD      102      5     32     34
CROD      103      5     35     36
CROD      104      5     34     37
CROD      105      5     33     38
CROD      106      5     36     39
CROD      107      5     37     40
CROD      108      5     38     41
CROD      109      6     39     42
CROD      110      6     40     43
CROD      111      6     41     44
CROD      112      6     42     45
CROD      113      6     43     46
CROD      114      6     44     47
CROD      115      7     45     48
CROD      116      7     46     49
CROD      117      7     47     50
CROD      118      7     48     51
CROD      119      7     49     52
CROD      120      7     50     53
CROD      121      8     51     54
CROD      122      8     52     55
CROD      123      8     53     56
CROD      124      8     54     57
CROD      125      8     55     58
CROD      126      8     56     59
CROD      127      9     33     34
CROD      128      9     34     35
CROD      129      9     38     37
CROD      130      9     37     36
CROD      131      9     41     40
CROD      132      9     40     39
CROD      133     10     44     43
CROD      134     10     43     42
CROD      135     10     47     46
CROD      136     10     46     45
CROD      137     10     50     49
CROD      138     10     49     48
CROD      139     11     53     52
CROD      140     11     52     51
CROD      141     11     56     55
CROD      142     11     55     54
CROD      143     11     59     58
CROD      144     11     58     57
CTRIA3    145     12     32     34     33     0.0
CQUAD4    146     12     35     34     32     31     0.0
CQUAD4    147     12     37     38     33     34     0.0
CQUAD4    148     12     36     37     34     35     0.0
```

```
CQUAD4    149    12    40    41    38    37    0.0
CQUAD4    150    12    39    40    37    36    0.0
CQUAD4    151    13    43    44    41    40    0.0
CQUAD4    152    13    42    43    40    39    0.0
CQUAD4    153    13    46    47    44    43    0.0
CQUAD4    154    13    45    46    43    42    0.0
CQUAD4    155    13    49    50    47    46    0.0
CQUAD4    156    13    48    49    46    45    0.0
CQUAD4    157    14    52    53    50    49    0.0
CQUAD4    158    14    51    52    49    48    0.0
CQUAD4    159    14    55    56    53    52    0.0
CQUAD4    160    14    54    55    52    51    0.0
CQUAD4    161    14    58    59    56    55    0.0
CQUAD4    162    14    57    58    55    54    0.0
CROD      201    1     35    5
CROD      202    1     34    4
CROD      203    1     36    6
CROD      204    1     37    7
CROD      205    1     38    8
CROD      206    2     39    9
CROD      207    2     40    10
CROD      208    2     41    11
CROD      209    2     42    12
CROD      210    2     43    13
CROD      211    2     44    14
CROD      212    3     45    15
CROD      213    3     46    16
CROD      214    3     47    17
CROD      215    3     48    18
CROD      216    3     49    19
CROD      217    3     50    20
CROD      218    4     51    21
CROD      219    4     52    22
CROD      220    4     53    23
CROD      221    4     54    24
CROD      222    4     55    25
CROD      223    4     56    26
CROD      224    4     57    27
CROD      225    4     58    28
CROD      226    4     59    29
CQUAD4    227    15    31    35    5     1     0.0
CQUAD4    228    15    32    34    4     2     0.0
CQUAD4    229    15    35    36    6     5     0.0
CQUAD4    230    15    34    37    7     4     0.0
CQUAD4    231    15    33    38    8     3     0.0
CQUAD4    232    15    36    39    9     6     0.0
CQUAD4    233    15    37    40    10    7     0.0
CQUAD4    234    15    38    41    11    8     0.0
CQUAD4    235    16    39    42    12    9     0.0
CQUAD4    236    16    40    43    13    10    0.0
```

```
CQUAD4    237    16    41    44    14    11    0.0
CQUAD4    238    16    42    45    15    12    0.0
CQUAD4    239    16    43    46    16    13    0.0
CQUAD4    240    16    44    47    17    14    0.0
CQUAD4    241    17    45    48    18    15    0.0
CQUAD4    242    17    46    49    19    16    0.0
CQUAD4    243    17    47    50    20    17    0.0
CQUAD4    244    17    48    5     21    18    0.0
CQUAD4    245    17    49    52    22    19    0.0
CQUAD4    246    17    50    53    23    20    0.0
CQUAD4    247    18    51    54    24    21    0.0
CQUAD4    248    18    52    55    25    22    0.0
CQUAD4    249    18    53    56    26    23    0.0
CQUAD4    250    18    54    57    27    24    0.0
CQUAD4    251    18    55    58    28    25    0.0
CQUAD4    252    18    56    59    29    26    0.0
CQUAD4    253    19    35    5     4     34    0.0
CQUAD4    254    19    34    4     3     33    0.0
CQUAD4    255    19    36    6     7     37    0.0
CQUAD4    256    19    37    7     8     38    0.0
CQUAD4    257    19    39    9     10    40    0.0
CQUAD4    258    19    40    10    11    41    0.0
CQUAD4    259    20    42    12    13    43    0.0
CQUAD4    260    20    43    13    14    44    0.0
CQUAD4    261    20    45    15    16    46    0.0
CQUAD4    262    20    46    16    17    47    0.0
CQUAD4    263    20    48    18    19    49    0.0
CQUAD4    264    20    49    19    20    50    0.0
CQUAD4    265    21    51    21    22    52    0.0
CQUAD4    266    21    52    22    23    53    0.0
CQUAD4    267    21    54    24    25    55    0.0
CQUAD4    268    21    55    25    26    56    0.0
CQUAD4    269    21    57    27    28    58    0.0
CQUAD4    270    21    58    28    29    59    0.0
ENDDATA
```

Structural Optimization Analysis

This is a sample listing from the 21 design variable input deck. The constraints which are active are stress, minimum gauge, and tip deflection (node 28). The applied force is the rigid aerodynamic loads for Mach number = 0.4 and the angle of attack = 30 degrees.

```
ID OPTIMIZE,STATIC
SOL 200 $ Static Analysis & Optimization
```

```
TIME 120
CEND
TITLE = STRENGTH OPTIMIZATION OF WINGBOX
SPC = 1
PARAM, APPC, STATICS
LOAD  = 31
DISP  = ALL
STRESS = ALL
BEGIN BULK
$
$        MODEL MEASURED IN SI UNITS
$           LENGTH = M
$           FORCE  = NEWTONS
$           TIME   = SECONDS
$           GRAV   = 9.81 M/S^2
$
$#########################################################
$                DESIGN  MODEL
$
$
$
$  DESVAR(1,2,3,4)   = Posts
$  DESVAR(5,6,7,8)   = Spars
$  DESVAR(9,10,11)   = Ribs
$  DESVAR(12,13,14)  = Skin
$  DESVAR(15,16,17,18) = SparShear
$  DESVAR(19,20,21)  = RibShear
$
$       DESVAR : Design Variable Definition
$          ID  Label  Start    Minimum  Maximum
$                     Value     Value    Value
$
DESVAR       1  ST11 .100E-04  1.E-5     10.
DESVAR       2  ST12 .151E-04  1.E-5     10.
DESVAR       3  ST13 .151E-04  1.E-5     10.
DESVAR       4  ST14 .851E-04  1.E-5     10.
DESVAR       5  ST15 .514E-04  1.E-5     10.
DESVAR       6  ST16 .731E-04  1.E-5     10.
DESVAR       7  ST17 .751E-04  1.E-5     10.
DESVAR       8  ST18 .598E-04  1.E-5     10.
DESVAR       9  ST19 .411E-04  1.E-5     10.
DESVAR      10  ST20 .801E-04  1.E-5     10.
DESVAR      11  ST21 .801E-04  1.E-5     10.
$
DESVAR      12  SP22 .227E-02  1.E-3      .1
DESVAR      13  SP23 .100E-02  1.E-3      .1
DESVAR      14  SP24 .132E-02  1.E-3      .1
DESVAR      15  SP25 .161E-02  1.E-3      .1
DESVAR      16  SP26 .195E-02  1.E-3      .1
DESVAR      17  SP27 .169E-02  1.E-3      .1
```

```
DESVAR      18  SP28 .101E-02  1.E-3     .1
DESVAR      19  SP29 .964E-02  1.E-3     .1
DESVAR      20  SP30 .992E-02  1.E-3     .1
DESVAR      21  SP31 .940E-02  1.E-3     .1
$
$       DVPREL1 : Corrolation between design variables and structural
$           properties (Property Cards)
$
DVPREL1       1   PROD      1     4  1.E-5              +DP1
+DP1          1   1.0
DVPREL1       2   PROD      2     4  1.E-5              +DP2
+DP2          2   1.0
DVPREL1       3   PROD      3     4  1.E-5              +DP3
+DP3          3   1.0
DVPREL1       4   PROD      4     4  1.E-5              +DP4
+DP4          4   1.0
DVPREL1       5   PROD      5     4  1.E-5              +DP5
+DP5          5   1.0
DVPREL1       6   PROD      6     4  1.E-5              +DP6
+DP6          6   1.0
DVPREL1       7   PROD      7     4  1.E-5              +DP7
+DP7          7   1.0
DVPREL1       8   PROD      8     4  1.E-5              +DP8
+DP8          8   1.0
DVPREL1       9   PROD      9     4  1.E-5              +DP9
+DP9          9   1.0
DVPREL1      10   PROD     10     4  1.E-5              +DP10
+DP10        10   1.0
DVPREL1      11   PROD     11     4  1.E-5              +DP11
+DP11        11   1.0
$
DVPREL1      12  PSHELL    12     4  1.E-3              +DP12
+DP12        12   1.0
DVPREL1      13  PSHELL    13     4  1.E-3              +DP13
+DP13        13   1.0
DVPREL1      14  PSHELL    14     4  1.E-3              +DP14
+DP14        14   1.0
DVPREL1      15  PSHELL    15     4  1.E-3              +DP15
+DP15        15   1.0
DVPREL1      16  PSHELL    16     4  1.E-3              +DP16
+DP16        16   1.0
DVPREL1      17  PSHELL    17     4  1.E-3              +DP17
+DP17        17   1.0
DVPREL1      18  PSHELL    18     4  1.E-3              +DP18
+DP18        18   1.0
DVPREL1      19  PSHELL    19     4  1.E-3              +DP19
+DP19        19   1.0
DVPREL1      20  PSHELL    20     4  1.E-3              +DP20
+DP20        20   1.0
DVPREL1      21  PSHELL    21     4  1.E-3              +DP21
```

```
+DP21       21    1.0
$
DRESP1       1     S1  STRESS    PROD          2          1
DRESP1       2     S2  STRESS    PROD          2          2
DRESP1       3     S3  STRESS    PROD          2          3
DRESP1       4     S4  STRESS    PROD          2          4
DRESP1       5     S5  STRESS    PROD          2          5
DRESP1       6     S6  STRESS    PROD          2          6
DRESP1       7     S7  STRESS    PROD          2          7
DRESP1       8     S8  STRESS    PROD          2          8
DRESP1       9     S9  STRESS    PROD          2          9
DRESP1      10    S10  STRESS    PROD          2         10
DRESP1      11    S11  STRESS    PROD          2         11
DRESP1      12    S12  STRESS  PSHELL          7         12
DRESP1      13    S13  STRESS  PSHELL          7         13
DRESP1      14    S14  STRESS  PSHELL          7         14
DRESP1      15    S15  STRESS  PSHELL          7         15
DRESP1      16    S16  STRESS  PSHELL          7         16
DRESP1      17    S17  STRESS  PSHELL          7         17
DRESP1      18    S18  STRESS  PSHELL          7         18
DRESP1      19    S19  STRESS  PSHELL          7         19
DRESP1      20    S20  STRESS  PSHELL          7         20
DRESP1      21    S21  STRESS  PSHELL          7         21
DRESP1      22    S22  STRESS  PSHELL          8         12
DRESP1      23    S23  STRESS  PSHELL          8         13
DRESP1      24    S24  STRESS  PSHELL          8         14
DRESP1      25    S25  STRESS  PSHELL          8         15
DRESP1      26    S26  STRESS  PSHELL          8         16
DRESP1      27    S27  STRESS  PSHELL          8         17
DRESP1      28    S28  STRESS  PSHELL          8         18
DRESP1      29    S29  STRESS  PSHELL          8         19
DRESP1      30    S30  STRESS  PSHELL          8         20
DRESP1      31    S31  STRESS  PSHELL          8         21
DRESP1      32    S32  STRESS  PSHELL          9         12
DRESP1      33    S33  STRESS  PSHELL          9         13
DRESP1      34    S34  STRESS  PSHELL          9         14
DRESP1      35    S35  STRESS  PSHELL          9         15
DRESP1      36    S36  STRESS  PSHELL          9         16
DRESP1      37    S37  STRESS  PSHELL          9         17
DRESP1      38    S38  STRESS  PSHELL          9         18
DRESP1      39    S39  STRESS  PSHELL          9         19
DRESP1      40    S40  STRESS  PSHELL          9         20
DRESP1      41    S41  STRESS  PSHELL          9         21
DRESP1      43    D43  DISP                    3         28
DRESP1      45      W  WEIGHT
$
DESOBJ      45      W         MIN
$
$       Stress Constraint Definitions
$
```

```
DCONSTR      1    ALL -2.76E8  2.76E8
DCONSTR      2    ALL -2.76E8  2.76E8
DCONSTR      3    ALL -2.76E8  2.76E8
DCONSTR      4    ALL -2.76E8  2.76E8
DCONSTR      5    ALL -2.76E8  2.76E8
DCONSTR      6    ALL -2.76E8  2.76E8
DCONSTR      7    ALL -2.76E8  2.76E8
DCONSTR      8    ALL -2.76E8  2.76E8
DCONSTR      9    ALL -2.76E8  2.76E8
DCONSTR     10    ALL -2.76E8  2.76E8
DCONSTR     11    ALL -2.76E8  2.76E8
DCONSTR     12    ALL -2.76E8  2.76E8
DCONSTR     13    ALL -2.76E8  2.76E8
DCONSTR     14    ALL -2.76E8  2.76E8
DCONSTR     15    ALL -2.76E8  2.76E8
DCONSTR     16    ALL -2.76E8  2.76E8
DCONSTR     17    ALL -2.76E8  2.76E8
DCONSTR     18    ALL -2.76E8  2.76E8
DCONSTR     19    ALL -2.76E8  2.76E8
DCONSTR     20    ALL -2.76E8  2.76E8
DCONSTR     21    ALL -2.76E8  2.76E8
DCONSTR     22    ALL -2.76E8  2.76E8
DCONSTR     23    ALL -2.76E8  2.76E8
DCONSTR     24    ALL -2.76E8  2.76E8
DCONSTR     25    ALL -2.76E8  2.76E8
DCONSTR     26    ALL -2.76E8  2.76E8
DCONSTR     27    ALL -2.76E8  2.76E8
DCONSTR     28    ALL -2.76E8  2.76E8
DCONSTR     29    ALL -2.76E8  2.76E8
DCONSTR     30    ALL -2.76E8  2.76E8
DCONSTR     31    ALL -2.76E8  2.76E8
DCONSTR     32    ALL -2.76E8  2.76E8
DCONSTR     33    ALL -2.76E8  2.76E8
DCONSTR     34    ALL -2.76E8  2.76E8
DCONSTR     35    ALL -2.76E8  2.76E8
DCONSTR     36    ALL -2.76E8  2.76E8
DCONSTR     37    ALL -2.76E8  2.76E8
DCONSTR     38    ALL -2.76E8  2.76E8
DCONSTR     39    ALL -2.76E8  2.76E8
DCONSTR     40    ALL -2.76E8  2.76E8
DCONSTR     41    ALL -2.76E8  2.76E8
DCONSTR     43    ALL   -.10    .10
$
DSCREEN      1 STRESS    -.1
DSCREEN      2   DISP    -1.
DOPTPRM      2           20
$
$    *    *    *    *    *    *    *    *    *
$##################################################
$        ANALYSIS MODEL
```

```
$
$
PARAM    AUTOSPC     YES
$
$    *      *      *      *      *      *      *      *      *
$  Nodal Forces from aerodynamic loads at M=0.4 aoa = 10 deg. This
$  data was collected from aeroelastic analysis.
$
FORCE       30      5          11502.     0.     0.     1.
FORCE       30      4             13.     0.     0.     1.
FORCE       30      6           2463.     0.     0.     1.
FORCE       30      7          -3545.     0.     0.     1.
FORCE       30      8           1752.     0.     0.     1.
FORCE       30      9           5186.     0.     0.     1.
FORCE       30     10          -1645.     0.     0.     1.
FORCE       30     11           1159.     0.     0.     1.
FORCE       30     12           4698.     0.     0.     1.
FORCE       30     13          -1988.     0.     0.     1.
FORCE       30     14           1223.     0.     0.     1.
FORCE       30     15           4691.     0.     0.     1.
FORCE       30     16          -1935.     0.     0.     1.
FORCE       30     17           1177.     0.     0.     1.
FORCE       30     18           4477.     0.     0.     1.
FORCE       30     19          -1885.     0.     0.     1.
FORCE       30     20           1071.     0.     0.     1.
FORCE       30     21           4122.     0.     0.     1.
FORCE       30     22          -1756.     0.     0.     1.
FORCE       30     23            882.     0.     0.     1.
FORCE       30     24           3467.     0.     0.     1.
FORCE       30     27           1746.     0.     0.     1.
FORCE       30     25          -1406.     0.     0.     1.
FORCE       30     26            735.     0.     0.     1.
FORCE       30     28           -810.     0.     0.     1.
FORCE       30     29           -431.     0.     0.     1.
$  TOTAL AERODYNAMIC LIFT =     34963.6 NEWTONS.
$    *      *      *      *      *      *      *      *      *
$ The forces are incremented to a 30 deg aoa by multiplying the forces
$ by 3.0 since for rigid aerodynamics the force is linear with respect
$ to aoa.
$              <...>
LOAD        31    3.0    1.0     30
$    *      *      *      *      *      *      *      *      *
```

Static Aeroelasticity

The following data deck is a sample deck from the aeroelastic analysis of one of the designs at an angle of attack of 30 degrees at a Mach number of 0.4. (dynamic

pressure of 11348 N/m^2)

```
NASTRAN
ID AERO,STATIC
SOL 21 $ Static Aero Analysis
TIME 5
COMPILE SOL21 SOUIN=MSCSOU NOLIST NOREF
$
$  This alter section forces the output to split the aerodynamic
$  loads into the rigid contribution and the flexible contribution.
$ >>>>>>>>
alter 1102 $ V66A & V67
IF ( NORSET>-1 ) UPARTN   USET,KAAa/KaALL,,,/'A'/'L'/'R'/0 $
ALTER 1169 $ V66A
MPYAD KALX, UX, /ALOAD/ $
SMPYAD   MSLR,RT,TRX,ux,,/ILOAD/4/////1 $
ADD ILOAD, ALOAD/ TLOAD/ $
 MATGPR GPL, USET, SIL, ILOAD//'X'/'L'/ $
 MATGPR GPL, USET, SIL, ALOAD//'X'/'L'/ $
 MATGPR GPL, USET, SIL, TLOAD//'X'/'L'/ $
 MATGPR GPL, USET, SIL, PLX//'X'/'L'/ $
alter 1170 $ V66A
mpyad kaall, ul, /aeload/ $
 MATGPR GPL, USET, SIL, aeload//'X'/'L'/ $
$<<<<<<<<<<
CEND
TITLE =  3 SPAR SWEPT WING
SUBTI = STATIC AERODYNAMICS (Cantilevered Wing)
$
$
SEALL = ALL
SPC    = 1
LOAD   = 30    $ only for stab. der. (supported structure case)
DISP   = ALL
STRESS = ALL
AEROF  = ALL
APRES  = ALL
subcase 1
 TRIM   = 1001
subcase 2
 trim   = 1002
$
BEGIN BULK
$          MODEL MEASURED IN SI UNITS
$             LENGTH = M
$             FORCE  = NEWTONS
$             TIME   = SECONDS
$             GRAV   = 9.81 M/S^2
$
$   STEADY AERO MODEL
```

```
$
$      for sea level      P = 101325. N/m^2   dens = 1.225 kg/m^3
$                         a = 340.290 m/s
$
PARAM   COUPMASS      1
PARAM    GRDPNT     60
$############## Restraint/Lump Mass ####################
SUPORT       60    345
ASET1         3     4   THRU     29
ASET1         3    34   THRU     59
SPC1          1   126     60
SPC1          1   456      4   thru     29
SPC1          1   456     34   thru     59
RBE2        301     60  123456     32     31      1      2      3+RB2
+RB2         33
$
GRAV          10          9.810    0.0    0.0   -1.0
FORCE         20     60          1.+11    0.0    0.0    1.0
LOAD          30    1.0    1.0     10    1.0     20
CONM2        310     60      0  1.+11                          +CM2
+CM2       1.+11          1.+11
PARAM     WTMASS.1019368
PARAM     AUNITS.1019368
$****************** Wing Position Axis *********************************
$      CID     RID     A1      A2      A3      B1      B2      B3
CORD2R 2             0.0     0.0     0.0     0.      0.      15.0    +CORD2
$      C1      C2      C3
+CORD2 2.0     0.0     15.0
$
$****************** Wing Stability Axis ********************************
$      CID     RID     A1      A2      A3      B1      B2      B3
$      *       *       *       *       *       *       *       *       *
CORD2R 11      2       1.1     0.0     0.0     1.1     0.0     1.0     +CORD11
$      C1      C2      C3
+CORD11 2.0    0.0     1.0
$*************************************************************************
$                                       SYMXZ   SYMXY
AEROS              11    2.4     6.0    5.40       1
CAERO1      2001    2000       2      10       8                  1+CARO
+CARO        0.0     0.0     0.0   2.400   3.000   3.000     0.0   1.200
PAERO1      2000
$
$########################## Trim Conditions ############################
$
AESTAT       500  ANGLEA
AESTAT       501  PITCH
AESTAT       503  URDD3
AESTAT       504  URDD5
AESTAT       505  URDD4
$
```

```
TRIM        1001    0.40  11348.  ANGLEA 0.52360   PITCH     0.0
$
$#########################################################################
$
$     5 deg = .08727      20 deg = .34910     35 deg = .61087
$    10 deg = .17453      25 deg = .43633     40 deg = .69813
$    15 deg = .26180      30 deg = .52360     45 deg = .78540
$
$          AERODYNAMICS  ==>  STRUCTURE
$
SPLINE1     2000    2001    2001    2080      17      0.
SET1         17      4    thru      29
$
$
$ !!!!!!! Insert Structural Data Here. !!!!!!!!!!!!!!!!!!!!!!!!!!!!!!!!!!!!
```

Flutter Analysis

The following input deck provided the data necessary to estimate the flutter speed of the vertical tail design.

```
ID KMETHOD,FLUTTER
SOL 75  $  FLUTTER ANALYSIS
TIME 10
CEND
TITLE =  SWEPT WING
LABEL =  FLUTTER ANALYSIS  (K-Method)
SEALL = ALL
SPC = 1
METHOD = 2
CMETHOD = 4          $ K-Method
FMETHOD = 3
SVEC = ALL           $ Vibration Modes
$Disp = all          $ Flutter Modes
$
BEGIN BULK
PARAM   COUPMASS      1
PARAM    GRDPNT      60
PARAM    LMODES       6
$
$******************** Wing Position Axis **********************************
$      CID     RID     A1      A2      A3      B1      B2      B3
CORD2R  2              0.0     0.0     1.0     0.      0.      15.0    +CORD2
$      C1      C2      C3
+CORD2  2.0     0.0     15.0
$
$   UNSTEADY AERO CARDS
```

```
$
AERO        0     1.   1.20   1.23      1      1
CAERO1     1001   1000      2     10      8                    1+CARO
+CARO      0.0    0.0    0.0   2.400   3.000   3.000    0.0   1.200
PAERO1     1000
$
$   AERO-STRUCTURE
$
SPLINE1      8   1001   1001   1080     17     0.
SET1        17     4   thru     29
$
$    FLUTTER FLIGHT CONDITION
$
FLUTTER      3      K    911    912    913     1      4
FLFACT     911      1.
$              Mach #
FLFACT     912     .8
$
$  for varying MACH #  change (1) MKAERO1 and (2) FLFACT 912
$
FLFACT     913   0.99    .800   .700   .600   .500   .450   .400+FLF1
+FLF1      .360   .340   .320   .300   .290   .280   .270   .260+FLF2
+FLF2      .255   .250   .245   .240   .235   .230   .225   .220+FLF3
+FLF3      .215   .205   .190   .180   .170   .160   .150   .140
MKAERO1      .8                                              +MKAROa
+MKAROa    1.00   .700   .600   .500   .400   .320   .300   .290
MKAERO1      .8                                              +MKAROb
+MKAROb    .280   .270   .260   .240   .225   .210   .205   .200
MKAERO1      .8                                              +MKAROc
+MKAROc    .195   .190   .180   .170   .160   .150   .140   .130
$
EIGR         2    GIV                      6
EIGC         4    HESS    MAX                              +EGC
+EGC                                          6
SPC1         1    123      1      2      3     31     32     33
SPC1         1    123     60
$ restrict modal analysis to displacements in the '3' coordinate direction.
$
ASET1        3      4   THRU     29
ASET1        3     34   THRU     59
$
$  Concentrated masses at selected nodal points.
$
CONM2      501      5            2.    0.0
CONM2      502      6            2.    0.0
CONM2      503      9            2.    0.0
CONM2      504     12            2.    0.0
CONM2      505     15            2.    0.0
CONM2      506     18            2.    0.0
CONM2      507     21            2.    0.0
```

```
CONM2     508     24          2.    0.0
CONM2     509     27          2.    0.0
CONM2     510     36          2.    0.0
CONM2     511     42          2.    0.0
CONM2     512     48          2.    0.0
CONM2     513     54          2.    0.0
CONM2     514     10          2.    0.0
CONM2     515     16          2.    0.0
CONM2     516     22          2.    0.0
CONM2     517     29          2.    0.0
$
$
$!!!!!!!!!!!! Put Structural Definition Data in here.!!!!!!!!!!!!!!!!!!
```

VITA

Captain David G. Miller was born on 17 July 1964 in Ankara, Turkey to U.S. Parents. He graduated from Civic Memorial High School, Bethalto, Illinois in 1983 and entered the University of Missouri-Rolla from which he received the Bachelor of Aerospace Engineering in 1987. Upon graduation, he was commissioned a second lieutenant in the USAF through the AFROTC program. He entered active duty at the Aeronautical Systems Division, Engineering Support Organization at Wright-Patterson AFB, Ohio where he served as an air transportable engineer. David entered the School of Engineering, Air Force Institute of Technology, in June 1991. His follow on assignment from AFIT is in the structures division at the Sacramento ALC.

Permanent Address :

1807 Bronzeleaf
Dayton, OH
45424

REPORT DOCUMENTATION PAGE

1. AGENCY USE ONLY (Leave blank)	2. REPORT DATE	3. REPORT TYPE AND DATES COVERED
	December 1992	Master's Thesis

4. TITLE AND SUBTITLE
THE INFLUENCE OF STRUCTURAL OPTIMIZATION ON THE AEROELASTIC PROPERTIES OF A VERTICAL TAIL

5. FUNDING NUMBERS

6. AUTHOR(S)
David G. Miller, Captain, USAF

7. PERFORMING ORGANIZATION NAME(S) AND ADDRESS(ES)
Air Force Institute of Technology
WPAFB OH 45433

8. PERFORMING ORGANIZATION REPORT NUMBER
AFIT/GAE/ENY/92D-24

9. SPONSORING/MONITORING AGENCY NAME(S) AND ADDRESS(ES)
Dr. James Olsen
WL/FI
Wright-Patterson AFB OH 45433

10. SPONSORING/MONITORING AGENCY REPORT NUMBER

11. SUPPLEMENTARY NOTES

12a. DISTRIBUTION/AVAILABILITY STATEMENT
Approved for public release;
distribution unlimited

12b. DISTRIBUTION CODE

13. ABSTRACT (Maximum 200 words)

The purpose of this thesis is to investigate the influence of structural optimization parameters on the structural and aeroelastic behavior of a vertical tail. The outside geometry of the tail is assumed fixed. The objective of the optimization is to reduce the structural member sizes so that the overall weight of the tail is minimized. The influence that design loads, design constraints, and design variable linking has on the optimal design is observed by examining several design cases. The static aeroelastic properties and flutter speeds of the various design cases are then compared. The doublet lattice method is used to calculate the steady and unsteady subsonic aerodynamic loads and finite element theory is used to model the vertical tail structure.

14. SUBJECT TERMS	15. NUMBER OF PAGES
Structural Optimization, Structural Analysis, Aeroelasticity.	149
	16. PRICE CODE

17. SECURITY CLASSIFICATION OF REPORT	18. SECURITY CLASSIFICATION OF THIS PAGE	19. SECURITY CLASSIFICATION OF ABSTRACT	20. LIMITATION OF ABSTRACT
Unclassified	Unclassified	Unclassified	UL

NSN 7540-01-280-5500

Standard Form 298 (Rev. 2-89)
Prescribed by ANSI Std. 239-18
298-102